

# Assessing Permeability Across Bacterial Membranes

Kadie Anne Holsinger

B.S. Biochemistry, Messiah University, 2021

A Thesis

Presented to the Graduate Faculty of The University of Virginia in Candidacy for the  
Degree of Master of Science in Chemistry

Department of Chemistry

University of Virginia

April 2023



## Abstract

Bacterial infections and the continual rise of antibiotic resistance pose a serious threat to healthcare worldwide. According to the Centers for Disease Control and Prevention's (CDC) 2019 Antibiotic Resistance Threat Report, more than 2.8 million cases of antibiotic resistance are reported each year in the United States alone. Additionally, these antibiotic-resistant infections are the cause of about 35,000 deaths in the U.S. yearly. While scientists had previously made progress in combatting antibiotic resistance, the CDC states that the emergence of COVID-19 in 2020 caused a serious setback. In fact, from 2019 to 2020 alone, there was a 15% increase in the number of resistant bacterial infections beginning during hospitalization. The clear threat of antibiotic resistance calls for the development of new antibiotics. However, in order for drugs to be most effective, they must permeate across the bacterial cell membrane. Thus, determining modifications to make drugs more permeable and being able to monitor this permeability are of utmost importance in this fight against antibiotic resistance.

Chapter 1 will begin by describing the difference between commensal and pathogenic bacteria as well as provide some examples of common diseases caused by pathogenic bacteria. Next, the classes of bacteria and how they differ from each other will be described. In particular, each section of the cell envelope will be discussed for each class of bacteria. The peptidoglycan (PG) layer will be discussed in more detail since this layer is conserved across all bacteria and is essential for bacterial survival. More specifically, the process of PG biosynthesis and the steps involved in PG cross-linking will be explained. Since bacterial infections are treated with antibiotics, Chapter 2 walks through the discovery of antibiotics beginning with the discovery of the first natural antibiotic, penicillin. Next, the rise in antibiotic resistance will be discussed. In particular, the mechanisms of resistance will be described in depth. These mechanisms include drug target modification, drug inactivation, drug efflux, and decreased drug uptake.

Chapter 3 describes the threat of a particular bacterial species, *Mycobacteria tuberculosis*, and the need to develop new antibiotics because of its increasing death toll and resistance. As such, the stipulations that dictate a drug-like molecule will be discussed. However, a common problem seen in drug development is the permeability of drugs into bacteria, especially mycobacteria. Thus, this chapter explores a particular modification, *N*-methylation, to examine its effects on peptide permeability into mycobacteria due to its ability to eliminate hydrogen-bond donors from the molecule. In addition, another hydrogen-bond donor eliminating modification,

peptoid substitution, is briefly explored in this chapter. The effects of these modifications are tested using a click-chemistry based assay to monitor the permeability across the mycomembrane.

Chapter 4 addresses permeability into *E. coli* cells with the goal of developing and optimizing a new, robust permeability assay. Current techniques to monitor permeability into *E. coli* have limitations such as significant structural modifications to the drug, low signal, or high background. In this chapter, we propose a luciferase-based assay that addresses these limitations for the assessment of permeability into Gram-negative bacteria, such as *E. coli*. The benefits of this assay (i.e., small modifications to the molecules of interest, no washing, good signal-to-noise ratio) will be discussed. In addition, the limitations and future applications of this assay will also be discussed.

## Acknowledgements

I would first like to thank Dr. Pires for his guidance in these projects. I would also like to thank my wonderful lab mates for keeping me laughing and encouraging me on the hard days. Research is better when I get to do it with you all! I would also like to thank my parents, Steve and Debbie, for their constant support throughout my whole life. You have always encouraged me and believed in me no matter what I'm doing, and I am blessed to have such a wonderful support system in you both. I would also like to thank my brother and sister-in-law, Brady and Lydia, for also always supporting me. You two never fail to make me laugh and to meet me where I am. Next, I would like to thank my wonderful parents-in-law, Steve and Angie, for supporting and loving me like your own daughter. Your support is so sweet and pure, and I'm thankful to have you both in my life! I would also like to thank my best friend, Krista, for sticking with me through everything, including another 2 years of long-distance friendship while I pursued my master's degree. Thank you for being the most loyal friend I've ever had. I love you all! And finally, I would like to thank my husband, Zach, for loving and supporting me through it all. You have walked with me through all the joys and all the trials and have constantly reminded me of my worth, strength, and faith. Thank you for always pointing me back to God and for loving me unconditionally. I couldn't have done this without you. I love you now and always.

## Table of Contents

<b>Abstract</b> .....	iii
<b>Chapter 1: Introduction</b> .....	8
1.1 Commensal and Pathogenic Bacteria .....	8
1.2 Classes of Bacteria .....	8
1.2.1 Gram-Negative Bacteria.....	9
1.2.2 Gram-Positive Bacteria.....	12
1.2.3 Mycobacteria.....	13
1.3 Peptidoglycan Biosynthesis .....	13
1.4 Peptidoglycan Crosslinking.....	15
1.5 Summary.....	17
1.6 References .....	18
<b>Chapter 2: Antibiotics and Resistance</b> .....	20
2.1 History of Antibiotics.....	20
2.2 Antibiotic Resistance in Bacteria.....	21
2.2.1 Drug Target Modifications.....	22
2.2.2 Drug Inactivation.....	24
2.2.3 Drug Efflux.....	25
2.2.4 Decreased Drug Uptake.....	27
2.3 Summary.....	28
2.4 References .....	29
<b>Chapter 3: Determining the Effects of <i>N</i>-methylation on Peptide Permeability into Mycobacteria</b> .....	32
3.1 Abstract .....	32
3.2 Introduction.....	32
3.3 Research Strategy and Assay Design.....	36
3.4 Results & Discussion .....	38
3.4.1 Metabolic Incorporation of tetraDBCO .....	38
3.4.2 Methylation Proof-of-Concept.....	39

3.4.3 Permeability of a Methylated Peptide Library .....	41
3.4.4 Peptoid-Peptide Hybrid Proof-of-Concept .....	44
3.5 Conclusions .....	46
3.6 Future Outlooks .....	46
3.7 Materials and Methods .....	48
3.8 References .....	52
<b>Chapter 4: Development of a Luciferase-based Assay to Assess Permeability into the Cytosol of <i>E. coli</i></b> .....	<b>55</b>
4.1 Abstract .....	55
4.2 Introduction .....	55
4.3 Results and Discussion .....	58
4.3.1 Luciferase Expression .....	58
4.3.2 Cyano Hydroxy Benzothiazole versus Cyano Amino Benzothioazole .....	59
4.3.3 CBT Concentration Scan .....	61
4.3.4 Addition of N-Ethylmaleimide .....	62
4.3.5 D-cystine-cipro-methyl-ester .....	63
4.4 Conclusions and Future Outlook .....	65
4.5 Materials and Methods .....	65
4.6 References .....	68
<b>Summary and Future Outlooks</b> .....	<b>70</b>
<b>Appendix</b> .....	<b>72</b>
A.3 Synthesis and Characterization of Compounds in Chapter 3 .....	72
A.4 Synthesis and Characterization of Compounds in Chapter 4 .....	98

## Chapter 1: Introduction

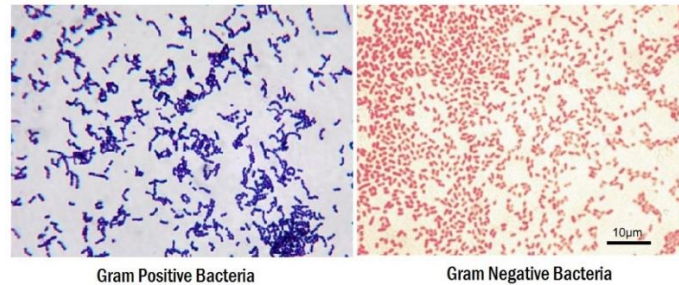
### 1.1 Commensal and Pathogenic Bacteria

Bacteria are unicellular prokaryotic microorganisms that are prevalent in most ecosystems, including humans. In fact, the Human Genome Project discovered that there are ten times more bacterial cells than human cells in the average person.<sup>1</sup> These microbes, also referred to as commensal bacteria, are found throughout the human body within the skin, gut, nose, and mouth. Not only do commensal bacteria live in harmony with human cells, but they can also enhance the human immune system, especially against pathogenic bacteria.<sup>2</sup>

In contrast, pathogenic bacteria impart disease to their host. Infections begin with entrance of the pathogenic bacteria into the host followed by their replication. The severity of the effects that a bacterial infection imparts on the host is called its virulence. This virulence is impacted by several features such as the initial infection load, the bacteria's interactions with the host through its effector proteins, and the host's response to the infection.<sup>3</sup> Common diseases caused by bacterial infections include pneumonia (*Streptococcus*), tuberculosis (*Mycobacterium tuberculosis*), salmonella (*Salmonella*), and MRSA (*Methicillin-resistant Staphylococcus aureus*). According to a report by US News, 1 in 8 deaths around the world are caused by a bacterial infection.<sup>4</sup> Therefore, pathogenic bacteria pose a serious health threat.

### 1.2 Classes of Bacteria

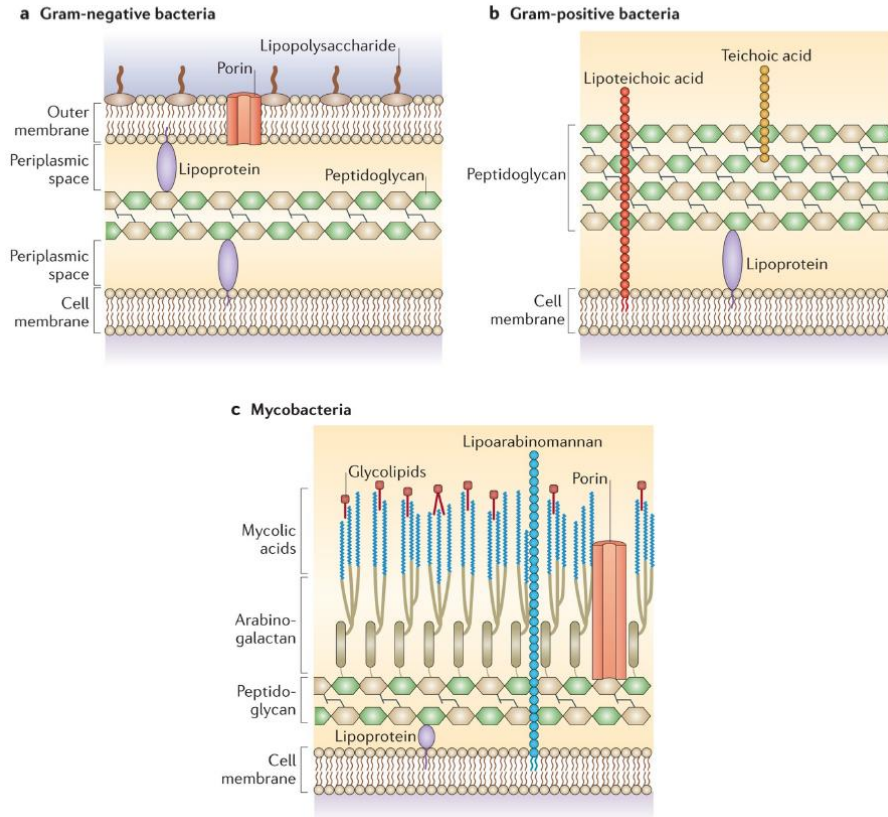
Bacteria are divided into two main classes based on the composition of their cellular envelope: Gram-negative and Gram-positive. These classifications were named for their appearance after a staining procedure developed by Hans Christian Gram in the late 1800s. Gram added crystal violet to bacterial cells and observed that some cells retained the stain while other cells did not; thus, the cell species were referred to as Gram-positive and Gram-negative, respectively (**Figure 1.1**).<sup>5</sup> The difference in staining is attributed to the different cell envelope composition observed in Gram-negative versus Gram-positive bacteria. This staining procedure, known today as Gram staining, was subsequently used to identify and characterize bacteria species.



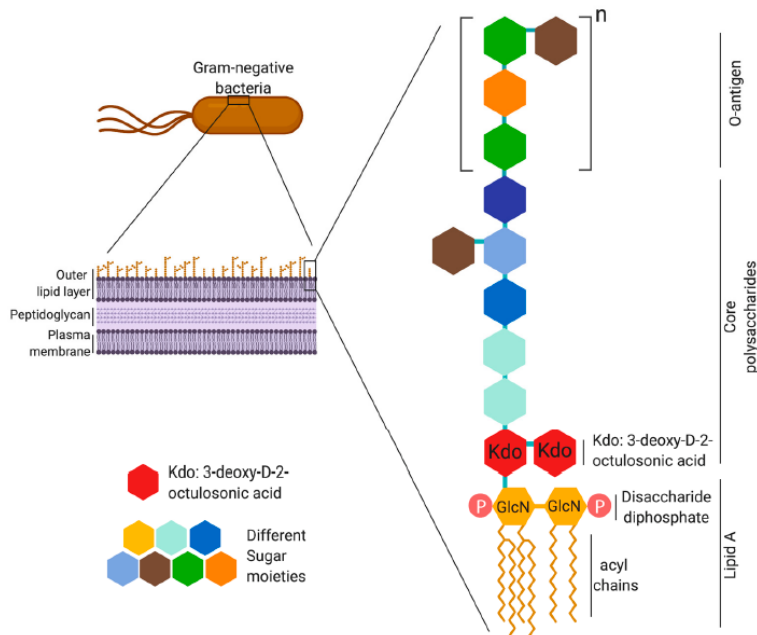
**Figure 1.1** Differences in Gram-positive (left) and Gram-negative (right) to gram staining observed using brightfield microscopy. Reproduced from<sup>6</sup>.

### 1.2.1 Gram-Negative Bacteria

The cell envelope of Gram-negative bacteria consists of three major components: the outer membrane, the peptidoglycan layer, and the inner membrane (**Figure 1.2**). The outer membrane is an asymmetric lipid bilayer composed of phospholipids in the inner leaflet and glycolipids in the outer leaflet, with the major glycolipid being lipopolysaccharide (LPS).<sup>7,8</sup> LPS is composed of three parts, each with a different function (**Figure 1.3**). The innermost part of LPS is lipid A, which is the endotoxic hydrophobic tail, and it serves as the immunostimulatory moiety.<sup>9,10</sup> More specifically, lipid A is recognized by toll-like receptor-4 (TLR4), which is present in phagocytic cells (i.e., macrophages, neutrophils, dendritic cells).<sup>10</sup> After recognition occurs, a signaling cascade promotes the production of pro-inflammatory cytokines to help eliminate the bacterial cells.<sup>10</sup> Lipid A is composed of an acylated  $\beta$ -1'-6-linked glucosamine disaccharide and is the most conserved part of LPS among species.<sup>8</sup> The second component of LPS is the core oligosaccharide, which is linked to the glucosamines of lipid A. This oligosaccharide component is non-repeating and varies from species-to-species but typically includes 3-deoxy-d-manno-oct-2-ulosonic acid (Kdo) residues, heptoses, and various hexoses. The final component of LPS is the O-antigen, which is a polysaccharide of two-eight sugars attached to the core oligosaccharide.<sup>8</sup> The O-antigen is the most variable part of LPS, and it aids the bacteria in evading the immune system due to it being the outermost component.<sup>8,10</sup> Apart from LPS, outer membrane proteins (OMPs) are also important components in the outer membrane of Gram-negative bacteria.<sup>11</sup>

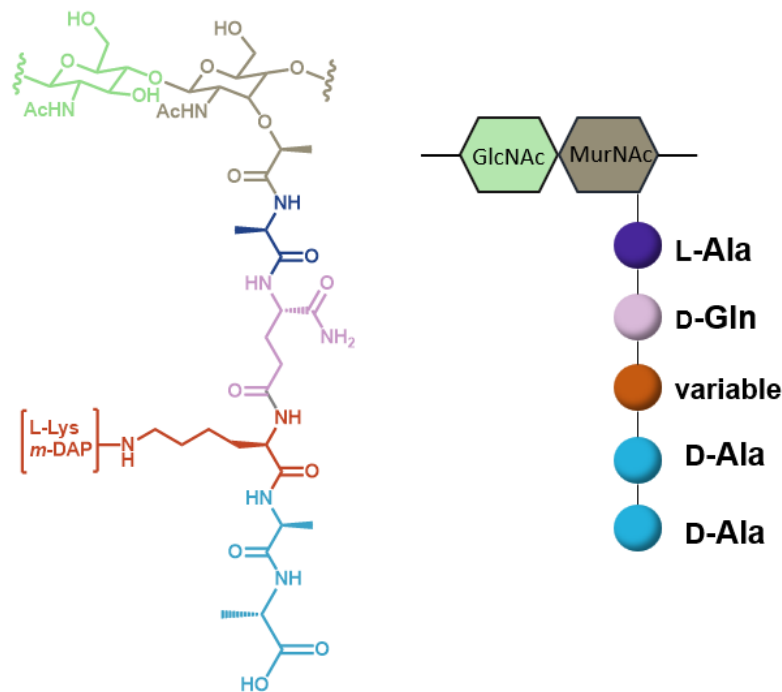


**Figure 1.2** The cell-envelope compositions of Gram-negative bacteria (a), Gram-positive bacteria (b) and mycobacteria (c). Reproduced from<sup>12</sup>.



**Figure 1.3** Depiction of Gram-negative bacteria, its cell envelope, and the lipopolysaccharide (LPS) components. Reproduced from<sup>10</sup>.

Underneath the outer membrane lies the peptidoglycan layer. The peptidoglycan (PG) consists of a repeating disaccharide polymer of *N*-acetylglucosamine (GlcNAc) and *N*-acetylmuramic acid (MurNAc). Covalently attached to the MurNAc is a stem peptide with the sequence: L-alanine, iso-D-glutamate, meso-diaminopimelic acid (m-DAP) or L-Lys, D-alanine, D-alanine (**Figure 1.4**). These stem peptides get crosslinked together by transpeptidases to form a mesh-like scaffold. The presence of PG is conserved across all bacteria, and it helps provide structure and fortify the bacterial cells against cytoplasmic osmotic pressure. Furthermore, while all bacteria contain PG, its third stem peptide residue and the types of crosslinks can vary per species. In Gram-negative bacteria, the PG is a relatively thin component between the inner and outer membranes.<sup>7</sup>



**Figure 1.4** Chemical structure (left) and cartoon depiction (right) of a peptidoglycan unit.

Just beneath the PG and just above the inner membrane lies an aqueous environment called the periplasmic space. A periplasmic space also exists between the outer membrane and the PG. The periplasm contains many proteins, including RNase and alkaline phosphatase, that could be toxic when present in the cytoplasm.<sup>7</sup> Furthermore, the periplasm performs many functions such as protein folding, protein oxidation, lipoprotein secretion, and environmental sensing.<sup>13</sup> Separating the periplasm from the cytoplasm is the inner membrane, which is a classic phospholipid bilayer and is the inner-most component of Gram-negative cell envelopes. This

membrane is also involved in environmental sensing, and it serves as the first exit point for waste produced inside the cell and the last entry point for nutrients.<sup>7</sup> The inner membrane is also responsible for many of the processes that usually occur within the organelles of eukaryotic cells such as energy production and lipid biosynthesis.<sup>7</sup>

### 1.2.2 Gram-Positive Bacteria

Two main differences exist between Gram-negative and Gram-positive: (1) the presence of an outer membrane and (2) the size of the PG. Gram-positive bacteria lack the outer membrane that Gram-negative bacteria possess. Instead, Gram-positive bacteria have a thick PG layer for protection and structure (**Figure 1.2**). In fact, the Gram-positive PG is about 30-100 nm thick, while Gram-negative PG is only a few nanometers in thickness.<sup>7</sup> Sandwiched between the PG in Gram-positive bacteria are teichoic acids (TA), which are comprised of repeats of one of the following: glycerol phosphate, glucosyl phosphate, or ribitol phosphate.<sup>7</sup> Different types of TAs are anchored in different places such as the PG itself (wall teichoic acids, WTAs) or the lipid head groups on the inner phospholipid membrane (lipoteichoic acids, LTAs).<sup>7</sup>

Embedded within the PG layer of Gram-positive bacteria are anchored proteins. In pathogenic Gram-positive bacteria, many of these proteins contribute to their virulence since they are displayed on the surface of the cell given that the PG is the outermost layer.<sup>14</sup> Enzymes known as sortases facilitate the cross-linking of proteins onto the stem peptides in the PG to anchor them onto the cell wall. These displayed proteins have several different functions depending on the class of sortase involved including: invasion or adhesion of host cells/tissues, evasion of the immune system, uptake of iron, and assembly of pili.<sup>14,15</sup> The most well-known sortase enzyme is Sortase A, which is found in *Staphylococcus aureus*. Sortase A recognizes the sequence LPXTG (where X is any amino acid) on a protein and mediates the formation of an amide bond between the protein and the pentaglycine cross bridge off the side chain of the third residue of the stem peptide.<sup>14,16,17</sup> More specifically, the active site cysteine in Sortase A cleaves the sorting sequence between the T and the G, forming a thioacyl intermediate between Sortase A and the threonine of the protein containing LPXT.<sup>14,16,17</sup> Then, the *N*-terminal amino group on the pentaglycine cross bridge in the PG nucleophilically attacks this intermediate, transferring the LPXT-containing protein to the PG.<sup>14,16,17</sup> Several other less known sortase enzymes also exist that recognize different motifs for subsequent cross-linking to the PG.<sup>14</sup>

### 1.2.3 Mycobacteria

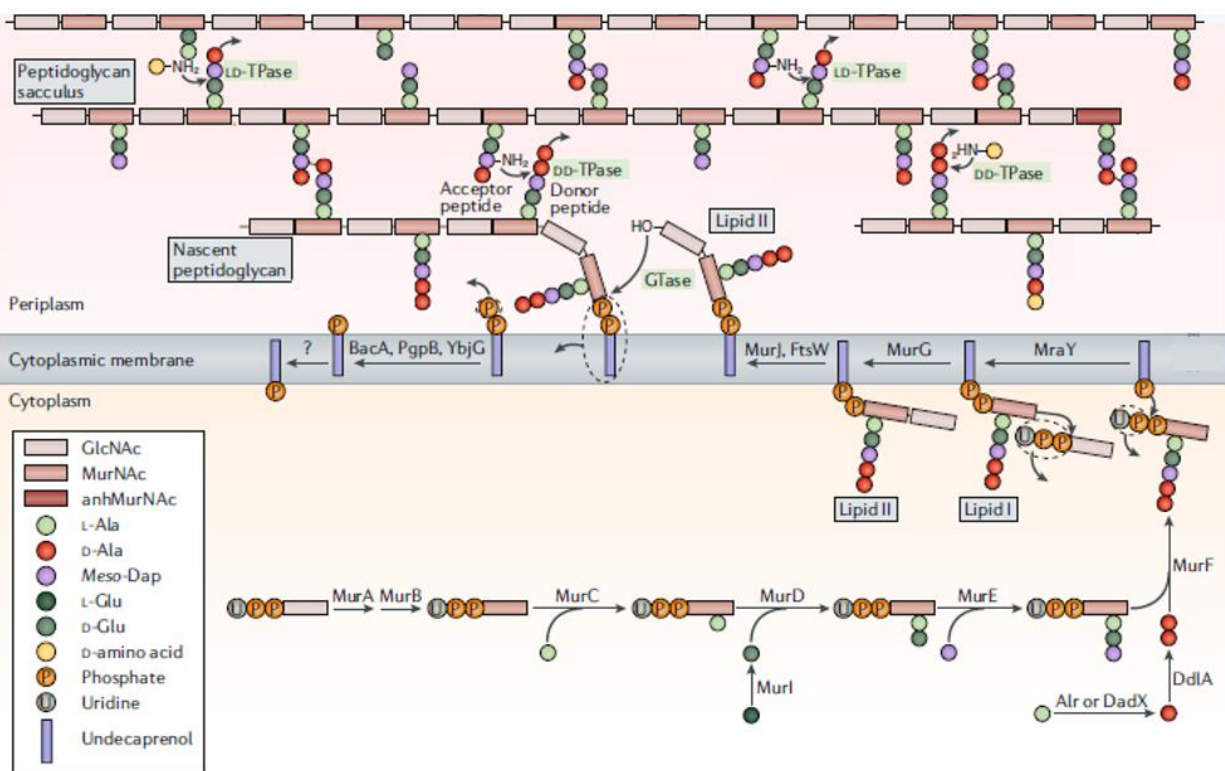
Although Gram-negative and Gram-positive comprise the majority of bacteria species, another type of bacteria consisting of a different cell wall composition is mycobacteria. The mycobacterial cell envelope consists of four components: the mycomembrane, the arabinogalactan layer, the PG, and the inner membrane (**Figure 1.2**). While the mycomembrane may be considered an outer membrane, its composition varies greatly from the outer membrane of Gram-negative bacteria. The mycomembrane is a ~8 nm thick lipid membrane with an outer and inner leaflet, both of which contain mycolic acids.<sup>18,19</sup> These mycolic acids are long-chain  $\alpha$ -alkyl- $\beta$ -hydroxy fatty acids, and they comprise a large percentage of the mycobacterial cell envelope.<sup>20</sup> In addition to the presence of free mycolic acids, the outer leaflet also contains trehalose monomycolate (TMM) and trehalose dimycolate (TDM) which are formed when mycolic acids attach to trehalose sugars.<sup>18,20</sup> Meanwhile, the mycolic acids in the inner leaflet are covalently attached to the arabinogalactan layer, which lies directly below the mycomembrane. Given the highly lipidic composition of the mycomembrane, this outer layer renders most compounds impermeable to the bacteria.<sup>18,20</sup> In fact, beta-lactam antibiotics are 100-1000 times less likely to permeate across the mycomembrane than the outer membrane of Gram-negative bacteria.<sup>18</sup>

As mentioned, the layer below the mycomembrane is the arabinogalactan (AG) layer, which is covalently attached to the PG layer beneath. As indicated by the name, the AG layer is comprised of arabinose and galactose sugars connected in a polymeric manner.<sup>18</sup> The galactose sugars play a role in the covalent link to the PG by binding to the rhamnose part of a rhamnose-GlcNAc dipeptide linker.<sup>18</sup> The GlcNAc then binds to MurNAc in the PG through a phosphodiester bond, which occurs at about 10-12% of the MurNAc residues.<sup>21</sup> Lastly, below the PG sits the inner membrane, which divides the rest of the cell envelope from the cytosol.

### 1.3 Peptidoglycan Biosynthesis

As mentioned above, the peptidoglycan is a common, crucial component to all bacteria cell envelopes due to its role in adding structural support and preventing cell lysis from cytosolic turgor pressure.<sup>22</sup> As such, its structure, biosynthesis, and remodeling has been studied extensively.<sup>22,23</sup> Although the PG exists outside the inner membrane of all bacterial cells, its synthesis begins within the cytoplasm. The first PG precursor is uridine diphosphate (UDP)-GlcNAc, which is generated from fructose-6-phosphate in the cytoplasm.<sup>23</sup> Next, two enzymes

(MurA and MurB) convert GlcNAc to MurNAc to form UDP-MurNAc. Following this conversion, MurC stereo-specifically ligates an L-alanine onto the lactic acid portion of MurNAc.<sup>22,23</sup> MurI then converts an L-Glu to a D-Glu, which gets coupled onto the L-Ala to form a dipeptide off of UDP-MurNAc.<sup>22</sup> As mentioned previously, the third amino acid on the stem peptide is variable, but MurE is typically the enzyme to incorporate this third residue (i.e., L-Lys or *m*-DAP).<sup>22,23</sup> The incorporation of the last two amino acids on the stem peptide is a step-wise process. First, Alr or DadX converts two L-Ala to two D-Ala. DdlA then links the two alanine residues together, and MurF couples the D-Ala-D-Ala dipeptide to the growing stem peptide off of the UDP-MurNAc to complete the pentapeptide (**Figure 1.5**).<sup>22</sup>



**Figure 1.5** Pathway of peptidoglycan biosynthesis. Adapted from Reference 22. Reproduced from<sup>22</sup>.

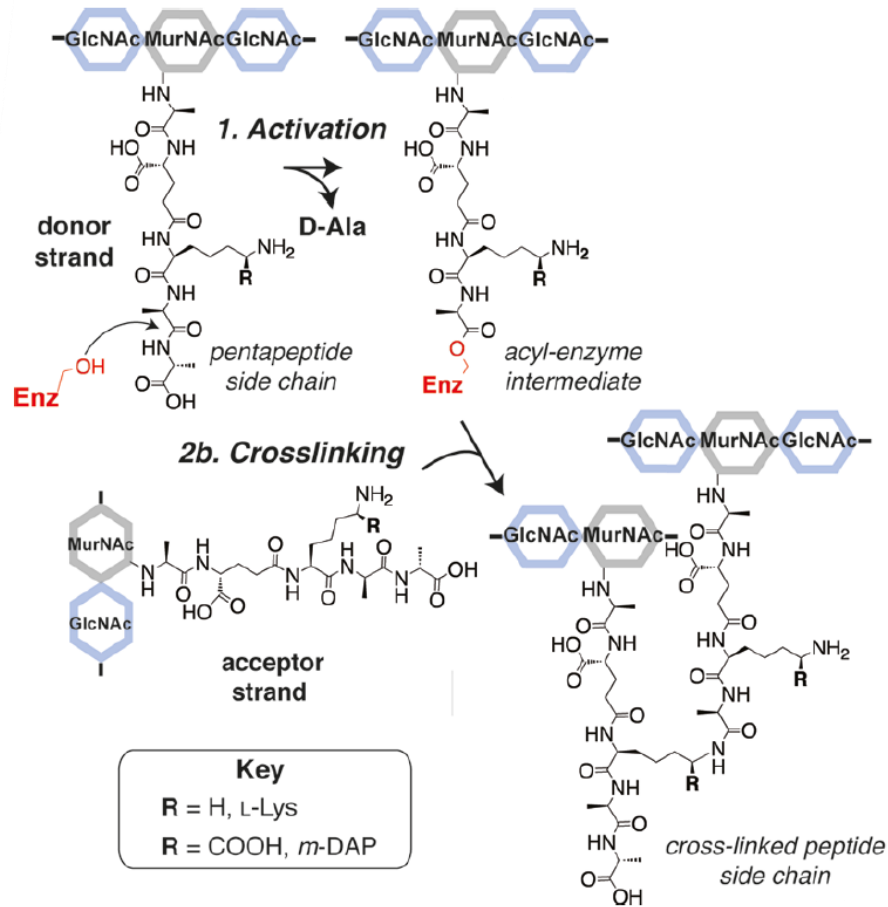
After the synthesis of the UDP-MurNAc-stem peptide complex in the cytoplasm, this PG building block interacts with an inner membrane-imbedded lipid called undecaprenol. This lipid is 55 carbons in length with a phosphate group on the cytoplasmic end of the lipid. The terminal phosphate on undecaprenol attacks between the two phosphates on UDP with uridine phosphate as the leaving group. This reaction is catalyzed by MraY. Now, the building block PP-MurNAc-

stem peptide is tethered to the membrane *via* undecaprenol in a complex known as Lipid I. MurG catalyzes the MurNAc sugar to attack between the phosphate and the sugar of unconverted UDP-GlcNAc, resulting in a PG precursor known as Lipid II.<sup>22</sup>

Subsequently, Lipid II is flipped by MurJ or FstW across the plasma membrane from the cytosol to the periplasmic space where the PG precursors are linked to form the PG scaffold. The first step in the periplasmic space involves glycosyltransferases catalyzing the reaction between the OH group on the GlcNAc of Lipid II and the phosphate-MurNAc linkage of another Lipid II molecule (**Figure 1.5**). This reaction releases the PG subunit from the plasma membrane. This process is repeated by more Lipid II molecules as they are flipped across the membrane to form the glycan polymer found in PG.<sup>22</sup>

#### *1.4 Peptidoglycan Crosslinking*

Once this polymer has formed, stem peptides are in close proximity to one another, which allows for the crosslinking of stem peptides to occur. Cross-linking is an essential step in PG synthesis as it links the strands together to form a rigid scaffold for cell shape and rigor. Two types of cross-linking occur in the PG: 4-3 crosslinks and 3-3 crosslinks. Enzymes called Penicillin Binding Proteins (PBPs), also known as D,D-transpeptidases (Ddts), are responsible for the 4-3 crosslinks. PBPs first bind to the terminal D-Ala-D-Ala of a stem pentapeptide *via* a serine residue in the active site. Upon binding to the stem peptide, which is referred to as the acyl donor, the PBP clips off the terminal D-ala.<sup>24</sup> The side chain on the third position (L-Lys or *m*-DAP) of a neighboring stem peptide (the acyl acceptor) then reacts with the acyl-enzyme intermediate, kicking off the enzyme and forming an amide bond between the two stem peptides (**Figure 1.6**). Thus, the crosslink is named 4-3 since the bond is formed between the fourth residue of one stem peptide (D-ala) and the third residue of the other stem peptide (variable).



**Figure 1.6** Mechanism of stem peptide activation and cross-linking via a transpeptidase enzyme. Reproduced from<sup>24</sup>.

The second type of crosslink (3-3) is mediated by L,D-transpeptidases (Ldts). The acyl donor in this case is a stem tetrapeptide (lacking the terminal D-Ala) as opposed to the stem pentapeptide used in 4-3 crosslinks. Ldts have a cysteine instead of a serine in the active site that clips between the third and fourth residue on the acyl donor peptide, forming another acyl-enzyme intermediate and sacrificing the terminal D-Ala. The next step is the same as before in which the side chain on the third position of a neighboring stem peptide attacks the intermediate, forming a 3-3 crosslink. Importantly, while the length of the acyl donor (penta- or tetrapeptide) dictates the type of crosslink formed, the acyl acceptor can be a tri-, tetra- or pentapeptide since all three contain the third residue.

### 1.5 Summary

Chapter 1 summarizes the difference between commensal and pathogenic bacteria, the classifications of bacteria, peptidoglycan biosynthesis, and peptidoglycan crosslinking. While commensal bacteria comprise the majority of cells in humans, pathogenic bacteria can cause great harm. Both types of bacteria can be one of the three classes that are differentiated by their cell envelope. Gram-negative bacteria possess an outer membrane, thin peptidoglycan layer, and an inner membrane, while Gram-positive bacteria lack an outer membrane but possess a thick PG layer and an inner membrane. Mycobacteria cell envelopes contain a unique outer membrane called the mycomembrane followed by the arabinogalactan layer, PG layer, and an inner membrane. The common thread between all bacterial strains is the peptidoglycan, which is important for cell wall shape and integrity. PG synthesis begins in the cytoplasm with a series of enzymes, and precursors are flipped to the periplasmic space where the glycan polymer is linked together by glycosyltransferases. The stem peptides on the glycan polymer are then cross-linked together either by Penicillin Binding Proteins or L,D-transpeptidases to form a mesh-like scaffold. Given the importance of PG to bacterial shape and integrity, it is imperative to the survival of bacterial cells.

## 1.6 References

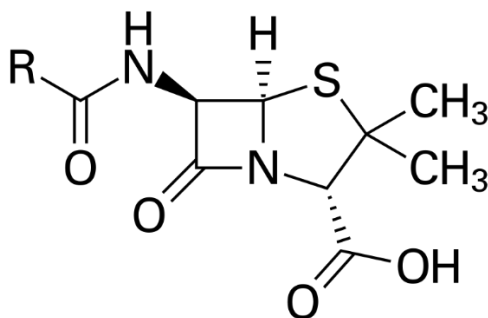
1. “NIH Human Microbiome Project defines normal bacterial makeup of the body.” National Institutes of Health (NIH). Available at: <https://www.nih.gov/news-events/news-releases/nih-human-microbiome-project-defines-normal-bacterial-makeup-body>. Accessed February 12, 2023.
2. Khan, R., Petersen, F. C., and Shekhar, S. “Commensal Bacteria: An Emerging Player in Defense Against Respiratory Pathogens,” *Frontiers in Immunology*, V. 10, 2019, p. 1203.
3. “Bacterial Pathogenesis - Medical Microbiology - NCBI Bookshelf.” Available at: <https://www.ncbi.nlm.nih.gov/books/NBK8526/>. Accessed February 12, 2023.
4. “Bacterial Infections to Blame for 1 in Every 8 Deaths Worldwide.” Available at: <https://www.usnews.com/news/health-news/articles/2022-11-22/bacterial-infections-to-blame-for-1-in-every-8-deaths-worldwide>. Accessed February 12, 2023.
5. Tripathi, N., and Sapra, A. “Gram Staining.” StatPearls. Treasure Island (FL), StatPearls Publishing, 2022.
6. “gram-positive-vs-gram-negative.png (1042×440).” Available at: <https://laboratoryinfo.com/wp-content/uploads/2016/01/gram-positive-vs-gram-negative.png>. Accessed March 5, 2023.
7. Silhavy, T. J., Kahne, D., and Walker, S. “The Bacterial Cell Envelope,” *Cold Spring Harbor Perspectives in Biology*, V. 2, No. 5, 2010, pp. a000414–a000414.
8. Bertani, B., and Ruiz, N. “Function and Biogenesis of Lipopolysaccharides,” *EcoSal Plus*, V. 8, No. 1, 2018, p. ecosalplus.ESP-0001-2018.
9. Farhana, A., and Khan, Y. S. “Biochemistry, Lipopolysaccharide.” StatPearls. Treasure Island (FL), StatPearls Publishing, 2022.
10. Mazgaeen, L., and Gurung, P. “Recent Advances in Lipopolysaccharide Recognition Systems,” *International Journal of Molecular Sciences*, V. 21, No. 2, 2020, p. 379.
11. Koebnik, R., Locher, K. P., and Van Gelder, P. “Structure and function of bacterial outer membrane proteins: barrels in a nutshell,” *Molecular Microbiology*, V. 37, No. 2, 2000, pp. 239–53.
12. Brown, L., Wolf, J. M., Prados-Rosales, R., et al. “Through the wall: extracellular vesicles in Gram-positive bacteria, mycobacteria and fungi,” *Nature Reviews Microbiology*, V. 13, No. 10, 2015, pp. 620–30.
13. Miller, S. I., and Salama, N. R. “The gram-negative bacterial periplasm: Size matters,” *PLOS Biology*, V. 16, No. 1, 2018, p. e2004935.

14. Spirig, T., Weiner, E. M., and Clubb, R. T. "Sortase enzymes in Gram-positive bacteria: Sortase enzymes in Gram-positive bacteria," *Molecular Microbiology*, V. 82, No. 5, 2011, pp. 1044–59.
15. Bradshaw, W. J., Davies, A. H., Chambers, C. J., et al. "Molecular features of the sortase enzyme family," *FEBS Journal*, V. 282, No. 11, 2015, pp. 2097–114.
16. Apostolos, A. J., Kelly, J. J., Ongwae, G. M., et al. "Structure Activity Relationship of the Stem Peptide in Sortase A Mediated Ligation from *Staphylococcus aureus* \*\*," *ChemBioChem*, V. 23, No. 20, 2022.
17. Pishesha, N., Ingram, J. R., and Ploegh, H. L. "Sortase A: A Model for Transpeptidation and Its Biological Applications," *Annual Review of Cell and Developmental Biology*, V. 34, No. 1, 2018, pp. 163–88.
18. Dulberger, C. L., Rubin, E. J., and Boutte, C. C. "The mycobacterial cell envelope — a moving target," *Nature Reviews Microbiology*, V. 18, No. 1, 2020, pp. 47–59.
19. Hoffmann, C., Leis, A., Niederweis, M., et al. "Disclosure of the mycobacterial outer membrane: Cryo-electron tomography and vitreous sections reveal the lipid bilayer structure," *Proceedings of the National Academy of Sciences*, V. 105, No. 10, 2008, pp. 3963–7.
20. Batt, S. M., Minnikin, D. E., and Besra, G. S. "The thick waxy coat of mycobacteria, a protective layer against antibiotics and the host's immune system," *Biochemical Journal*, V. 477, No. 10, 2020, pp. 1983–2006.
21. Alderwick, L. J., Harrison, J., Lloyd, G. S., et al. "The Mycobacterial Cell Wall—Peptidoglycan and Arabinogalactan," *Cold Spring Harbor Perspectives in Medicine*, V. 5, No. 8, 2015, p. a021113.
22. Egan, A. J. F., Errington, J., and Vollmer, W. "Regulation of peptidoglycan synthesis and remodelling," *Nature Reviews Microbiology*, V. 18, No. 8, 2020, pp. 446–60.
23. Barreteau, H., Kovač, A., Boniface, A., et al. "Cytoplasmic steps of peptidoglycan biosynthesis," *FEMS Microbiology Reviews*, V. 32, No. 2, 2008, pp. 168–207.
24. Lupoli, T. J., Tsukamoto, H., Doud, E. H., et al. "Transpeptidase-Mediated Incorporation of D -Amino Acids into Bacterial Peptidoglycan," *Journal of the American Chemical Society*, V. 133, No. 28, 2011, pp. 10748–51.

## Chapter 2: Antibiotics and Resistance

### 2.1 History of Antibiotics

The first natural antibiotic discovered was penicillin, which was found in 1928 by a Scottish physician/scientist named Alexander Fleming (**Figure 2.1**).<sup>1,2</sup> This discovery was made when Fleming had left some *Staphylococcus petri* dishes growing for some time. One dish contained some mold, and the area immediately around the mold was void of bacterial colonies. This observation led Fleming to believe that the mold was secreting a bacterial growth inhibitor, and he set out with his assistants to isolate the culprit, which they named penicillin. This antibiotic has since been used to kill a wide range of Gram-positive bacteria.<sup>2,3</sup>



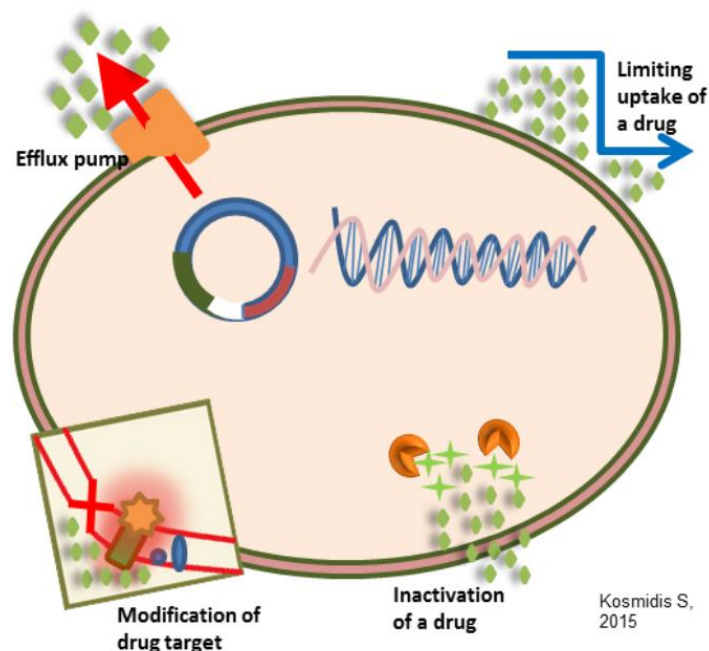
**Figure 2.1** Structure of penicillin.

In 1943, soon after the discovery of penicillin, Selman Abram Waksman and his student Albert Schatz discovered another antibiotic: streptomycin.<sup>4</sup> This antibiotic was discovered when studying soil microbiology. Since penicillin only worked to treat Gram-positive bacteria, streptomycin filled an important gap in treating Gram-negative bacteria and even some mild mycobacterial infections.<sup>4</sup> Waksman, who coined the term “antibiotic,” later won the 1952 Nobel Prize in Physiology or Medicine for his work in discovering streptomycin.<sup>4,5</sup>

The discovery of both penicillin and streptomycin launched the beginning of the Golden Age of Antibiotics, which lasted for about 20 years. During this time, many antibiotics were discovered either from actinomyces (a type of bacteria) natural products, other bacterial natural products, or synthetic strategies (**Figure 2.2**). Antibiotics isolated from actinomyces included macrolides, glycopeptides, and cycloserine. The most popular antibiotics isolated from other bacteria are polymyxins. Lastly, synthetic antibiotics included pyridinamines, quinolones,



In order to effectively circumvent resistance and intelligently design new antibiotics, the types of resistance and the mechanisms by which bacteria resist antibiotics must be understood. Three types of resistance exist in bacteria. The first is intrinsic resistance in which all bacteria in a certain species naturally resist antibiotics in the same way.<sup>10</sup> The second type of resistance is induced, meaning the bacteria express a naturally-occurring gene only after exposure to antibiotics.<sup>10</sup> The last type of resistance is called acquired resistance in which bacteria either take in genetic material from other cells or simply accumulate mutations on their own DNA that confer resistance to antibiotics. These three types of resistance manifest in four main mechanisms: (1) making modifications to the drug targets, (2) rendering the drug inactive, (3) pumping the drug out of the cell (efflux), and (4) decreasing permeability of the drugs through the cell envelope (**Figure 2.3**).<sup>10</sup> While some bacteria many only employ one of these mechanisms, many bacteria will use these mechanisms in conjunction to increase their resistance to antibiotics.

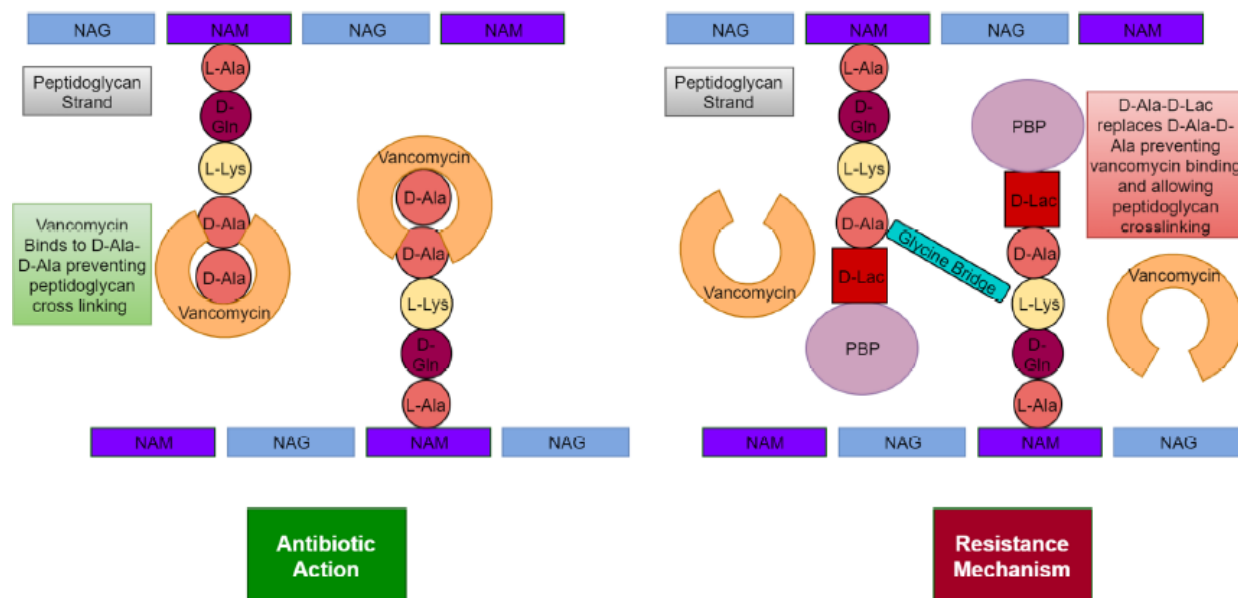


**Figure 2.3** Mechanisms of antibiotic resistance employed by bacteria. Reproduced from<sup>10</sup>.

### 2.2.1 Drug Target Modifications

Modifying the drug target within the bacteria cell is an effective resistance mechanism since the target can evade being recognized by the antibiotic. One example of this is Gram-positive bacterial resistance to the antibiotic vancomycin. Vancomycin is part of a class of antibiotics called glycopeptides. Its mechanism of action (MOA) is to bind to the terminal D-Ala-

D-Ala on the peptidoglycan stem peptide and thereby inhibit cross-linking (transpeptidation) and polymerization of MurNAc and GlcNAc (transglycosylation) (**Figure 2.4, left**).<sup>11,12</sup> Without transpeptidation and transglycosylation occurring, the bacterial cell wall becomes weak and results in lysis. The most common way that Gram-positive bacteria resist vancomycin is by synthesizing their stem peptides with D-Ala-D-Lac (lactate) instead of D-Ala-D-Ala (**Figure 2.4, right**).<sup>11–14</sup> The affinity of vancomycin for D-Ala-D-Lac is three orders of magnitude smaller than for D-Ala-D-Ala.<sup>15</sup> Thus, vancomycin no longer has a strong affinity for the PG, effectively prohibiting the antibiotic from killing the cells.



**Figure 2.4** Left) Mechanism of action of susceptible *S. aureus* cells. Right) Mechanism of vancomycin resistance by conversion of D-Ala-D-Ala to D-Ala-D-Lac. Reproduced from<sup>14</sup>.

Another example of drug target modifications to resist treatment is with the class of antibiotics called quinolones. Typically quinolones act upon DNA gyrase or DNA topoisomerase IV to inhibit DNA synthesis in the bacteria, thus inhibiting proper DNA replication.<sup>10,16</sup> DNA gyrase is the main target in Gram-negative bacteria while DNA topoisomerase IV is the main target in Gram-positive bacteria. These bacteria confer resistance *via* mutations in either the *gyrA* gene (Gram-negative) or the *parC* gene (Gram-positive). These mutations are thought to decrease the binding affinity of the quinolones to the enzymes, allowing the enzymes to continue their proper functions in DNA replication.<sup>16</sup>

An example of drug target modification-mediated resistance that is solely found in Gram-negative bacteria is involving the drug polymyxin. In susceptible bacteria, polymyxin binds to the lipid A component of LPS, causing the displacement of calcium and magnesium. These metals are typically chelated by the phosphate groups to stabilize the LPS, and their displacement causes destabilization of the outer membrane.<sup>12,17</sup> Once destabilized, the bacteria are hypothesized to have membrane leakage, mixing of the inner and outer membranes, inactivation of protein targets, and/or creation of radical oxygen species, resulting in cell death.<sup>12,17</sup> Resistance to polymyxin ensues when the bacteria alter their lipid A composition. The most common modification is the addition of 4-amino-L-arabinose, which contains a positive charge, to the lipid A 4' phosphate group. By switching the charge of the lipid A from negative to positive, the polymyxin is repelled and can no longer bind.<sup>12,17</sup>

### 2.2.2 Drug Inactivation

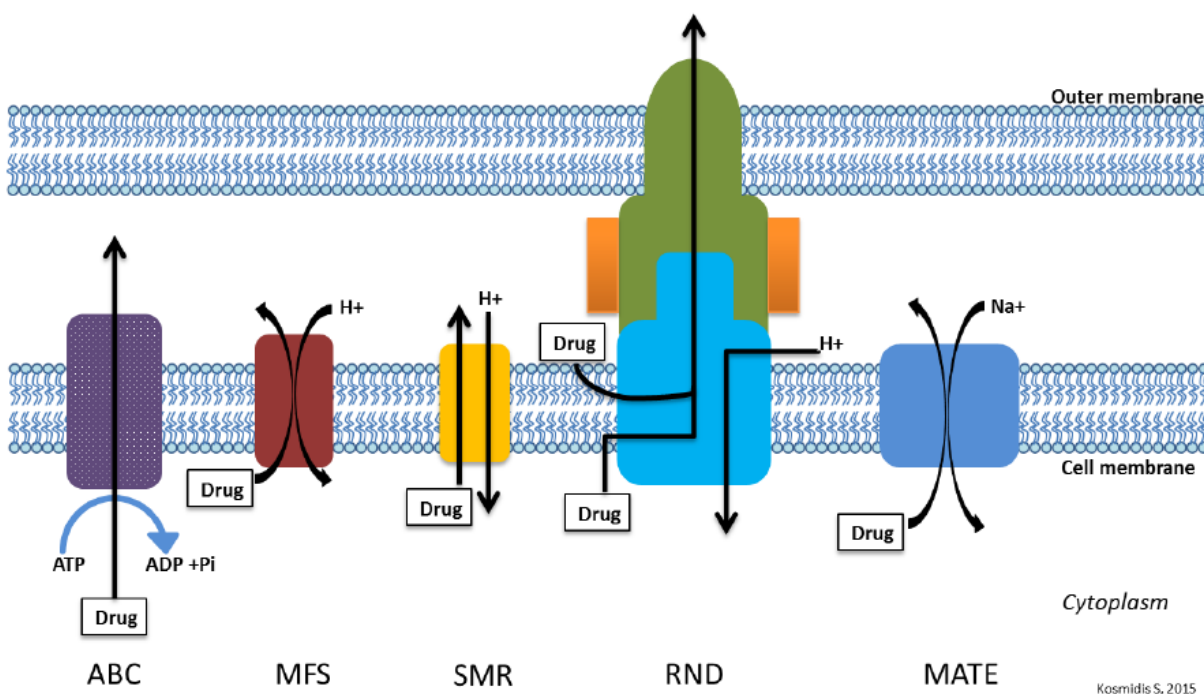
A drug can be rendered inactive by being either degraded or modified by the bacteria. The most known drug-inactivation as a means of resistance *via* degradation is with  $\beta$ -lactam antibiotics, which is the largest used class of antibiotics.  $\beta$ -lactams drugs are structurally similar to D-Ala-D-Ala, and thus, in susceptible bacteria, PBPs see these drugs as substrates.  $\beta$ -lactam antibiotics work binding to the active site of PBPs, which inhibits the PBPs from interacting with the stem peptides.<sup>18</sup> Thus, transpeptidases are no longer available to cross-link the PG.<sup>18</sup> In response, bacteria begin producing enzymes called  $\beta$ -lactamases that hydrolyze the four-membered  $\beta$ -lactam ring found within all drugs in this class of antibiotic.<sup>10,18</sup> Once hydrolyzed, the drugs can no longer bind to PBPs, allowing usual cross-linking to continue.<sup>10</sup> Fortunately, many researchers have focused their efforts on designing  $\beta$ -lactamase inhibitors to use in conjunction with the  $\beta$ -lactam antibiotics.<sup>18</sup>

An example of resistance *via* modification of the antibiotic involves the aminoglycoside class of antibiotics. Typically, aminoglycosides bind to 16S rRNA, which is a component of the ribosome. This binding triggers a conformational change in the A site of the ribosome, which is where tRNAs bring in the next amino acid for protein synthesis. Consequently, the proofreading mechanism is impaired, and mistranslation of the mRNA ensues, causing either inaccurate or truncated proteins, both of which result in cell death. Bacteria resist aminoglycosides by utilizing acetyltransferases (AACs), nucleotidyltransferases (ANTs), or phosphotransferases (APHs). When AACs are used, the 1, 3, 5' or 6' positions on the drug are acetylated. ANTs transfer AMP

from ATP to one of the hydroxyl groups on the aminoglycoside. Lastly, APHs phosphorylate the drugs. All three aminoglycoside-modifying enzymes significantly reduce the antibacterial effects of the drugs. As with  $\beta$ -lactamases, researchers have also developed aminoglycoside-modifying enzyme inhibitors to be used in conjunction with aminoglycosides to treat these resistant bacteria.<sup>19</sup>

### 2.2.3 Drug Efflux

Efflux pumps are transport proteins that deliver an antibiotic out of the cell, preventing the antibiotic from interacting with its target.<sup>20</sup> The pumps are chromosomally encoded in the bacteria and can either be intrinsically expressed or expressed upon exposure to an antibiotic.<sup>10</sup> Bacteria contain five types of efflux pumps: ATP binding cassette (ABC), multidrug and toxic compound extrusion (MATE), major facilitator (MF), small multidrug resistance (SMR), and resistance-nodulation-division (RND) (**Figure 2.5**).<sup>10,20</sup>



**Figure 2.5** Depictions of the five different types of efflux pumps. Reproduced from<sup>10</sup>.

ABC efflux pumps obtain energy through ATP hydrolysis, and they typically have a degree of substrate specificity; however, they can transport a wide variety of molecules such as amino acids, proteins, sugars, and ions. Importantly, some ABC efflux pumps have been shown to efflux

fluoroquinolones and tetracyclines.<sup>10</sup> MATE efflux pumps obtain energy through a sodium gradient. These pumps are majorly found in Gram-negative bacteria, and some can efflux cationic dyes, fluoroquinolones, and aminoglycosides.<sup>10</sup> SMR efflux pumps obtain energy through a proton-motive force. These pumps are highly substrate selective due to hydrophobic composition. Typically, SMR efflux pumps excrete lipophilic cations, but some have also been shown to pump out  $\beta$ -lactams and aminoglycosides.<sup>10</sup> MF efflux pumps export their substrates *via* a solute/proton or sodium symport or *via* solute/proton antiport. As an efflux family, substrate specificity is broad, but each individual pump is specific to a substrate. For instance, *E. coli* cells contain a separate MF efflux pump for macrolides, fluoroquinolones, and trimethoprim.<sup>10</sup> RND efflux pumps also export substrates *via* a proton antiport. These pumps are only found in Gram-negative bacteria and mycobacteria since they are multicomponent efflux pumps, meaning they extend the entire cell envelope from the cytosol to the extracellular space, while the aforementioned pumps only traverse the cytoplasmic membrane (single-component).<sup>21,22</sup> Additionally, these pumps have broad substrate specificity, allowing for the efflux of many different antibiotics.<sup>10</sup> In general, overexpression of more than one type of efflux pump has been shown to have additive, and in some cases synergistic, effects of antibiotic efflux.<sup>23</sup>

While overexpression of the pumps to allow faster excretion of the antibiotic can be used as a resistance mechanism, overexpression alone is rarely sufficient for significant resistance.<sup>20</sup> Instead, the extra efflux pumps aid in bacterial survival to antibiotic pressure and allow the opportunity for mutations that will subsequently confer resistance.<sup>20</sup> For example, Wang et al. studied 30 strains of fluoroquinolone-resistant *E. coli* from a hospital in China. They found that these bacteria had increased expression of AcrAB/TolC, which is a multidrug efflux pump. While overexpression of this pump was found to help increase resistance to fluoroquinolones, other mechanisms of resistance were also at play. The *E. coli* also overexpressed the genes *marA* and *soxS*, which ultimately led to the decreased synthesis of OmpF, which is a porin that many antibiotics use to enter the cells. In addition, Wang et al. also found several mutations in the topoisomerase genes. Therefore, this research effectively showed that while efflux pumps are employed as a resistance mechanism, they are usually combined with at least one of the other three mechanisms.<sup>21</sup>

### 2.2.4 Decreased Drug Uptake

Limiting the amount of antibiotic uptake into bacterial cells is an effective resistance strategy. Some bacteria have intrinsic resistance to antibiotic permeability simply by the composition of their cell wall. More specifically, Gram-negative bacteria have two membranes (inner and outer) that are comprised of different components, providing resistance by having two barriers for penetration. Even if an antibiotic is permeable through one membrane, the drug may not pass through the other. In addition, these bacteria are intrinsically more resistant than Gram-positive bacteria to PG-targeting antibiotics since the PG is harder to access and is smaller in size. However, individual species in the Gram-negative class have different levels of intrinsic resistance. Differences in the exact composition of the outer membrane (i.e., number of LPS molecules, charge distribution, etc.) accounts for the differences in resistance at the outer membrane level.<sup>24</sup> Despite intrinsic resistance to drug uptake, bacteria also have other mechanisms to reduce drug permeability. Gram-negative bacteria contain outer membrane proteins that usually assemble in a  $\beta$ -barrel formation, creating a hydrophilic pore in the membrane through which some antibiotics enter rather than by passive diffusion through the membrane. In such cases, bacteria can either reduce the number of expressed porins or mutate the porin to change selectivity of the channel.<sup>10,25</sup> For instance, deleting the OmpF porin gene led to increased resistance of *E. coli* to various antibiotics.<sup>26</sup> Additionally, others discovered that *E. aerogenes* can mutate a glycine to an arginine in its Omp36 porin, which decreased the porin's activity by three-fold.<sup>25</sup>

Mycobacteria have similar intrinsic resistance properties as Gram-negative bacteria. However, the mycomembrane is considered to be 100-1000 times less permeable than Gram-negative bacteria's outer membrane.<sup>27</sup> The mycomembrane is a waxy and highly hydrophobic, providing a formidable barrier to many antibiotics, especially hydrophilic ones.<sup>22</sup> In addition to the hydrophobic nature, Bertozzi and coworkers discovered that the mycomembrane has a low level of fluidity, which contributes to the low permeability nature of the membrane.<sup>28</sup> In fact, when *M. smegmatis* cells were treated with a common tuberculosis antibiotic (ethambutol), the fluidity of the mycomembrane increased.<sup>28</sup> This result could explain why ethambutol is most effective for treating tuberculosis when combined with other drugs since it can make the mycomembrane more permeable. Another part of the membrane composition that contributes to mycobacteria's intrinsic resistance is the low number of expressed porins or transporters.<sup>29</sup> Several drugs, particularly hydrophilic ones, have been shown to enter mycobacterial cells *via* porins or transporters.<sup>30</sup>

Therefore, the limited number of porins limits the amount of antibiotic that can enter the cells and subsequently reach their targets.

While Gram-positive bacteria are considered more permeable than Gram-negative and mycobacteria, they also have the ability to make their cellular envelope less permeable. For instance, vancomycin-intermediate *S. aureus* (VISA) is a strain of Gram-positive bacteria that is not yet resistant to vancomycin, but it does have reduced sensitivity to the drug.<sup>31</sup> This reduced sensitivity is conducted in two ways. First, PG synthesis is ramped up, causing a thickened cell wall that is shaped irregularly. Second, less cross-linking occurs, meaning that more D-Ala-D-Ala sites are exposed for the vancomycin to bind to. Once bound, these vancomycin molecules sterically hinder either more vancomycin molecules or other drugs from permeating the cell envelope to reach their targets.<sup>13</sup>

### 2.3 Summary

Chapter 2 walks through the discovery of antibiotics and the subsequent rise in antibiotic resistance *via* several resistance mechanisms. The first natural antibiotic discovered was penicillin, which helped to launch the Golden Age of Antibiotics during which several new classes of antibiotics were discovered. However, the rise in new antibiotic treatments was accompanied by the rise in resistance to antibiotics. Resistance mechanisms developed by bacteria fall into four categories: drug target modification, drug inactivation, drug efflux, or decreased drug uptake. Drug target modifications are usually executed *via* structural changes to the target (i.e., D-Ala-D-Lac in vancomycin-resistant bacteria) or *via* in the target gene, which leads to changes in the target structure (i.e., mutations to *gyrA* and *parC* in quinolone resistant bacteria). Inactivation of drugs is typically manifested in either modifications to the drug or degradation of the drug. Drug efflux is mediated by one or more efflux pumps from the five categories: ATP binding cassette (ABC), multidrug and toxic compound extrusion (MATE), major facilitator (MF), small multidrug resistance (SMR), and resistance-nodulation-division (RND). Lastly, bacteria can resist antibiotics by limiting the uptake of drugs, which is carried out by either intrinsic resistance or alterations to the composition of the cell wall (i.e., rigidity, number of porins).

## 2.4 References

1. Tan, S., and Tatsumura, Y. "Alexander Fleming (1881–1955): Discoverer of penicillin," *Singapore Medical Journal*, V. 56, No. 07, 2015, pp. 366–7.
2. "Alexander Fleming Discovery and Development of Penicillin - Landmark." American Chemical Society. Available at: <https://www.acs.org/education/whatischemistry/landmarks/flemingpenicillin.html>. Accessed February 19, 2023.
3. Zaffiri, L., Gardner, J., and Toledo-Pereyra, L. H. "History of Antibiotics. From Salvarsan to Cephalosporins," *Journal of Investigative Surgery*, V. 25, No. 2, 2012, pp. 67–77.
4. Wainwright, M. "Streptomycin: Discovery and Resultant Controversy," *History and Philosophy of the Life Sciences*, V. 13, No. 1, 1991, pp. 97–124.
5. Davies, J., and Davies, D. "Origins and Evolution of Antibiotic Resistance," *Microbiology and Molecular Biology Reviews*, V. 74, No. 3, 2010, pp. 417–33.
6. Hutchings, M. I., Truman, A. W., and Wilkinson, B. "Antibiotics: past, present and future," *Current Opinion in Microbiology*, V. 51, 2019, pp. 72–80.
7. Davies, J. "Where Have all the Antibiotics Gone?," *Canadian Journal of Infectious Diseases and Medical Microbiology*, V. 17, No. 5, 2006, pp. 287–90.
8. CDC. "What Exactly is Antibiotic Resistance?" Centers for Disease Control and Prevention. Available at: <https://www.cdc.gov/drugresistance/about.html>. Accessed March 5, 2023.
9. Silver, L. L. "Challenges of Antibacterial Discovery," *Clinical Microbiology Reviews*, V. 24, No. 1, 2011, pp. 71–109.
10. C Reygaert, W. and Department of Biomedical Sciences, Oakland University William Beaumont School of Medicine, Rochester, MI, USA "An overview of the antimicrobial resistance mechanisms of bacteria," *AIMS Microbiology*, V. 4, No. 3, 2018, pp. 482–501.
11. Mühlberg, E., Umstätter, F., Kleist, C., et al. "Renaissance of vancomycin: approaches for breaking antibiotic resistance in multidrug-resistant bacteria," *Canadian Journal of Microbiology*, V. 66, No. 1, 2020, pp. 11–6.
12. Schaenzer, A. J., and Wright, G. D. "Antibiotic Resistance by Enzymatic Modification of Antibiotic Targets," *Trends in Molecular Medicine*, V. 26, No. 8, 2020, pp. 768–82.
13. Lowy, F. D. "Antimicrobial resistance: the example of *Staphylococcus aureus*," *Journal of Clinical Investigation*, V. 111, No. 9, 2003, pp. 1265–73.

14. Nikolic, P., and Mudgil, P. "The Cell Wall, Cell Membrane and Virulence Factors of *Staphylococcus aureus* and Their Role in Antibiotic Resistance," *Microorganisms*, V. 11, No. 2, 2023, p. 259.
15. Healy, V. L., Lessard, I. A., Roper, D. I., et al. "Vancomycin resistance in enterococci: reprogramming of the d-Ala–d-Ala ligases in bacterial peptidoglycan biosynthesis," *Chemistry & Biology*, V. 7, No. 5, 2000, pp. R109–19.
16. Jacoby, G. A. "Mechanisms of Resistance to Quinolones," n.d.
17. Li, J., Nation, R. L., and Kaye, K. S., eds. "Polymyxin Antibiotics: From Laboratory Bench to Bedside," v. vol. 1145, Cham, Springer International Publishing, 2019.
18. Bush, K., and Bradford, P. A. "β-Lactams and β-Lactamase Inhibitors: An Overview," *Cold Spring Harbor Perspectives in Medicine*, V. 6, No. 8, 2016, p. a025247.
19. Ramirez, M. S., and Tolmasky, M. E. "Aminoglycoside modifying enzymes," *Drug Resistance Updates*, V. 13, No. 6, 2010, pp. 151–71.
20. Webber, M. A. "The importance of efflux pumps in bacterial antibiotic resistance," *Journal of Antimicrobial Chemotherapy*, V. 51, No. 1, 2003, pp. 9–11.
21. Wang, H., Dzink-Fox, J. L., Chen, M., et al. "Genetic Characterization of Highly Fluoroquinolone-Resistant Clinical *Escherichia coli* Strains from China: Role of *acrR* Mutations," *Antimicrobial Agents and Chemotherapy*, V. 45, No. 5, 2001, pp. 1515–21.
22. Batt, S. M., Minnikin, D. E., and Besra, G. S. "The thick waxy coat of mycobacteria, a protective layer against antibiotics and the host's immune system," *Biochemical Journal*, V. 477, No. 10, 2020, pp. 1983–2006.
23. Lee, A., Mao, W., Warren, M. S., et al. "Interplay between Efflux Pumps May Provide Either Additive or Multiplicative Effects on Drug Resistance," *Journal of Bacteriology*, V. 182, No. 11, 2000, pp. 3142–50.
24. Zgurskaya, H. I., and Rybenkov, V. V. "Permeability barriers of Gram-negative pathogens," *Annals of the New York Academy of Sciences*, V. 1459, No. 1, 2020, pp. 5–18.
25. Delcour, A. H. "Outer membrane permeability and antibiotic resistance," *Biochimica et Biophysica Acta (BBA) - Proteins and Proteomics*, V. 1794, No. 5, 2009, pp. 808–16.
26. Choi, U., and Lee, C.-R. "Distinct Roles of Outer Membrane Porins in Antibiotic Resistance and Membrane Integrity in *Escherichia coli*," *Frontiers in Microbiology*, V. 10, 2019, p. 953.
27. Kartmann, B., Stenger, S., and Niederweis, M. "Porins in the Cell Wall of *Mycobacterium tuberculosis*," *J. BACTERIOL.*, n.d.

28. Rodriguez-Rivera, F. P., Zhou, X., Theriot, J. A., et al. "Visualization of mycobacterial membrane dynamics in live cells," *Journal of the American Chemical Society*, V. 139, No. 9, 2017, pp. 3488–95.
29. Gygli, S. M., Borrell, S., Trauner, A., et al. "Antimicrobial resistance in *Mycobacterium tuberculosis*: mechanistic and evolutionary perspectives," *FEMS Microbiology Reviews*, V. 41, No. 3, 2017, pp. 354–73.
30. Danilchanka, O., Pavlenok, M., and Niederweis, M. "Role of Porins for Uptake of Antibiotics by *Mycobacterium smegmatis*," *Antimicrobial Agents and Chemotherapy*, V. 52, No. 9, 2008, pp. 3127–34.
31. Cui, J., Zhang, H., Mo, Z., et al. "Cell wall thickness and the molecular mechanism of heterogeneous vancomycin-intermediate *Staphylococcus aureus*," *Letters in Applied Microbiology*, V. 72, No. 5, 2021, pp. 604–9.

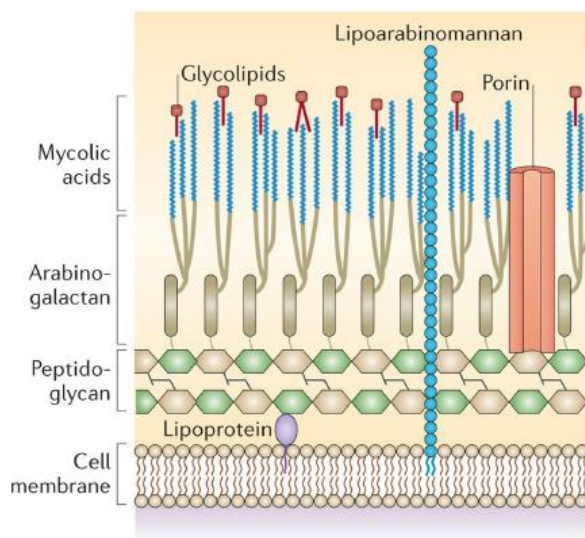
## Chapter 3: Determining the Effects of *N*-methylation on Peptide Permeability into Mycobacteria

### 3.1 Abstract

Tuberculosis (TB) is an infectious disease caused by *Mycobacterium tuberculosis* (*Mtb*) that results in about 2 million deaths per year, and resistant strains of *Mtb* continue to persist. As such, the CDC classifies TB as a serious threat. TB is difficult to treat due to its complex cell wall structure, including a mycomembrane outer layer that is the major permeation barrier for antibiotics. Furthermore, the prevalence of resistant TB stains necessitates the development of new treatments. However, one common problem with antibiotic treatment is the ability to permeate across the thick, waxy mycomembrane. Efforts to improve permeability into mammalian cells resulted in the discovery that *N*-methylation of the peptide backbone tends to modulate permeability of peptides. Therefore, we hypothesize that *N*-methylation of the peptide backbone could also improve permeability into mycobacterial cells. To test this hypothesis, we installed a bioorthogonal tag within the peptidoglycan, which is a layer of the cell wall beneath the mycomembrane. This tag reports on the abilities of peptides with different degrees of methylation to permeate across the mycomembrane *via* a permeability assay using click chemistry. Results from this work show that *N*-methylating the peptide backbone has the potential to increase permeability across the mycomembrane. However, increasing the degree of methylation does not necessarily correlate with increased permeability. Peptoid substitutions, an alternative to *N*-methylation, was also briefly studied and was found to have an impact on permeability.

### 3.2 Introduction

*Mycobacterium tuberculosis* (*Mtb*), the causative agent of tuberculosis (TB), imparts pathogenicity by infecting and residing in the lungs.<sup>1</sup> About one-fourth of the global population has a latent TB infection, causing approximately 1.5 million deaths per year, and the number of deaths by TB has since increased upon the emergence of COVID-19.<sup>2</sup> TB is particularly difficult to treat due to the presence of a complex cell wall that consists of a mycomembrane, an arabinogalactan (AG) layer, and peptidoglycan (PG) (**Figure 3.1**).<sup>3</sup> Moreover, drugs that have cytosolic or cell wall targets must cross the mycomembrane, which is the major permeability barrier to the cell.<sup>4</sup>



**Figure 3.1** Structure of the mycobacterial cell wall. The outermost layer is the mycomembrane, followed by the arabinogalactan layer (AG), the peptidoglycan (PG), and inner plasma membrane. Reproduced from<sup>5</sup>.

Current treatments for TB include four small molecule antibiotics: Isoniazid, Ethambutol, Rifampin, and Pyrazinamide. However, these drugs were FDA-approved many decades ago, and *Mtb* cells have since developed resistance.<sup>6</sup> A combination of antibiotics is often used to treat drug-resistant TB, but resistance has emerged even to this more intense regimen.<sup>7</sup> More recently, two drugs Bedaquiline and Delamanid were discovered for treatment of TB, but *Mtb* developed resistance to these within three years.<sup>8</sup> The continual resistance of *Mtb* to traditional antibiotics calls for the consideration of alternate treatment methods or modifications of drugs.

In order to design effective antibiotics for both susceptible and resistant bacteria, two important factors must be taken into account: (1) oral bioavailability and (2) permeability. Oral bioavailability is important because the drug must arrive at the bacterial cells without being degraded. Furthermore, orally administered antibiotics are more convenient and a more distributable way to treat bacterial infections. Simultaneously, permeability is important because the drug must be able to reach its target. Bacterial cells can alter their porins to decrease drug influx, and they can alter their membrane composition to decrease passive permeability of molecules, owing to the bacteria's ability to resist antibiotic treatment.<sup>9</sup> In addition, researching new drugs for mycobacterial infections proves difficult due to the intrinsic permeability resistance from the highly hydrophobic mycomembrane. Thus, permeability is arguably the highest priority problem that needs to be addressed in developing new antibiotics for mycobacteria.

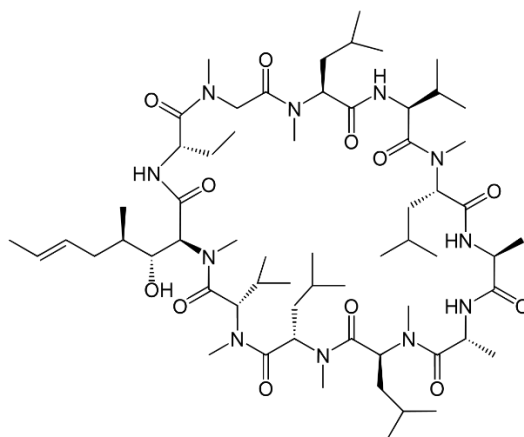
Many years ago, Christopher Lipinski developed a framework for determining if a molecule is drug-like (i.e., orally bioavailable and permeable) called the Rule of 5 (Ro5). Lipinski's Rule of 5 states that for a molecule to be drug-like, it must follow at least two of these stipulations: be less than 500 Da, contain less than 5 hydrogen bond donors, contain less than 10 hydrogen bond acceptors, and have a ClogP of less than 5.<sup>10</sup> Lipinski suggests that breaking even one of these four principles may cause a molecule to be a poor drug.<sup>10</sup> Nowadays, the Ro5 is considered more of a guideline rather than a rule since several effective drugs break one or more of these "rules."<sup>11</sup>

For instance, peptide drugs are becoming more popular therapeutic treatment options.<sup>12</sup> However, peptides tend to break the Ro5 because each peptide bond includes one hydrogen-bond donor and two hydrogen-bond acceptors.<sup>13</sup> Therefore, a peptide consisting of five nonpolar amino acids already exceeds two guiding principles in the Ro5.<sup>13</sup> Furthermore, given that peptides tend to be 2-50 amino acids long, they likely have a molecular weight greater than 500 Da.<sup>14</sup> For example, a hepta-peptide consisting of only alanine, the second smallest amino acid, is 515 Da. Since CLogP describes the lipophilicity of a peptide, this value varies based on amino acid composition. Therefore, almost all peptide drugs break at least one of the four guiding principles, limiting their drug-likeness, including permeability.

One strategy to broadly address permeability issues is *N*-methylation. This strategy has been studied recently in the literature to address the impact of hydrogen-bond donors on the permeability of drugs.<sup>15-17</sup> In a normal peptide bond, a hydrogen atom is bonded with the backbone nitrogen atom. In solution, this hydrogen atom can participate in hydrogen bonding with the solvent molecules. Therefore, when the drug permeates across the membrane, the hydrogen bonding gets disrupted, which results in an enthalpic desolvation penalty. However, if the hydrogen atom is replaced by a methyl group, a hydrogen bond can no longer form, and less energy is required for this methylated peptide to cross the membrane compared to its unmethylated counterpart. *N*-methylation successfully eliminates one hydrogen-bond donor, placing the molecule closer to the constraints of the Ro5. Peptides are an appropriate place to begin addressing the effects of *N*-methylation on permeability due to their accessible synthetic strategies.

Although peptides have been emerging as a promising treatment option for many diseases, they have poor membrane permeability, which is a particular challenge with the complex cell wall of mycobacteria. However, since certain FDA-approved peptides can cross

mammalian cell membranes, these peptides can serve as inspiration for designing peptides that are permeable across mycobacteria's more complex cell wall. For instance, the peptide Cyclosporine is an FDA-approved immunosuppressant drug used to treat the rejection of organs after a transplant (**Figure 3.2**).<sup>18</sup> When taking a closer look at Cyclosporine, multiple methyl groups on the backbone nitrogen atoms are present (**Figure 3.2**). This *N*-methylation strategy has been shown by several groups to improve peptide permeability into mammalian cells.<sup>15</sup> For instance, the Lokey group found that increasing the degree of methylation of large molecular weight lariat peptides led to an increase in their permeability.<sup>19</sup> Additionally, the group also made sanguinamide A analogues, which is another cyclic peptide. They found that adding methyl groups to solvent-exposed backbone nitrogen atoms significantly improved the permeability of these peptides into mammalian cells.<sup>16</sup>



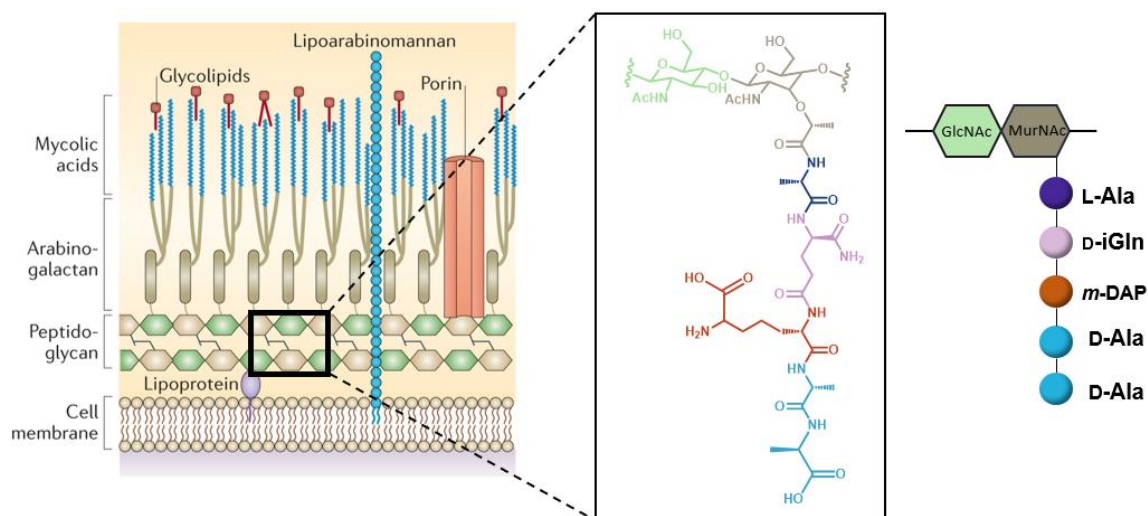
**Figure 3.2.** Structure of Cyclosporine.

Some groups have also studied the effects of *N*-methylation of peptides on permeability into Gram-negative bacteria. For instance, the Ni group looked at the peptide Anoplin, which can bind to bacterial DNA and/or inhibit ATP synthesis.<sup>17,20</sup> The intracellular targets indicate that the peptide must either passively permeate through the membrane or be actively transported across. The Ni group tested the ability of a few *N*-methylated and lipid-tail conjugated analogs of Anoplin to permeate across the outer membrane of *E. coli* using an N-Phenyl-1-naphthylamine (NPN) dye, which will only fluoresce when bound to hydrophobic regions.<sup>17</sup> They found that within one minute of adding their peptides to the cells, fluorescence of NPN increased significantly, with some analogs outperforming the original Anoplin peptide, indicating rapid uptake.<sup>17</sup>

Taking inspiration from these studies with mammalian cells and Gram-negative cells, this project seeks to investigate *N*-methylation as a strategy to make peptides permeable into mycobacteria using a systematic approach. We hypothesize that methylating peptides will increase their permeability into mycobacteria as has been seen with mammalian and Gram-negative bacterial cells. To study the relationship between *N*-methylation and permeability in the context of mycobacteria, we have chosen to use peptides as they are synthetically accessible; however, the results found can be applied to small molecule drugs as well.

### 3.3 Research Strategy and Assay Design

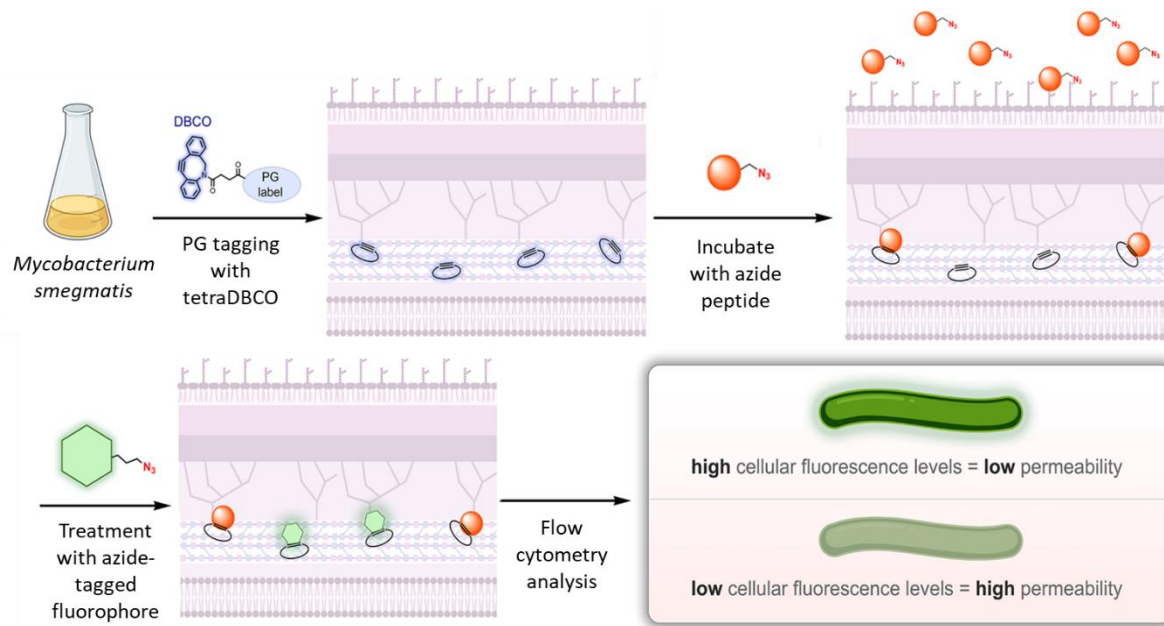
In order to probe for permeability across the mycomembrane, this project takes advantage of the peptidoglycan layer of the mycobacterial cell wall, which sits beneath the highly hydrophobic mycomembrane (**Figure 3.1**). PG is a cell wall component that is unique to all bacterial cells and has been increasingly studied over the past couple years.<sup>21</sup> The PG is comprised of a repeating disaccharide polymer of *N*-acetyl glucosamine (GlcNAc) and *N*-acetyl muramic acid (MurNAc) (**Figure 3.3**). Covalently attached to the MurNAc sugar is the stem peptide, which is a three-to-five-amino-acid long peptide with a relatively conserved sequence. This sequence found in mycobacteria is typically L-alanine, amidated *iso*-D-glutamate, *meso*-diaminopimelic acid (*m*-DAP), D-alanine, D-alanine.<sup>22</sup> These stem peptides are cross-linked together by transpeptidase enzymes to form a mesh-like scaffold.



**Figure 3.3.** Peptidoglycan composition. The PG sits beneath the mycomembrane and is comprised of a repeating disaccharide unit and stem peptides. The pentapeptide is depicted here. Leftmost portion of the figure reproduced from<sup>5</sup>.

Our lab previously investigated metabolic labeling of the PG. Pidgeon et al. synthesized a stem peptide analog with a fluorescein attached to the N-terminus of the tetrapeptide (tetraFI): fluorescein-L-ala-D-isoGln-L-Lys-D-ala.<sup>23</sup> When this peptide was added to *Mycobacterium smegmatis* (*Msm*) cell culture, Pidgeon et al. observed a significant rise in fluorescence levels compared to background and other structural variants when analyzing the cells *via* flow cytometry. Therefore, they concluded that tetraFI was recognized by the endogenous transpeptidases as a substrate and was covalently cross-linked into the existing PG scaffold. Additionally, a recent paper in our lab tested labeling of the PG with the tetrapeptide conjugated to a click handle and compared to labeling with a single amino acid (diaminopimelic acid, D-Dap) conjugated to a click handle.<sup>24</sup> Liu et al. found significantly higher labeling with the peptide rather than the single amino acid.<sup>24</sup>

Here, we also hope to take advantage of the PG cross-linking machinery using the same tetrapeptide label, which is a stem peptide analog with a dibenzo cyclooctyne (DBCO) click handle conjugated on the N-terminus. When incubated with *Msm* cells, which is a model for *Mtb*, the DBCO tetrapeptide (tetraDBCO) should be metabolically incorporated, displaying the DBCO on the PG for subsequent click chemistry (**Figure 3.4**). Azide reactive handles will be installed on a library of variably methylated peptides. Each azide-tagged peptide will be incubated with the cells. Permeable peptides that crossed the mycomembrane will encounter and react with the DBCO on the PG *via* a type of click chemistry reaction called Strain-Promoted Alkyne-Azide Cycloaddition (SPAAC). Then, the cells will be incubated with fluorescein-azide (FI-az) to react with free DBCO sites. Flow cytometry will be used to analyze the fluorescence levels of the cells. If a peptide is highly permeable, the peptide will occupy a high percentage of the DBCO sites; only a few DBCO sites will be free for reaction with FI-az, giving a low fluorescence signal. The opposite is also true: a poorly permeable azide peptide will give a high fluorescence signal (**Figure 3.4**).

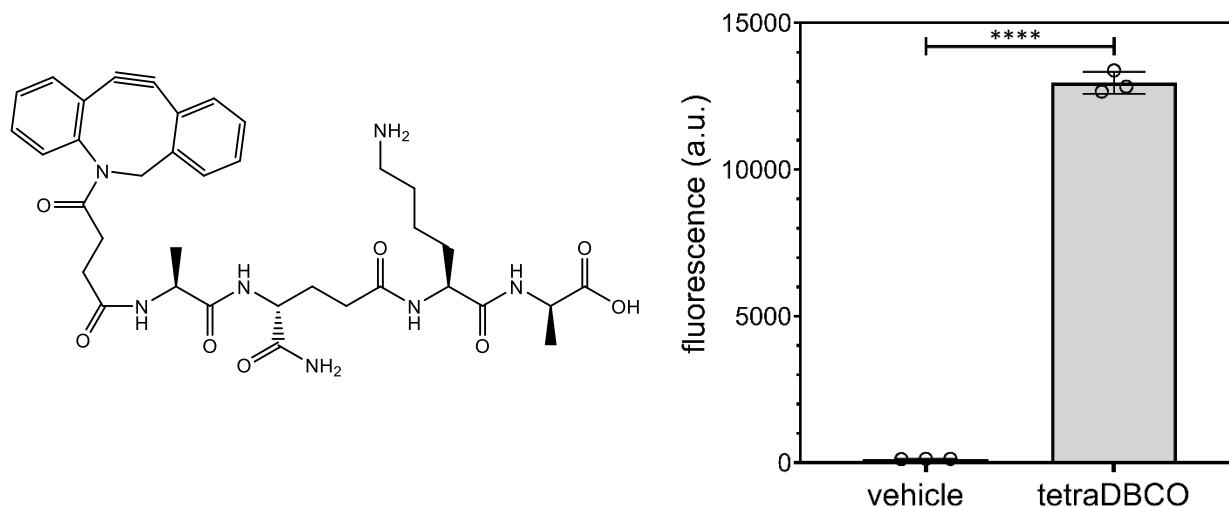


**Figure 3.4** Assay workflow. First, *Msm* cells are incubated with tetraDBCO to metabolically label the PG. Then, cells are treated with azide-tagged peptides followed by an azide-tagged fluorophore. Flow cytometry analysis will provide an inverse relationship between fluorescence levels and permeability.

### 3.4 Results & Discussion

#### 3.4.1 Metabolic Incorporation of tetraDBCO

First, the tetraDBCO peptide was synthesized using solid phase peptide synthesis (SPPS), purified by high-performance liquid chromatography (HPLC), and characterized using matrix-assisted laser desorption ionization (MALDI) mass spectrometry and UV-vis absorbance (**Figure 3.5, left**). Then, *Msm* ( $mc^2$  155) was tested for its ability to metabolically incorporate tetraDBCO into its PG. *Msm* cells were only treated with FI-az without tetraDBCO, which gave low fluorescence levels (**Figure 3.5, right**). Since DBCO is not present, SPAAC cannot occur, and the fluorophore cannot get anchored onto the cell wall. However, when *Msm* cells were incubated with tetraDBCO followed by an incubation with FI-az, fluorescence levels were high (**Figure 3.5, right**). Since fluorescence levels were only high in cells that were incubated with tetraDBCO, the stem peptide analog is likely incorporated into the *Msm* cell wall.



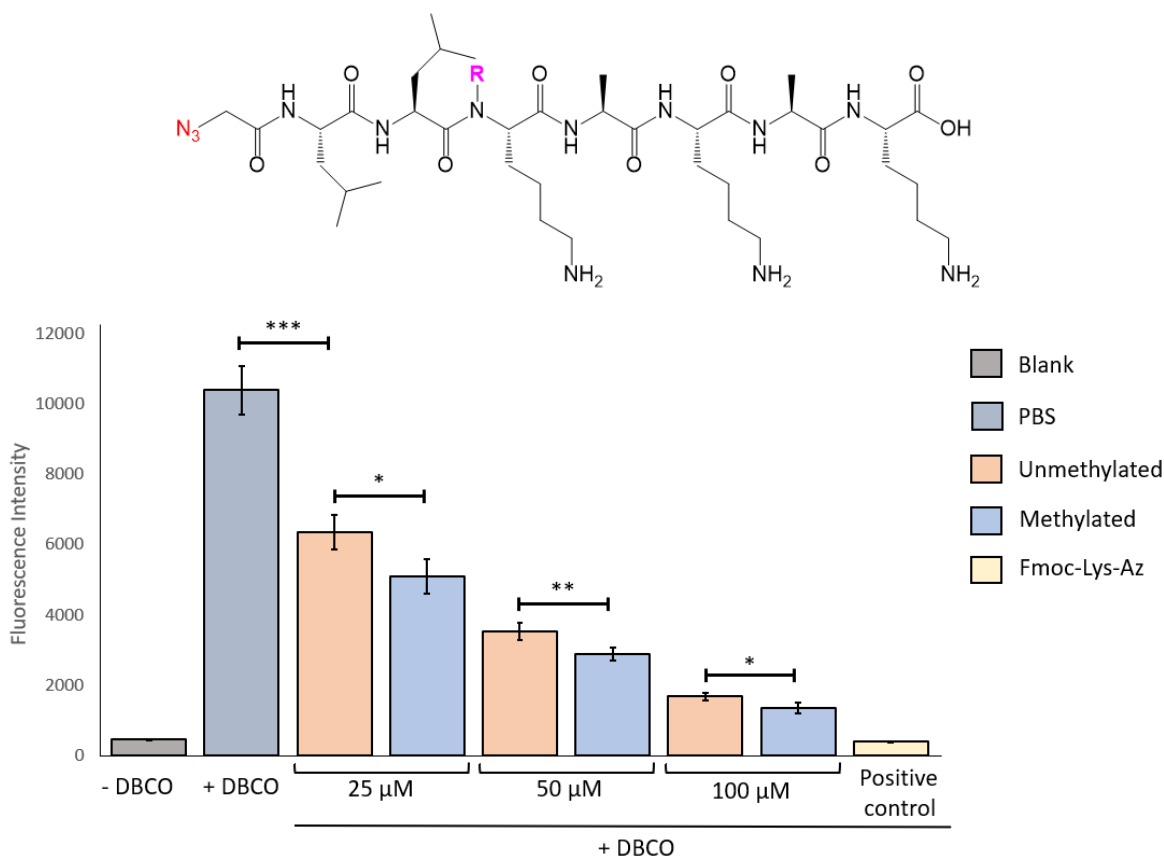
**Figure 3.5** Structure of tetraDBCO (left) and flow cytometry data showing labeling of the PG (right). Vehicle indicates cells that were not incubated with tetraDBCO but were treated with FI-az. The tetraDBCO column are cells incubated with tetraDBCO and then FI-az. The high fluorescence shows DBCO labeling. Data are presented as mean  $\pm$  SD ( $n=3$ ).  $P$ -values were determined by a two-tailed  $t$ -test (\*\*\*\* denotes a  $p$ -value  $< 0.0001$ ).

### 3.4.2 Methylation Proof-of-Concept

Next, test peptides were synthesized to use as proof-of-concept with the assay design. The peptide sequence tested was AzLLKAKAK, which was chosen for its hypothesized ease of purification and characterization (**Figure 3.6, top**). SPPS was used to synthesize the peptide, and the methylation was performed during SPPS at the lysine closest to the N-terminus using a protocol from Kessler and coworkers.<sup>25</sup> A control peptide with no methyl groups was also synthesized using SPPS. 2-Azidoacetic acid was then coupled to the N-terminus of both peptides to install the azide handle. These peptides were made on rink amide resin, producing an amidated C-terminus to eliminate the negative charge, which could hinder permeability. Both peptides were purified by HPLC and characterized by MALDI.

These two peptides were then tested using the assay described above. First, *Msm* cells were incubated with tetraDBCO for metabolic labeling. Then, 25  $\mu$ M of either the methylated or unmethylated peptide was incubated with the cells followed by incubation with FI-az. The positive control was Fmoc-Lys-Az, which was shown by Liu et al. to be highly permeable into *Msm* using the same assay.<sup>24</sup> According to the results generated from flow cytometry, both the methylated

and unmethylated peptides caused a decrease in fluorescence levels compared to the cells that were only incubated with PBS, indicating slight permeability of both peptides (**Figure 3.6, bottom**). Additionally, the methylated peptide had lower fluorescence than the unmethylated peptide, indicating a slightly higher permeability. The experiment was repeated at 50  $\mu\text{M}$  and 100  $\mu\text{M}$ , and the same trend was observed in a concentration-dependent manner (**Figure 3.6, bottom**). Therefore, the results from this assay indicate that the methylated peptide is slightly more permeable than its unmethylated counterpart. Thus, this experiment serves as proof-of-concept for using this assay to study the permeability of methylated peptides.



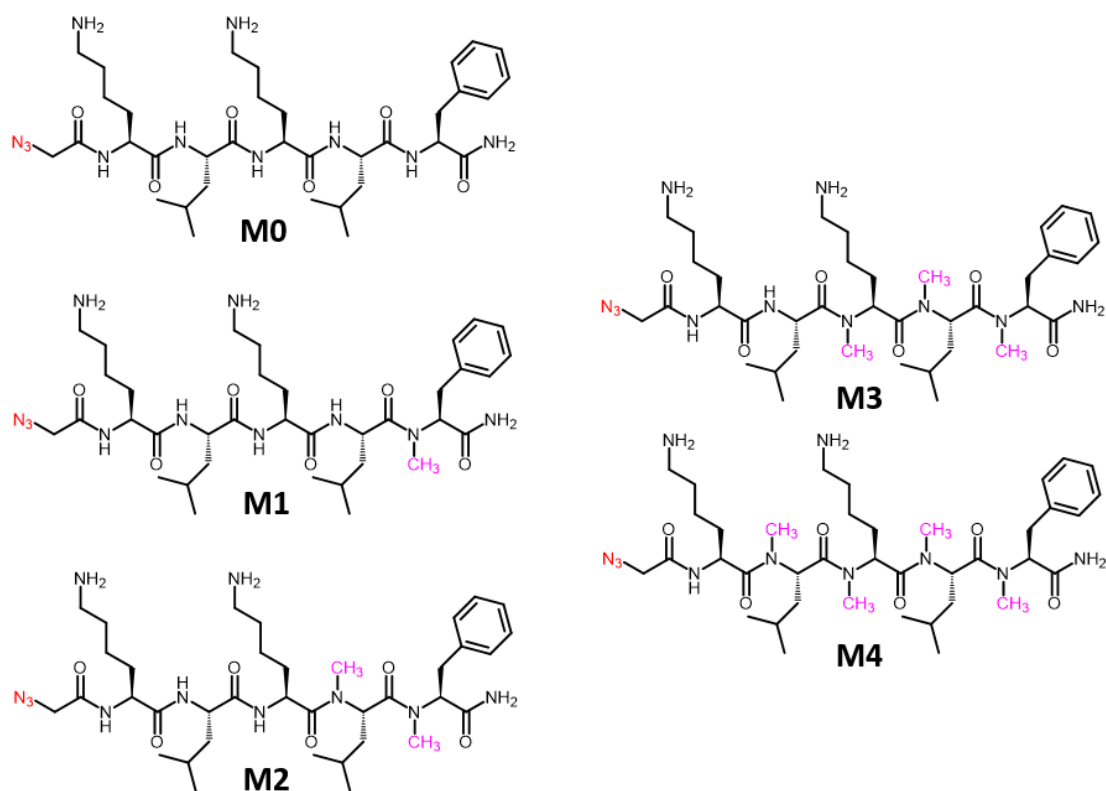
**Figure 3.6** (Top) Structure of the test peptides where  $R=H$  for the unmethylated peptide and  $R=CH_3$  for the methylated peptide. (Bottom) Flow cytometry data comparing unmethylated vs methylated AzLLKAKAK permeability. The - DBCO column depicts cells that were not metabolically labeled. The + DBCO column depicts cells labeled with tetraDBCO and then incubated with FI-Az. The unmethylated and methylated peptides were tested at 25, 50, and 100  $\mu\text{M}$ . The positive control was 100  $\mu\text{M}$  of a known permeable small molecule (Fmoc-Lys-azide) to benchmark the assay. Data are presented as mean  $\pm$  SD ( $n=3$ ).  $P$ -values were determined by a two-tailed  $t$ -test (\* denotes a  $p$ -value  $< 0.1$ , \*\* denotes a  $p$ -value  $< 0.05$ , \*\*\* denotes a  $p$ -value  $< 0.01$ , \*\*\*\* denotes a  $p$ -value  $< 0.001$ , n.s. denotes no significance).

### 3.4.3 Permeability of a Methylated Peptide Library

In order to study methylation in a more systematic way, a library of peptides must be synthesized. The first library sequence chosen was AzLSLSL. Leucine was included because it is prevalent in naturally occurring peptides that are permeable into mammalian cells.<sup>19</sup> The hydrophobicity of leucine was balanced by the addition of serine residues to make the peptides soluble and purifiable. Serine was chosen over lysine as the hydrophilic residue to reduce the number of charges on the peptide. However, the yield on the HPLC purified peptide was very low, causing two problems to surface. The first problem is the characterization of the peptide stock. Secondly, the yield needs to be improved in order to generate a peptide stock that is concentrated enough for subsequent assays.

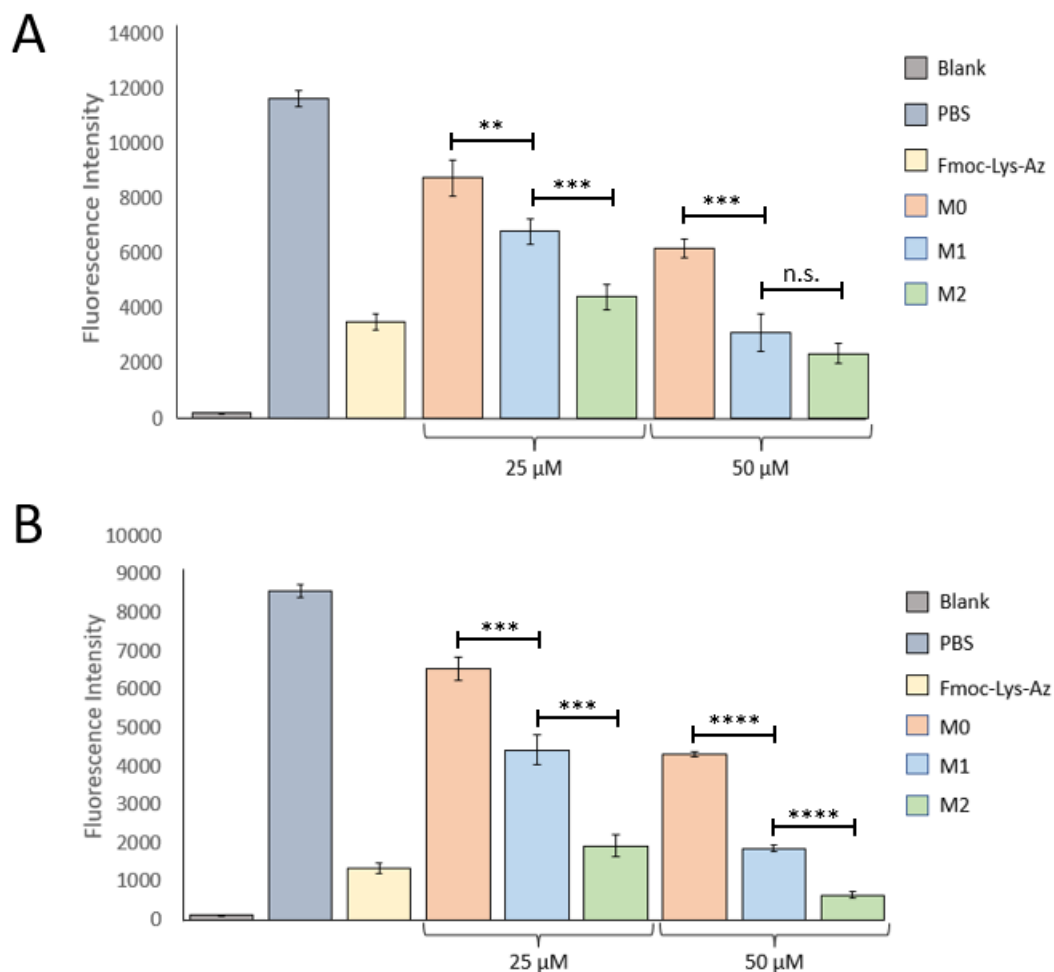
To solve the characterization problem, a single phenylalanine was added to each peptide, allowing for the determination of the concentration based on the absorbance of its aromatic side chain using the Beer-Lambert law. The new library consisted of the same peptide sequence except with the N-terminal leucine substituted with a phenylalanine (AzFSLSL). To solve the yield problem, the methylation step was allowed to react for longer, and more efficient coupling reagents were used. However, this new sequence had poor solubility in water, making the characterization *via* phenylalanine absorbance challenging. Furthermore, poor water solubility could potentially become problematic at the assay level as well since the assays are performed in PBS.

To increase the solubility of the peptide sequence, the serine residues were replaced with more hydrophilic lysine residues. Additionally, since the methylation procedure was still generating low yield, pre-methylated amino acids were used for the synthesis. The peptide sequence AzKLKLF was synthesized in a library from no backbone nitrogen atoms being methylated to four methyl groups, moving from C-terminus to N-terminus (**M0-M4, Figure 3.7**). This peptide sequence proved to be sufficiently water soluble while still being able to be retained on the HPLC column long enough for desirable separation.



**Figure 3.7** Structures of peptides M0-M4, which include different numbers of methyl groups on the backbone nitrogen atoms. Each contain an N-terminal azido-acetic acid moiety.

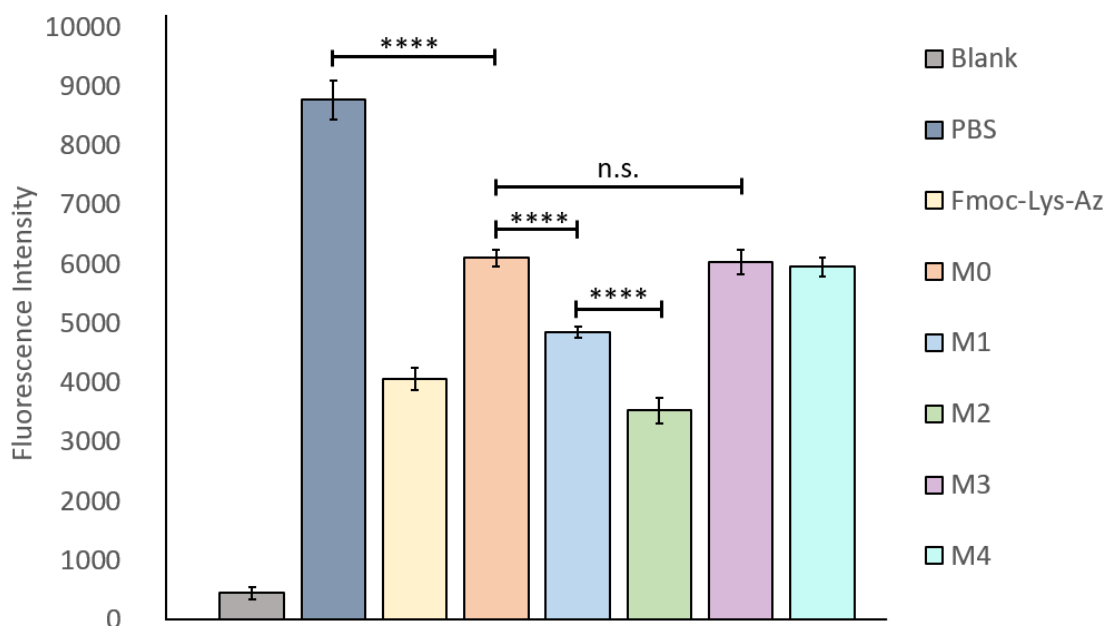
First, **M0-M2** were used to determine the ideal incubation time of the peptides as well as the ideal concentration to conduct the permeability assay described above. Peptides were incubated with the tetraDBCO-labeled *Msm* cells for either one or two hours at either 25 or 50  $\mu\text{M}$ . Cells were then washed, incubated with 50  $\mu\text{M}$  fluorescein-azide, and washed once more before being analyzed *via* flow cytometry. The same positive control (Fmoc-Lys-Az) was used. Assay conditions of a one-hour incubation and 25  $\mu\text{M}$  peptide concentration was chosen due to these conditions producing the best dynamic range. Therefore, the hypothesized continuing linear trend upon addition of more methyl groups should be visible in this dynamic range (**Figure 3.8**).



**Figure 3.8** One-hour (A) or two-hour (B) incubations of peptides M0-M2 at either 25  $\mu$ M or 50  $\mu$ M. PBS was used as a negative control, and Fmoc-Lys-Az was used as the positive control at 25  $\mu$ M. Data are presented as mean  $\pm$  SD ( $n=3$ ). P-values were determined by a two-tailed t-test (\*\* denotes a p-value < 0.05, \*\*\* denotes a p-value < 0.01, \*\*\*\* denotes a p-value < 0.001, n.s. denotes no significance).

The completed **M0-M4** library was tested using these optimized assay conditions. Peptides **M0-M2** follow the hypothesized trend of increasing methylation leading to increased permeability across the mycomembrane (**Figure 3.9**). Unexpectedly, **M3** and **M4** did not continue the downward trend in fluorescence. Instead, **M3** and **M4** exhibited similar permeability as the unmethylated peptide **M0** (**Figure 3.9**). One possible explanation for the decreased permeability of **M3** and **M4** is related to lipophilicity. Since these two peptides are more lipophilic due to the decreased number of hydrogen-bond donors, the peptides are more attracted to the greasy

mycomembrane. As such, these peptides may be interacting too much with the mycomembrane to be able to permeate through to the PG layer.



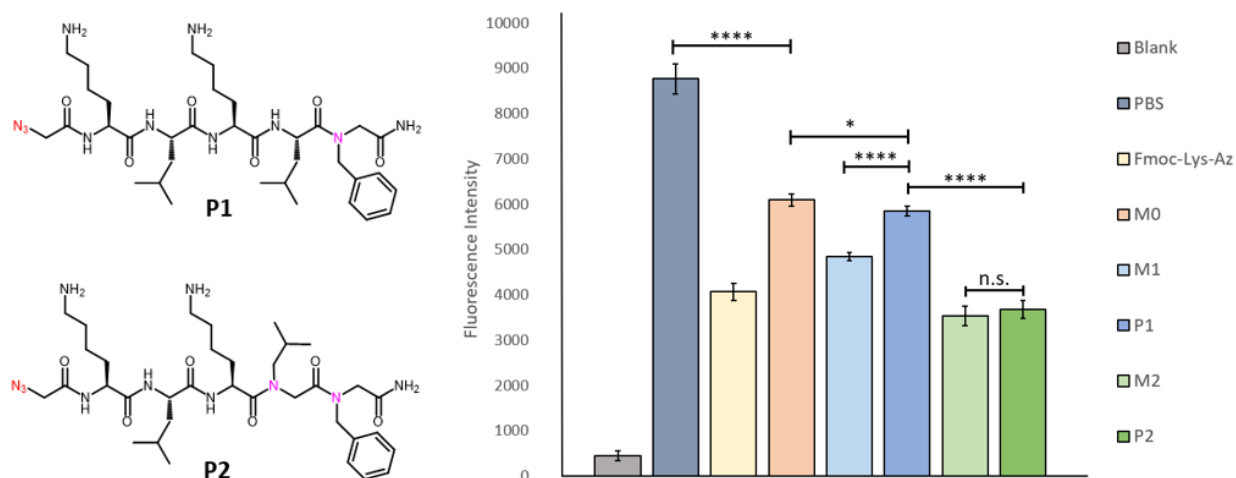
**Figure 3.9** One-hour incubation of methylated peptides (M0-M4) at 25  $\mu$ M. PBS was used as a negative control, and Fmoc-Lys-Az was used as the positive control at 25  $\mu$ M. Data are presented as mean  $\pm$  SD ( $n=4$ ). P-values were determined by a two-tailed t-test (\* denotes a p-value < 0.1, \*\* denotes a p-value < 0.05, \*\*\* denotes a p-value < 0.01, \*\*\*\* denotes a p-value < 0.001, n.s. denotes no significance).

#### 3.4.4 Peptoid-Peptide Hybrid Proof-of-Concept

Another way to test the idea of removing hydrogen-bond donors on peptides is to create peptoid analogs. Peptoids are comprised of amino acid analogs in which the side chain is attached to the backbone nitrogen instead of the  $\alpha$ -carbon. In this way, the backbone nitrogen is acylated without adding any atoms to the peptide. By comparing a peptide to its corresponding peptoid analog, the impact of removing a hydrogen-bond donor can be evaluated. The Lokey group previously studied the effects of peptoid modifications on cyclic hexapeptide permeability into mammalian cells.<sup>26</sup> They had originally identified a mammalian cell permeable *N*-methylated peptide scaffold (1NMe3) that contains three *N*-methylated amino acids. In their peptoid study, they substituted the *N*-methylated amino acids in 1NMe3 with peptoid monomers and compared the permeability to the parent compound. In general, they found that the peptoid monomer

substitutions maintained about the same permeability as the original compound with some performing worse and some performing better.

Given the literature precedence of peptoid substitutions modulating peptide permeability into mammalian cells, we hypothesized that peptoid-peptide hybrid analogs of the AzKLKLF library could also impact permeability into mycobacteria in a similar manner as the methylated peptides. The first peptoid-peptide hybrid included a peptoid monomer at the phenylalanine position (**P1**), and the second one included the same peptoid monomer in addition to a leucine monomer (**P2**) at the neighboring position (**Figure 3.10, left**). The same positive control was used. *Msm* cells were incubated with **P1** and **P2** for one hour at 25  $\mu$ M and compared to the corresponding methylated peptides using the same assay described above. Interestingly, **P1** permeability was more similar to **M0** than **M1** (**Figure 3.10, right**). However, the permeability of **P2** increased significantly and was on par with the permeability observed for **M2** (**Figure 3.10, right**). Thus, the data shows that peptoid substitutions can increase the permeability of peptides, but the trend differs slightly from their methylated counterparts.



**Figure 3.10** (Left) Structures of the two peptoid-peptide hybrids. (Right) One hour incubation of methylated peptides (**M0-M2**) and peptide-peptoid hybrids (**P1-P2**) at 25  $\mu$ M. PBS was used as a negative control, and Fmoc-Lys-Az was used as the positive control at 25  $\mu$ M. Data are presented as mean  $\pm$  SD ( $n=4$ ). *P*-values were determined by a two-tailed *t*-test (\* denotes a *p*-value < 0.1, \*\* denotes a *p*-value < 0.05, \*\*\* denotes a *p*-value < 0.01, \*\*\*\* denotes a *p*-value < 0.001, n.s. denotes no significance).

### 3.5 Conclusions

*N*-methylation has been shown as a useful strategy to make peptides more permeable across mammalian cell membranes. Our lab recently developed an assay to monitor the permeability of compounds into mycobacterial cells, which can be used to assess the effect of hydrogen-bond elimination on the permeability of peptides. Preliminary data with two test peptides, methylated and unmethylated AzLLKAKAK, showed promising results in that the methylated version showed higher permeability than the unmethylated peptide. To address the effect of *N*-methylation in a systematic manner, a library of peptides, AzLSLSL, was designed. However, this sequence was difficult to characterize. Therefore, a phenylalanine residue was introduced for characterization purposes. While the characterization issue was solved, the sequence had poor water solubility. The serine residues were thus replaced with lysine residues to improve the water solubility of the peptides. Additionally, pre-methylated amino acids were used in the peptide synthesis to improve the yield. Upon testing assay conditions, a one-hour incubation at 25  $\mu$ M of the peptides was chosen for the best dynamic range. Furthermore, as the degree of methylation increased from zero to two in the AzKLKLF peptide library (**M0-M2**), the permeability also increased. However, peptides **M3** and **M4** did not continue the trend and instead had similar permeability to the unmethylated peptide, potentially due to their increased lipophilicity. Lastly, two peptoid-peptide hybrids were tested and compared to their methylated counterparts to probe the effect of peptoid substitutions on permeability. While **P1** did not improve the permeability compared to **M0**, the permeability of **P2** greatly increased and was similar to the permeability of **M2**. Thus, both *N*-methylation and peptoid substitutions are promising routes for improving permeability of molecules across the mycomembrane.

### 3.6 Future Outlooks

The next experiment to run would be to determine why **M3** and **M4** are not permeating as expected. One explanation is that the increased lipophilicity of the peptides are causing them to get stuck in the mycomembrane. To test this hypothesis, the mycomembrane can be digested and its contents analyzed using liquid chromatography-mass spectrometry (LC-MS) to determine if the masses of the peptides are present. Another potential explanation would be that the increased methylation causes **M3** and **M4** to have different reactivity. Thus, we can assess the reactivity of each methylated peptide in the absence of a permeability barrier in order to determine that the observed decreased fluorescence is not related to reactivity differences. To do so,

polystyrene-amine beads can be conjugated with DBCO-NHS to display DBCO on the beads for subsequent SPAAC with the peptides using the same conditions as the assay above. After this incubation, the beads would be washed and then incubated with fluorescein-azide. Since there is no barrier to the click chemistry reaction occurring, this assay would allow for the relative determination of reactivity. If the bead assay shows a difference in reactivity, perhaps the additional methyl groups affect the reactivity of the azide moiety with the DBCO.

To expand upon this work, additional libraries of peptides and peptoid-peptide hybrids comprised of different amino acids can be tested to determine whether the results from the current library hold true for various sequences. For instance, libraries of peptides with polar or charged residues can be designed and tested with systematic methylation and/or peptoid substitution. Additionally, the location of the methyl groups or peptoid substitutions for peptides that are not fully methylated/substituted can be altered. For example, a single methyl group or peptoid monomer can exist at any of the five amino acids, allowing for five variations of the singly modified peptides that can be tested and compared. This experiment will determine if the location of the modification has an impact on the permeability. Furthermore, known impermeable peptides can be methylated or substituted with peptoid monomers to test if eliminating a hydrogen-bond donor modulates their permeability.

Another important future direction is to test permeability of the peptides into macrophages. During the majority of TB's infectious cycle, the *Mtb* cells live within macrophages.<sup>27</sup> Thus, peptide drugs must permeate across the macrophage membrane to reach the *Mtb* cells and then permeate across the mycomembrane to be an effective TB treatment. To test this, *Msm* cells can be labeled with tetraDBCO and then be taken up by macrophages. Extracellular bacteria can be killed using antibiotics to only monitor intracellular bacteria. The macrophages can then be incubated with the library of peptides followed by FI-az and analyzed using flow cytometry as described previously.

After gathering sufficient data with *Msm* from these several experiments, promising peptides will be sent to our collaborator Dr. Sloan Siegrist at the University of Massachusetts Amherst, where her lab can test the same peptides in *Mtb*, both extra- and intracellularly. A culmination of the results from all these experiments will allow us to make conclusions about the role that *N*-methylation plays in modulating permeability of peptides across the mycomembrane, which can better inform drug design for the treatment of TB.

In the effort to continue testing the effects of eliminating hydrogen bond donors on permeability, another modification to study is amide-to-ester substitution. Instead of a typical amide peptide bond, one or more amino acids can be conjugated *via* an ester bond. Recently, Honsono et al. tested the ability of cyclic peptides to permeate across mammalian membranes compared to their amide-to-ester and *N*-methylated counterparts.<sup>28</sup> Interestingly, while both modifications improved the permeability of cyclic peptides, the ester peptides (depsipeptides) tended to be more cell-permeable than even the *N*-methylated peptides. The study by Honsono et al. used cyclic peptides, which brings peptide conformation into account since certain peptide bonds expose the hydrogen to the solvent while other conformations may allow for intramolecular bonding. Therefore, the authors found the position of the ester bond to play a role.<sup>28</sup> However, linear peptides may not suffer from the same position dependency, especially if no secondary structures have formed. An extension of this work would be to test the effects of ester substitution on peptide permeability into mycobacteria, using both linear and cyclic peptides. An azide moiety can be installed in these peptides and tested using the same assay presented in this paper to determine the ability of these peptides to permeate into the mycobacteria.

### 3.7 Materials and Methods

**Materials.** All canonical amino acids were purchased from ChemImpex. *N*-Me amino acids were purchased from either ChemImpex, Ambeed, or Aapptec. All other peptide-related reagents were purchased from ChemImpex or TCI Chemicals. HPLC solvents were purchased from ChemImpex or Millipore Sigma.

**Solid phase peptide synthesis.** Standard Fmoc-based solid phase peptide synthesis (SPPS) procedures were performed. In short, each amino acid was coupled by dissolving 3 eq of the amino acid in DMF with 3 eq oxyma and 3 eq DIC, adding to the resin, and shaking for 2 hours. Washing was performed by alternating DCM and MeOH. Fmoc deprotection was performed by shaking the resin in 20% piperidine in DMF for 30 min followed by the same washing procedure. For amino acids coupling using the microwave synthesizer, 5 eq of each reagent was used. Peptides (except for tetraDBCO) were cleaved from resin using 95% TFA, 2.5% TIPS, and 2.5% H<sub>2</sub>O with a final volume of 10 mL. See Appendix A.3 for more details relating to each synthesized peptide.

**N-methylation procedure.** The N-methylation procedure was adopted from Kessler and coworkers.<sup>25</sup> First, the on-resin amino acid was Fmoc-deprotected using 20% piperidine in DMF for 30 min. Resin was washed with DCM and MeOH two-three times each. NBS-protection was performed by dissolving 4 eq 2-Nitrobenzenesulfonyl chloride (*o*-NBS-Cl) and 10 eq *sym*-collidine in DMF. This solution was added to the resin and shook at room temperature for 15 min. The resin was then washed 1x with DMF, and the protection procedure was repeated with 10 min shaking. The resin was then washed with DCM, MeOH, and DMF 5x. The procedure was later changed to 30 min shaking for both protection steps to bring the reaction to completion. Next, to perform the methylation, 3 eq of DBU was dissolved in DMF and added to the resin. The resin shook vigorously for 3 min. 10 eq of DMS was then added to the resin (without draining DBU) and shook vigorously for 2 min. The resin was then washed 1x with DMF, and the protection procedure was repeated and washed with DCM, MeOH, and DMF 5x. The procedure was later changed to 15 min shaking with DBU and 30 min shaking with DMS to bring the reaction to completion. A test cleave was performed to ensure proper methylation. To do so, a few resin beads were transferred to an Eppendorf tube and 1 mL cleaving solution (95% TFA, 2.5% TIPS, 2.5% H<sub>2</sub>O) was added. After shaking for 2 hours, the TFA was blown off with air. 1 mL of cold ether was added to crash out the peptide. The tube was centrifuged at 14000 rpm for 3 min to pellet the resin and peptide, and the supernatant was discarded. MeOH was added to dissolve the peptide, and its mass was analyzed using either ESI and/or MADLI. If the unmethylated mass was present, the methylation procedure was performed 1-2 more times. If only the methylated mass was present, the *o*-NBS deprotection was performed. 10 eq of 2-mercaptoethanol (BME) and 5 eq of DBU were dissolved in DMF. This was added to the resin and shook for 5 min. The resin was then washed 1x with DMF, and the deprotection procedure was repeated and washed with DCM, MeOH, and DMF 5x. The procedure was later changed to a 1-hour deprotection followed by a 30 min deprotection. Another test cleave was performed using the same method to ensure complete deprotection. If the mass with *o*-NBS was still present, the deprotection procedure was performed another 1-2x. The resin was transferred to a microwave synthesizer to couple any amino acid following a methylated amino acid. Any peptides using pre-methylated amino acids were synthesized on the microwave synthesizer using 5 eq of each amino acid.

**Peptoid synthesis procedure.** In short, synthesis began on 100 mg of rink amide resin (loading capacity of 0.48 mmol/g). The resin was deprotected by shaking with 20% piperidine in DMF for 30 minutes. The resin was then washed with DMF 3x. A 0.6 M bromoacetic acid solution was made in DMF, and 1 mL was added to the resin. A solution of 50% DIC in DMF was also made,

and 200  $\mu\text{L}$  were added to the resin. This mixture shook for 20 minutes and was then washed with DMF 3x. A 1.5 M solution of the desired amine was made in DMF, and 1 mL was added to the resin to shake for one hour. The resin was then washed with DMF. If another peptoid monomer needed to be added, the same procedure was repeated. If an amino acid was the next residue, 5 eq of the amino acid, 5 eq oxyma, and 5 eq DIC were dissolved in DMF, and the solution shook with the resin overnight. The resin was then washed with alternating DCM and MeOH, ending with DCM 2x. Then, normal SPPS was used to finish the rest of the synthesis of the peptoid-peptide hybrids.

**Peptide/peptoid purification and characterization.** Peptides were purified using a Waters 1525 reverse-phase high performance liquid chromatograph (RT-HPLC) with 2489 UV/Visible Detector on a Phenomenex Luna 10  $\mu\text{m}$  C8(2) 100  $\text{\AA}$  (250 x 21.2 mm) column. The solvents ( $\text{H}_2\text{O}$  + 0.1% TFA and ACN + 0.1% TFA) were run through the system in a gradient of 5-100% ACN at 1.5 mL/min rate of change. Collected fractions were run on the rotary evaporator to concentrate the peptide before being placed in a Labconco Freezone 4.5 L (-84oC) lyophilizer. The resulting peptide was then run on the same RT-HPLC but with a smaller column (Phenomenex Luna 5  $\mu\text{m}$  C8(2)) to check for purity. The solvents were the same but with 0.01% TFA. The mass of the peptides was confirmed using matrix-assisted laser desorption ionization (MALDI) mass spectrometry. Peptide stocks were made in DMSO, and the concentrations were determined using UV/vis spectroscopy; absorbance of peptides containing DBCO was measured at 309 nm ( $\epsilon = 12,000 \text{ cm}^{-1}\text{M}^{-1}$ ) while peptides containing phenylalanine was measured at 257 nm ( $\epsilon = 195 \text{ cm}^{-1}\text{M}^{-1}$ ).

***Mycobacterium smegmatis* cell culture.** 3 mL overnight cultures were prepared with 7H9 broth (containing 0.5% glycerol, 0.05% tween 80) and 1x ADC from a filtered 10x ADC stock. The 10X ADC stock was prepared by dissolving 500 mg bovine serum albumin and 200 mg dextrose in 10 mL of autoclaved  $\text{dH}_2\text{O}$ , filtering, and then dividing into 1 mL aliquots. 30  $\mu\text{L}$  of a 1 mg/mL catalase stock (made in autoclaved  $\text{dH}_2\text{O}$ ) were added to the 1 mL aliquots to create the 10X ADC. The catalase was only added on the days that the overnight cultures were being prepared. A *Msm* ( $\text{mc}^2$  155) glycerol stock aliquot (30% glycerol + cells from stationary phase growth) was thawed from the -80  $^\circ\text{C}$  and added to the media in a 1:1000 dilution.

**Permeability assay.** 3 mL overnight cultures were prepared as indicated above. 24 hours later, the DBCO-tetrapeptide was added to the culture in a final concentration of 25  $\mu\text{M}$ . The cultures

were incubated overnight at 37 °C. The following morning, the culture tubes were centrifuged at 4,000 rpm for 2 minutes to pellet the cells. The supernatant was discarded, and the cells were resuspended in 3 mL PBS-T (PBS + 0.5% Tween 80) to wash. Cells were centrifuged again at 4,000 rpm for 2 minutes. The washing was repeated once more, and the cells were resuspended in 3 mL PBS-T. Test peptides were added to a 96-well, clear, round-bottomed plate in a volume that ensured the desired concentration in a final assay volume of 100  $\mu$ L. The same volume of cells was added to each well, so PBS was used to make up the volume of any well that did not reach 100  $\mu$ L between the volume of test peptide and the volume of cells. The plate was then incubated for 1-2 hours at 37 °C. The plate was centrifuged at 4,000 rpm for 2 minutes, and then washed two times with PBS-T and resuspended. Then, fluorescein-azide was added to new wells for a final concentration of 50  $\mu$ M in 100  $\mu$ L. The volume was made up to 100  $\mu$ L with the cells and mixed. The plate was incubated at 37 °C for 1 hour. As before, the plate was washed twice, but this time, the cells were resuspended in 4% formaldehyde after the final wash. The cells incubated for 10 minutes before being diluted 1:10 and analyzed on Attune™ NxT Acoustic Focusing Cytometer.

### 3.8 References

1. Pai, M., Behr, M. A., Dowdy, D., et al. "Tuberculosis," *Nature Reviews Disease Primers*, V. 2, No. 1, 2016, p. 16076.
2. Trajman, A., Felker, I., Alves, L. C., et al. "The COVID-19 and TB syndemic: the way forward," *The International Journal of Tuberculosis and Lung Disease*, V. 26, No. 8, 2022, pp. 710–9.
3. Marrakchi, H., Lanéelle, M.-A., and Daffé, M. "Mycolic Acids: Structures, Biosynthesis, and Beyond," *Chemistry & Biology*, V. 21, No. 1, 2014, pp. 67–85.
4. Batt, S. M., Minnikin, D. E., and Besra, G. S. "The thick waxy coat of mycobacteria, a protective layer against antibiotics and the host's immune system," *Biochemical Journal*, V. 477, No. 10, 2020, pp. 1983–2006.
5. Brown, L., Wolf, J. M., Prados-Rosales, R., et al. "Through the wall: extracellular vesicles in Gram-positive bacteria, mycobacteria and fungi," *Nature Reviews Microbiology*, V. 13, No. 10, 2015, pp. 620–30.
6. Gygli, S. M., Borrell, S., Trauner, A., et al. "Antimicrobial resistance in *Mycobacterium tuberculosis*: mechanistic and evolutionary perspectives," *FEMS Microbiology Reviews*, V. 41, No. 3, 2017, pp. 354–73.
7. Dookie, N., Rambaran, S., Padayatchi, N., et al. "Evolution of drug resistance in *Mycobacterium tuberculosis*: a review on the molecular determinants of resistance and implications for personalized care," *Journal of Antimicrobial Chemotherapy*, V. 73, No. 5, 2018, pp. 1138–51.
8. Bloemberg, G. V., Keller, P. M., Stucki, D., et al. "Acquired Resistance to Bedaquiline and Delamanid in Therapy for Tuberculosis," *New England Journal of Medicine*, V. 373, No. 20, 2015, pp. 1986–8.
9. "Frontiers | *Mycobacterium tuberculosis* Cells Surviving in the Continued Presence of Bactericidal Concentrations of Rifampicin in vitro Develop Negatively Charged Thickened Capsular Outer Layer That Restricts Permeability to the Antibiotic." Available at: <https://www.frontiersin.org/articles/10.3389/fmicb.2020.554795/full>. Accessed March 27, 2023.
10. Lipinski, C. A., Lombardo, F., Dominy, B. W., et al. "Experimental and computational approaches to estimate solubility and permeability in drug discovery and development settings1PII of original article: S0169-409X(96)00423-1. The article was originally published in *Advanced Drug Delivery Reviews* 23 (1997) 3–25.1," *Advanced Drug Delivery Reviews*, V. 46, No. 1, 2001, pp. 3–26.

11. Benet, L. Z., Hosey, C. M., Ursu, O., et al. "BDDCS, the Rule of 5 and drugability," *Advanced Drug Delivery Reviews*, V. 101, 2016, pp. 89–98.
12. Muttenthaler, M., King, G. F., Adams, D. J., et al. "Trends in peptide drug discovery," *Nature Reviews Drug Discovery*, V. 20, No. 4, 2021, pp. 309–25.
13. Dougherty, P. G., Sahni, A., and Pei, D. "Understanding Cell Penetration of Cyclic Peptides," *Chem. Rev.*, 2019, p. 47.
14. Lau, J. L., and Dunn, M. K. "Therapeutic peptides: Historical perspectives, current development trends, and future directions," *Bioorganic & Medicinal Chemistry*, V. 26, No. 10, 2018, pp. 2700–7.
15. Lee, L. L. H., Buckton, L. K., and McAlpine, S. R. "Converting polar cyclic peptides into membrane permeable molecules using N-methylation," *Peptide Science*, V. 110, No. 3, 2018, p. e24063.
16. Bockus, A. T., Schwochert, J. A., Pye, C. R., et al. "Going Out on a Limb: Delineating The Effects of  $\beta$ -Branching, N -Methylation, and Side Chain Size on the Passive Permeability, Solubility, and Flexibility of Sanguinamide A Analogues," *Journal of Medicinal Chemistry*, V. 58, No. 18, 2015, pp. 7409–18.
17. Liu, T., Zhu, N., Zhong, C., et al. "Effect of N-methylated and fatty acid conjugation on analogs of antimicrobial peptide Anoplin," *European Journal of Pharmaceutical Sciences*, V. 152, 2020, p. 105453.
18. Tapia, C., Nessel, T. A., and Zito, P. M. "Cyclosporine." StatPearls. Treasure Island (FL), StatPearls Publishing, 2022.
19. Kelly, C. N., Townsend, C. E., Jain, A. N., et al. "Geometrically Diverse Lariat Peptide Scaffolds Reveal an Untapped Chemical Space of High Membrane Permeability," *Journal of the American Chemical Society*, V. 143, No. 2, 2021, pp. 705–14.
20. Wu, Y., Huang, R., Jin, J.-M., et al. "Advances in the Study of Structural Modification and Biological Activities of Anoplin," *Frontiers in Chemistry*, V. 8, 2020, p. 519.
21. Egan, A. J. F., Errington, J., and Vollmer, W. "Regulation of peptidoglycan synthesis and remodelling," *Nature Reviews Microbiology*, V. 18, No. 8, 2020, pp. 446–60.
22. Raghavendra, T., Patil, S., and Mukherjee, R. "Peptidoglycan in Mycobacteria: chemistry, biology and intervention," *Glycoconjugate Journal*, V. 35, No. 5, 2018, pp. 421–32.
23. Pidgeon, S. E., Apostolos, A. J., Nelson, J. M., et al. "L,D-Transpeptidase Specific Probe Reveals Spatial Activity of Peptidoglycan Cross-Linking," *ACS Chemical Biology*, 2019, p. acschembio.9b00427.

24. "A Metabolic-Tag-Based Method for Assessing the Permeation of Small Molecules Across the Mycomembrane in Live Mycobacteria - Liu - *Angewandte Chemie* - Wiley Online Library." Available at: <https://onlinelibrary.wiley.com/doi/abs/10.1002/ange.202217777>. Accessed March 4, 2023.
25. Chatterjee, J., Laufer, B., and Kessler, H. "Synthesis of N-methylated cyclic peptides," *Nature Protocols*, V. 7, No. 3, 2012, pp. 432–44.
26. Schwochert, J., Turner, R., Thang, M., et al. "Peptide to Peptoid Substitutions Increase Cell Permeability in Cyclic Hexapeptides," *Organic Letters*, V. 17, No. 12, 2015, pp. 2928–31.
27. Huang, L., Nazarova, E. V., and Russell, D. G. "*Mycobacterium tuberculosis*: Bacterial Fitness within the Host Macrophage," *Microbiology Spectrum*, V. 7, No. 2, 2019, p. 7.2.04.
28. Hosono, Y. "Amide-to-ester substitution as a stable alternative to N-methylation for increasing membrane permeability in cyclic peptides," *Nature Communications*, 2023.

## Chapter 4: Development of a Luciferase-based Assay to Assess Permeability into the Cytosol of *E. coli*

### 4.1 Abstract

Bacterial infections are the cause of millions of deaths worldwide, and this number has increased due to the growing trend of antibiotic resistance. Thus, new antibiotics must be developed to combat this global health threat. Part of screening new drugs involves permeability testing to ensure the drugs can reach their target, owing to the need of a robust permeability assay. Current techniques have limitations such as significant modifications to the drug, low signal, high background, and/or several washing steps. Herein, we propose a luciferase-based assay that addresses these limitations for the assessment of permeability into *E. coli* cells. The molecules to test need to be modified with a D-cysteine *via* a disulfide bond, which is a comparatively small modification, especially to peptides. Upon incubation of these molecules and CBT with luciferase-expressing *E. coli* cells, the disulfide bond will break if the molecule reaches the cytosol. The resulting free D-cysteine can combine with CBT to form D-luciferin, which is the substrate for luciferase, and produce light. We show that the signal-to-noise ratio is sufficient, allowing this assay to be used as a robust, high-throughput method for assessing the permeability of molecules into the cytosol of *E. coli* cells.

### 4.2 Introduction

Antibiotic resistance is increasing the threat of bacterial infections worldwide. According to the Centers for Disease Control and Prevention (CDC), antibiotic resistance was the cause of almost 5 million deaths in 2019 alone.<sup>1</sup> While scientists have made progress in combatting resistance, the emergence of COVID-19 in 2020 caused a setback in this fight. In fact, the CDC states that COVID-19 has made the threat of antibiotic resistance worse.<sup>2</sup> Thus, circumventing antibiotic resistance is vital. One of the major barriers for effective drugs is the permeability of these into bacterial cells. In particular, Gram-negative and mycobacteria have outer membranes that hinder antibiotics from entering the cell. Furthermore, while cell-wall targeting antibiotics do exist, the most potent antibiotics tend to have cytosolic targets.<sup>3</sup> Therefore, permeable drugs are arguably the most valuable. Thus, in the process of drug development, the existence of robust permeability assays is of utmost importance.

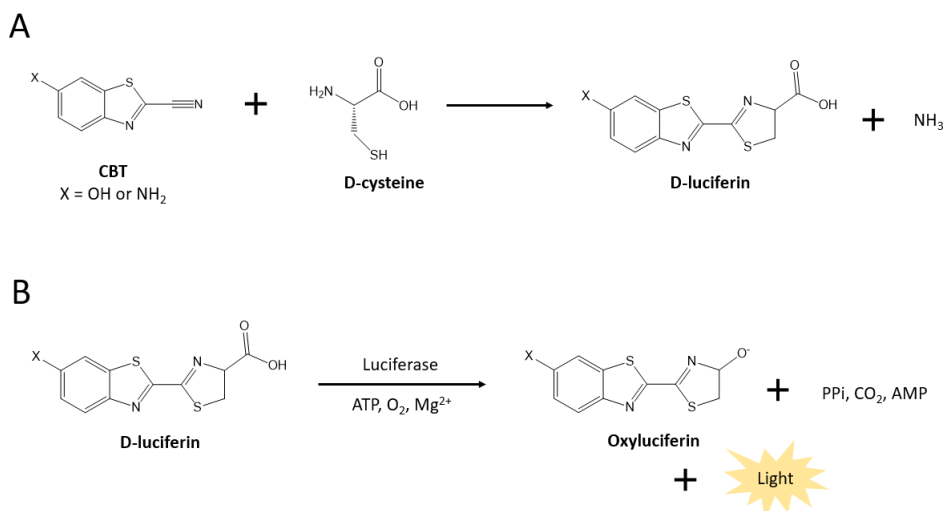
Currently, there are several methods for assessing the permeability of molecules into Gram-negative bacteria. The most popular method is optical imaging by attaching a fluorophore to the peptides and/or small molecules to observe if they entered the cell.<sup>4,5</sup> These assays are typically analyzed *via* flow cytometry or confocal microscopy. However, these methods are limited by the non-specific binding and quenching of the fluorophore molecules.<sup>6</sup> Furthermore, the conjugation of a fluorophore to the molecule of interest is a significant structural change, which could impact its permeability.

Another method to assess permeability was developed by our lab, which involves labeling the peptidoglycan (PG) layer of the bacterial cells with a stem peptide analog.<sup>3</sup> This analog includes an N-terminal click handle for reaction with an azide group on the molecules of interest. A fluorophore with an azide group follows the molecule incubation to react with any free click handles that did not react with the molecule of interest. This assay design gives an inverse relationship between permeability and fluorescence.<sup>3</sup> While this design works well for Gram-positive bacteria and even mycobacteria, the thin PG layer of Gram-negative bacteria is a limitation of this technique. Since the PG is not as thick, a smaller amount of label will become metabolically incorporated, leading to a low labeling level. Furthermore, this assay only assesses permeability to the PG layer.

Our lab also developed another method called Bacterial ChloroAlkane Penetration Assay (BaCAPA) for the measurement of small molecule accumulation in the intracellular space of *E. coli*. This method improved upon the PG-labeling assay since it can assess permeability to the cytosol rather than just to the PG. BaCAPA utilizes the expression of the enzyme Halo-tag in the cytoplasmic space, and its substrate is a chloroalkane chain. Thus, molecules of interest were modified with a chloroalkane chain and incubated with the bacteria. If they reach the cytosol, HaloTag will covalently anchor the molecule in its active site. Subsequently, the bacteria were incubated with rhodamine110-chloroalkane to bind any empty HaloTag active sites. This experimental setup also results in an inverse relationship between permeability and fluorescence, which can be measured using flow cytometry. While BaCAPA was used to successfully determine the permeability of molecules into *E. coli*, the approach possesses some inherent limitations.<sup>7</sup> For instance, the method requires a two-step process in which the target molecule is incubated first, followed by the fluorescent tag, both of which involve washing steps. Furthermore, the molecules of interest are modified with a chloroalkane chain, which could potentially alter the permeability of the molecule itself.

Given the limitations of current permeability assays, a novel, robust assay is needed. The goal of this project is to develop and optimize an assay for the assessment of molecule permeation into Gram-negative bacteria such as *E. coli*. To do so, we hypothesize that a luciferase-based enzymatic assay could fill in the gaps inherent to other methods. Luciferase is an enzyme that converts D-luciferin to oxyluciferin, producing light in the process (**Scheme 4.1B**). The substrate, D-luciferin, can be broken apart into two molecules – cyano benzothiazole (CBT) and D-cysteine – that can covalently react in a click reaction with each other to re-form D-luciferin (**Scheme 4.1A**).

Others have taken advantage of this system to detect D-cysteine in the body. For instance, Roychaudhuri et al. used this system to detect endogenous D-cysteine in the brain by taking cell/sample tissues and incubating them with the reagents indicated in **Scheme 4.1B**.<sup>8</sup> In addition, others have used this system to determine permeability of peptides into mammalian cells.<sup>9</sup> To do this, Karatas et al. developed a Split Luciferin Peptide (SLP) assay in which the D-cysteine is “caged” by the peptide of interest *via* a disulfide bond. After a CBT pre-incubation, the peptide is incubated with mammalian cells overexpressing luciferase in the cytosol. Upon permeating into the cytosol, the disulfide bond between the D-cysteine and the peptide will break apart due to the reducing environment of the cytosol. With D-cysteine now free, it can react with CBT to form D-luciferin, which is the substrate of luciferase. However, if the compound does not reach the cytosol, D-cysteine will not get released, resulting in low light production. Using this procedure, they were able to monitor the cellular uptake of peptides both *in vitro* and *in vivo*.<sup>9</sup>



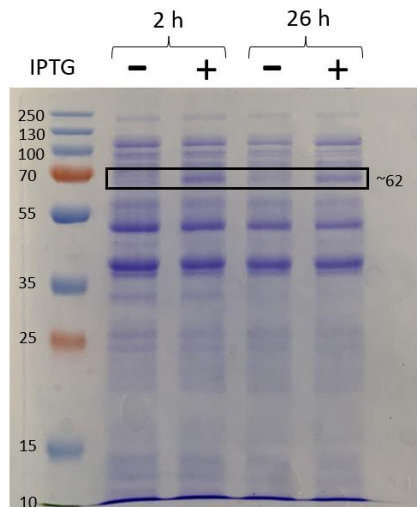
**Scheme 4.1** A) Combination of CBT and D-cysteine results in the formation of D-luciferin. B) In the presence of ATP, O<sub>2</sub>, Mg<sup>2+</sup>, and luciferase, D-luciferin is converted to oxyluciferin, which produces light in the process.

Given the precedence of using this luciferase-based assay to monitor permeability into mammalian cells, we envision using a similar assay to monitor permeability across the more complex Gram-negative cell wall. One advantage of this system is the one-step approach in which all molecules needed for the results are incubated in one step, reducing the time required for the assay and eliminating the need for washing. These two factors in addition to using a microplate reader for analysis allow for a high-throughput assay. Additionally, while this system still requires the modification of the target molecule, the addition of the D-cysteine is a smaller modification than the long chloroalkane chain needed for BaCAPA, especially for a peptide. Another advantage of the luciferase system is the measurement of luminescence. Some bacteria species exhibit some intrinsic fluorescence, which could potentially contribute to high background in assays using fluorescence as a readout method.<sup>10</sup> Since the readout of luciferase is luminescence and most bacteria do not naturally luminesce, the bacterial cells themselves are less likely to inherently interfere with the readout. Therefore, we hypothesize that by expressing luciferase in *E. coli* cells and incubating them with CBT and a molecule of interest caged by D-cysteine, the assay should output light that correlates with permeability of the peptide into Gram-negative bacteria.

### **4.3 Results and Discussion**

#### **4.3.1 Luciferase Expression**

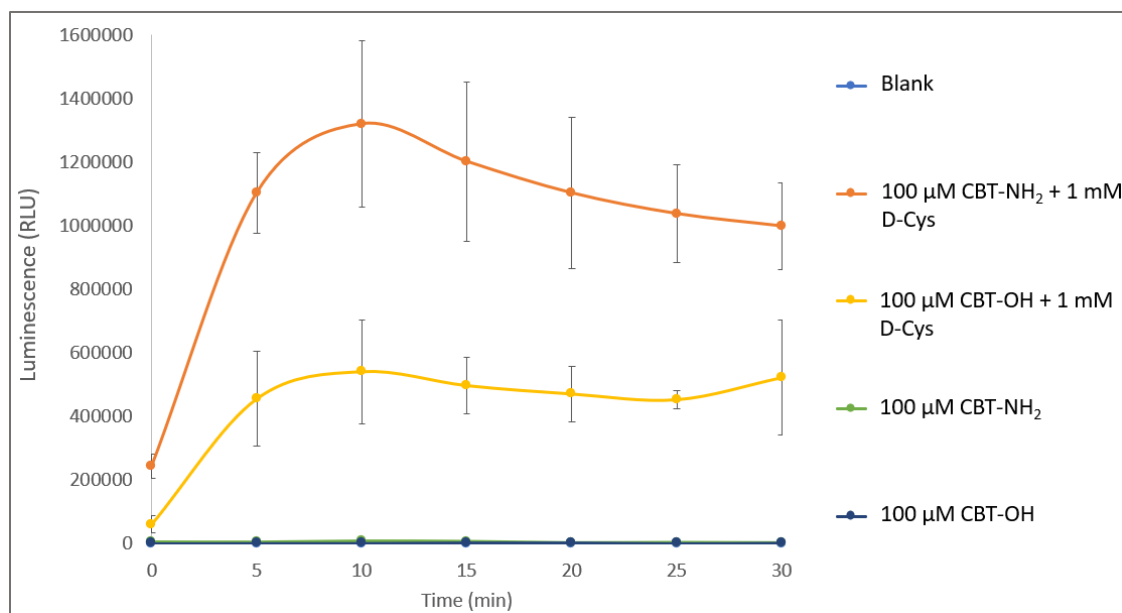
Before running any assays, the expression of luciferase first needed to be assessed. Two conditions were tested for the expression of luciferase: 2-hour induction and 26-hour induction. Cells were grown overnight and then diluted (1:10) the next morning. When the cells reached an OD600 between 0.6-0.8, IPTG was added to induce protein expression. After two hours, minus and plus IPTG samples were collected. Cells were then allowed to grow for a total of 26 hours, and minus and plus IPTG samples were collected again. Protein expression was visualized using sodium dodecyl sulfate polyacrylamide gel electrophoresis (SDS-PAGE). The presence of luciferase was identified using a standard protein ladder. At around 62 kDa, which is the molecular weight of luciferase, both samples with IPTG showed increased protein expression compared to the samples without IPTG (**Figure 4.1**). However, when comparing the two time points with IPTG, there is no clear difference (**Figure 4.1**). Thus, the two-hour induction time was chosen for future assays.



**Figure 4.1** SDS-PAGE results of luciferase protein expression after two hours or 26 hours. The ladder is Thermo Scientific™ PageRuler™ Plus Prestained Protein Ladder, 10 to 250 kDa. The weight of firefly luciferase is about 62 kDa.

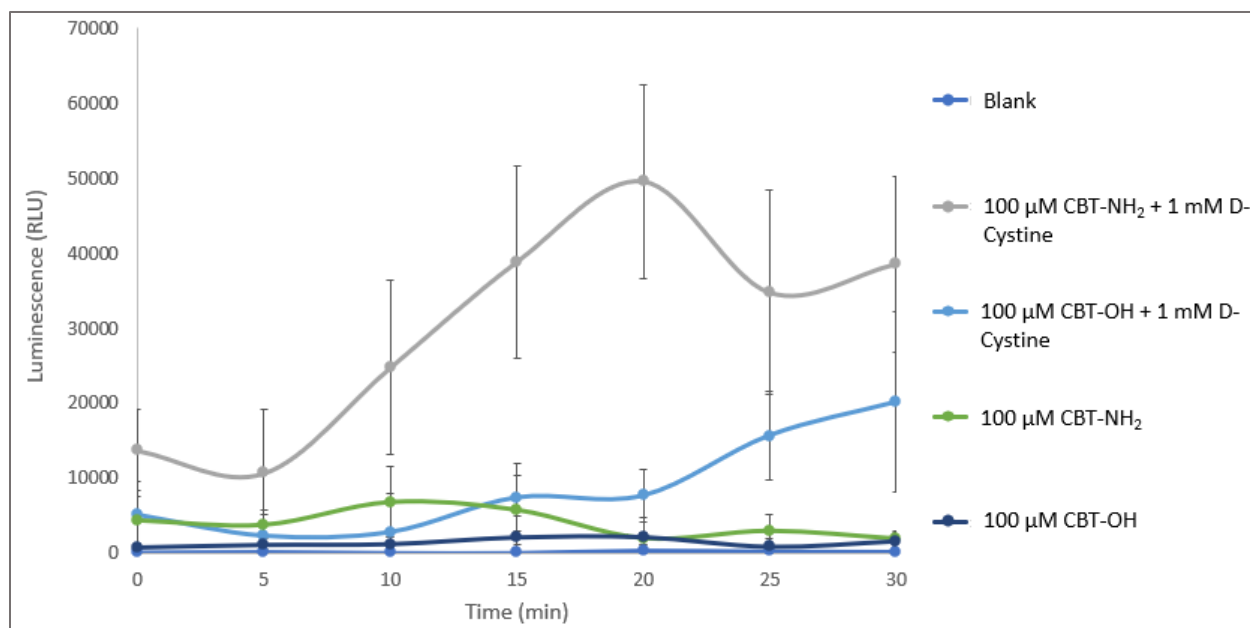
#### 4.3.2 Cyano Hydroxy Benzothiazole versus Cyano Amino Benzothioazole

A cyano benzothiazole substrate needed to be decided upon: CBT-NH<sub>2</sub> or CBT-OH (**Scheme 4.1A**). We incubated luciferase-expressing *E. coli* cells with the CBT variants for one hour, washed the cells, and then incubated with D-cysteine for 30 minutes. Stepwise addition was performed to prevent CBT and D-cysteine from forming D-luciferin outside the cell before permeating in. Controls consisted of incubation of the CBT variants alone to determine background levels of endogenous D-cysteine. Bioluminescence was analyzed using a microplate reader. As seen in **Figure 4.2**, cells treated with CBT containing the amino group (CBT-NH<sub>2</sub>) produced more light than the cells treated with CBT containing the hydroxy group (CBT-OH). The background light production of both CBTs was low compared to the signal with D-Cys. However, CBT-NH<sub>2</sub> produced a better signal-to-noise ratio than CBT-OH.



**Figure 4.2** Time course of CBT variant incubation followed by incubation of D-cysteine. Blank, 100 μM CBT-NH<sub>2</sub>, and 100 μM CBT-OH all overlap at background levels. Data are presented as mean +/- SD (n=4).

Next, D-cystine was tested instead of D-cysteine. This molecule consists of two D-cysteine molecules conjugated *via* a disulfide bond and thus better mimics the types of molecules the assay is designed to test. If D-cystine can enter the cell, the disulfide bond will be reduced by the internal reducing environment from the cells (i.e., thioredoxin and glutathione<sup>11</sup>) and release free D-cysteine for subsequent reaction with CBT. However, since D-cystine cannot react with CBT outside the cell, the two substrates were co-incubated, eliminating the washing step associated with pre-incubation of CBT. As seen previously with D-cysteine, cells incubated with CBT-NH<sub>2</sub> produced a significantly larger luminescence signal than CBT-OH (**Figure 4.3**). Therefore, CBT-NH<sub>2</sub> was chosen as a substrate for future assays. Furthermore, this assay shows that the D-cystine was sufficiently reduced to D-cysteine for light formation, providing some foundation for conjugating D-cysteine onto a molecule *via* a disulfide bond for permeability studies.



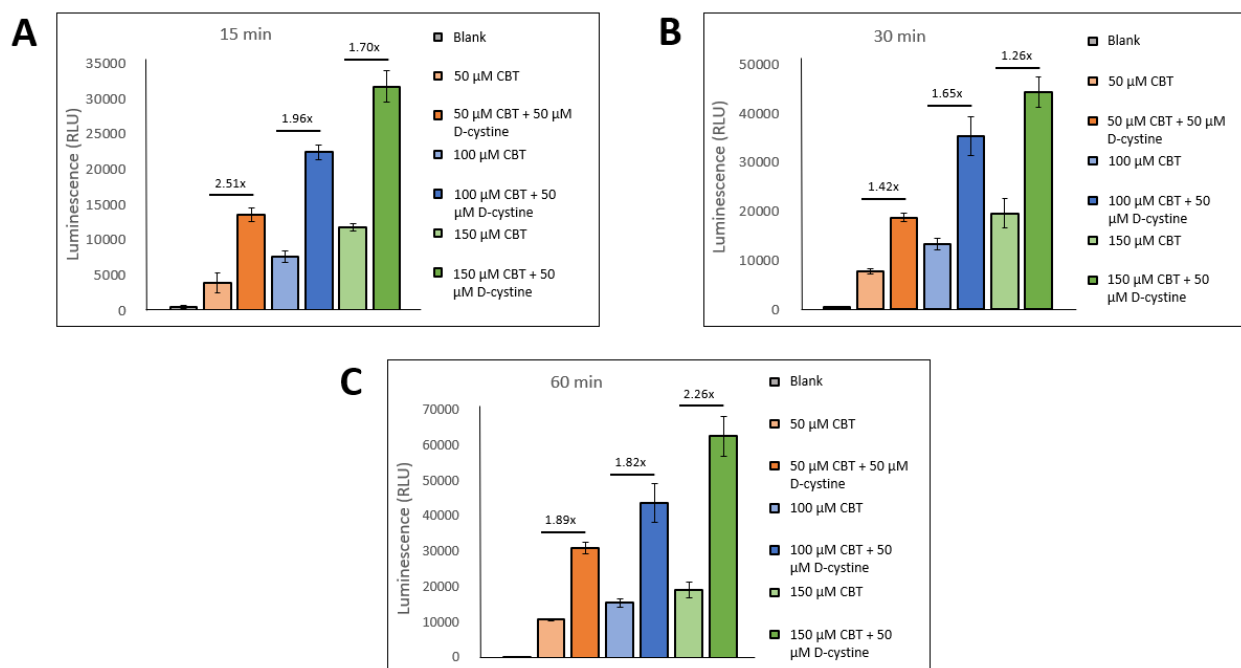
**Figure 4.3** Time course of CBT variant incubation followed by incubation of D-cystine. Data are presented as mean  $\pm$  SD ( $n=4$ ).

Since D-cystine is comprised of two D-cysteine molecules, incubation of cells with D-cystine was hypothesized to produce twice as much light upon reduction compared to D-cysteine. Interestingly, D-cystine incubation produced significantly more light than D-cysteine (**Figure 4.2**, **Figure 4.3**). However, Korshunov et al. found that *E. coli* contains D-cystine importers.<sup>12</sup> When D-cystine is detected, the bacteria import D-cystine inside the cell, reduce it, and then begin pumping D-cysteine out of the cell.<sup>12</sup> In fact, the import of D-cystine was found to induce activation of the exporter AlaE to pump the resulting D-cysteine out.<sup>12</sup> Therefore, the decreased luminescence signal of D-cystine compared to D-cysteine may result from the activation of the D-cysteine efflux mechanisms.

#### 4.3.3 CBT Concentration Scan

The next step was to determine the optimal concentration of CBT-NH<sub>2</sub>. Two hours after IPTG induction, the cells were washed and either co-incubated with varying concentrations of CBT-NH<sub>2</sub> and 50 μM D-cystine or incubated with CBT-NH<sub>2</sub> alone. Light production was then monitored over time using a microplate reader. After 15 minutes, the signal to noise ratio was determined at each CBT concentration. 50 μM CBT gave the best signal to noise ratio with a 2.51-fold increase over background compared to 100 μM (1.96-fold) and 150 μM (1.70-fold) (**Figure**

4.4). The signal to noise ratio was also determined at 30 minutes, which showed 100  $\mu\text{M}$  to be the best with a 1.65-fold increase compared to 50  $\mu\text{M}$  (1.42-fold) and 150  $\mu\text{M}$  (1.26-fold) (**Figure 4.4**). At 60 minutes, 150  $\mu\text{M}$  gave the best signal to noise ratio at a 2.26-fold increase compared to 50  $\mu\text{M}$  (1.89-fold) and 100  $\mu\text{M}$  (1.82-fold) (**Figure 4.4**). Since there was no consistency in which concentration gave the best signal to noise ratio over time, any concentration should be sufficient for the assay. The middle concentration, 100  $\mu\text{M}$ , was chosen for future assays in this study.

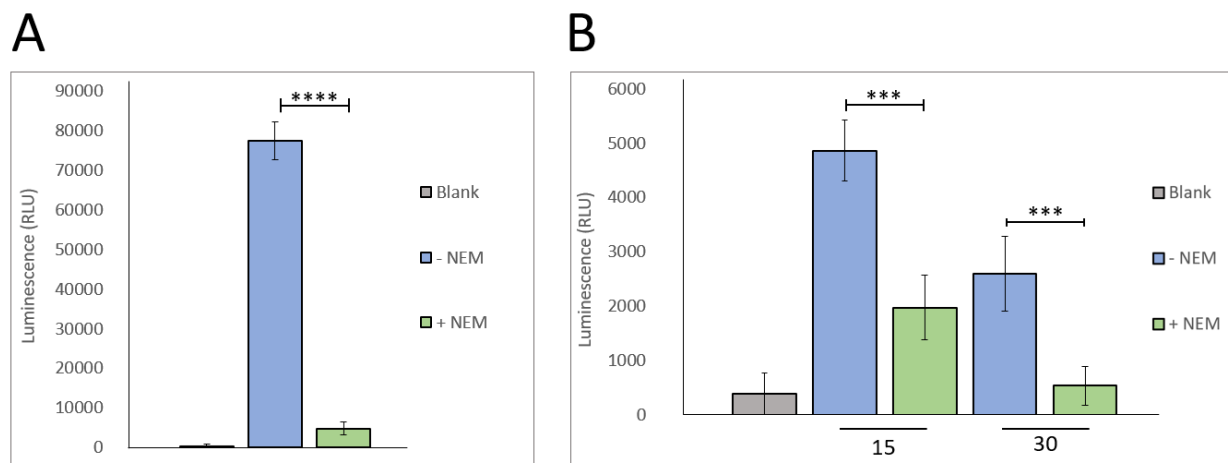


**Figure 4.4** Concentration scan of CBT. Charts show luminescence values at (A) 15 minutes, (B) 30 minutes, or (C) 60 minutes after addition of CBT and D-cystine. The numbers above the bars indicate the fold-difference in signal over background. Data are presented as mean  $\pm$  SD ( $n=4$ ).

#### 4.3.4 Addition of N-Ethylmaleimide

To ensure that light was being emitted from the hypothesized reaction, the addition of N-ethylmaleimide was tested. N-ethylmaleimide (NEM) is a thiol scavenger; therefore, when added to the reaction, this molecule is expected to react with the free D-cysteine, preventing its reaction with CBT and thus reducing the amount of light being produced by the luciferase. When CBT and D-cystine were incubated with the cells, light was produced (**Figure 4.5A**). However, when NEM was added to the reaction, a significant decrease in produced light was observed (**Figure 4.5A**). Therefore, the NEM is likely reacting with the free D-cysteine and preventing its conjugation with

CBT to form D-luciferin, meaning that light produced in the experiments is likely generated from the combination of CBT and free D-cysteine from D-cystine. Additionally, NEM was used to determine if the background signals resulted from endogenous D-cysteine. Incubation of 100  $\mu$ M CBT for 30 minutes was compared with and without the addition of 100  $\mu$ M NEM. As expected, the addition of NEM decreased the signal produced by the cells, indicating that at least a portion of the background signal results from endogenous cysteine (**Figure 4.5B**).

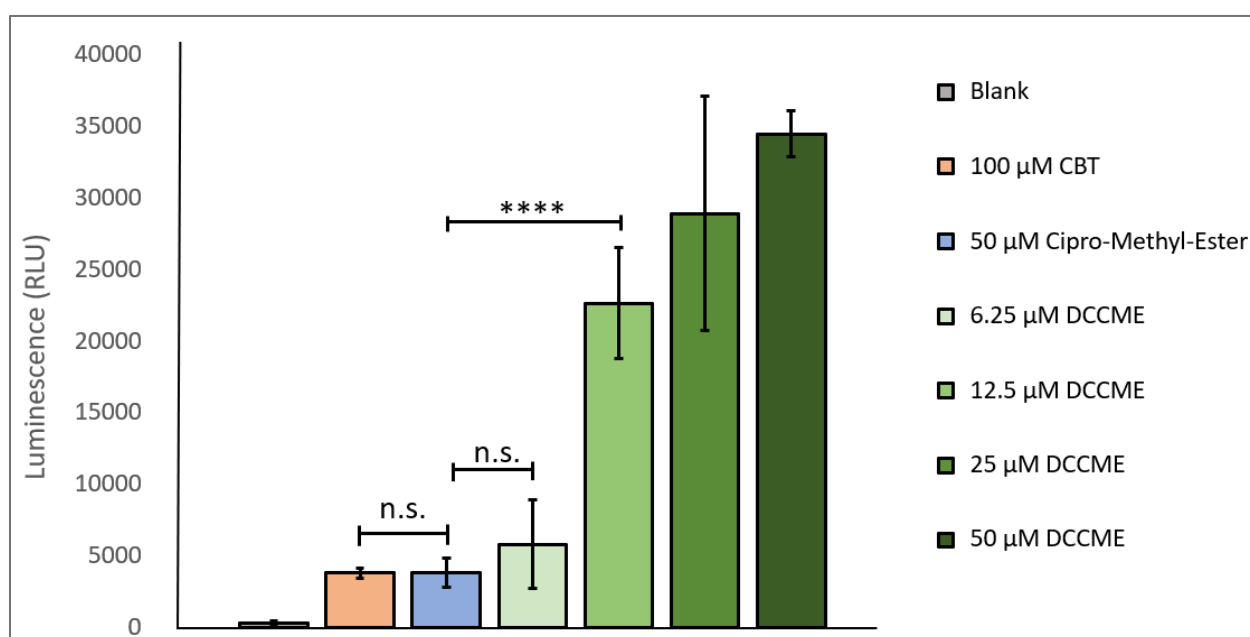


**Figure 4.5** (A) Blank cells were incubated with PBS. 100  $\mu$ M CBT and 50  $\mu$ M D-cystine were added to the – NEM cells immediately before analysis. 100  $\mu$ M CBT, 50  $\mu$ M D-cystine, and 100  $\mu$ M NEM were added to the + NEM cells immediately before analysis via the microplate reader. Values depicted here were at the 15-minute mark after analysis began. (B) Besides the blank, which were just incubated with PBS, cells were incubated with 100  $\mu$ M CBT for thirty minutes before imaging. Cells were washed and then 100  $\mu$ M NEM was added to + NEM immediately before analysis on the plate reader. 0, 15, and 30 refer to the minutes after analysis began that the data was collected. Data are presented as mean  $\pm$  SD ( $n=4$ ). P-values were determined by a two-tailed t-test (\* denotes a p-value < 0.1, \*\* denotes a p-value < 0.05, \*\*\* denotes a p-value < 0.01, \*\*\*\* denotes a p-value < 0.001, n.s. denotes no significance).

#### 4.3.5 D-cystine-cipro-methyl-ester

To test the assay on a molecule other than D-cystine, the antibiotic ciprofloxacin was chosen. Ciprofloxacin binds to DNA topoisomerase and DNA gyrase to inhibit DNA replication.<sup>13</sup> Since its target is intracellular, ciprofloxacin must penetrate through the bacterial cell envelope to reach the cytosol. Additionally, the O-methyl ester modification to the carboxylic acid has been shown to improve the permeability of ciprofloxacin into Gram-positive bacteria, so the same

modification was chosen for this study.<sup>14</sup> D-cystine was coupled onto the secondary amine in cipro-methyl-ester to serve as the reporter tag. Then, the molecule and CBT were co-incubated with the luciferase-expressing *E. coli*. The control of 50  $\mu$ M cipro-methyl-ester without the D-cystine showed background level luminescence as expected (**Figure 4.6**). In general, the luminescence intensity increased as concentration of D-cystine-cipro-methyl-ester increased (DCCME) up to 50  $\mu$ M DCCME (**Figure 4.6**). Additionally, there is a significant difference between the background and the luminescence values of DCCME starting at 12.5  $\mu$ M (**Figure 4.6**). While the DCCME compound has a slight impurity, the data shows promise for the ability of the assay to monitor the permeability of molecules to the cytosol of *E. coli*.



**Figure 4.6** Concentration scan of D-cystine-cipro-methyl-ester (DCCME). Besides the blank, each well was treated with 100  $\mu$ M CBT along with either 50  $\mu$ M cipro-methyl-ester as a control or varying concentrations of DCCME. The values indicate luminescence values 30 minutes after addition of the reagents. Data are presented as mean  $\pm$  SD ( $n=4$ ). *P*-values were determined by a two-tailed *t*-test (\* denotes a *p*-value < 0.1, \*\* denotes a *p*-value < 0.05, \*\*\* denotes a *p*-value < 0.01, \*\*\*\* denotes a *p*-value < 0.001, n.s. denotes no significance).

#### 4.4 Conclusions and Future Outlook

In order to combat antibiotic resistance, robust permeability assays can assist in drug molecule testing. As such, we propose a luciferase-based permeability assay that involves a one-step procedure that outputs light. *E. coli* cells expressed luciferase and were incubated with CBT and a D-cysteine “caged” molecule. Upon permeating to the cytosol, the D-cystine is released and reacts with CBT, forming the substrate for luciferase. Upon binding to the luciferase, light was produced, indicating its permeability into the cytosol. The best CBT variant was determined to be CBT-NH<sub>2</sub> as opposed to CBT-OH due to the better signal-to-noise ratio it produced. Furthermore, the CBT concentration was chosen to be 100 μM; although based on the results, any concentration from 50-150 μM would be sufficient due to good signal-to-noise ratios at any time point. Additionally, the dependence of light on D-cysteine was confirmed by adding a thiol scavenger, NEM, to the incubation. When NEM was added, the signal significantly decreased, indicating the role of D-cysteine in the production of light. However, a limitation of this assay is that the molecule of interest must include a cysteine or some sort of thiol group for disulfide conjugation of D-cysteine to the molecule.

If a molecule does contain an exposed thiol group, this assay can be used to monitor its permeability into the cytosol of *E. coli*. For instance, the effect of *N*-methylation or cyclization on permeability can be assessed using this assay. Peptides with varying degrees of *N*-methylation and/or cycle size can be synthesized, and a cysteine must be included in its sequence. After oxidizing a D-cysteine onto the sulfur atom, the peptides plus CBT can be co-incubated with the luciferase-expressing *E. coli* cells, and the resulting light can inform about the permeability of these peptides. Furthermore, this assay can be used to monitor permeability of a large library of small molecules in a quick, no washing, high throughput screening method.

#### 4.5 Materials and Methods

**Materials.** The FLUC2 pET28a plasmid was obtained from the Ai lab at the University of Virginia. All reagents for bacterial growth and all chemical building blocks for the assay were purchased from ChemImpex or TCI Chemicals.

**Transformation of plasmid into BL21.** First, the FLUC2 pET28a plasmid was transformed into DH5α *E. coli* cells *via* heat shock. In short, 50 μL of competent DH5α *E. coli* cells and 2-5 μL

plasmid were added to an Eppendorf tube and kept in ice. After 30 minutes, a water bath was heated to 42 °C and the tube containing the cells and plasmid was placed in the bath for 30 seconds followed by another 2 minutes on ice. One mL of sterile LB media was added to the tube, mixed, and transferred to a culture tube for 1 hour. Then, 25-200 µL of cells were added to a warmed culture plate containing kanamycin (KAN) and incubated overnight. A colony was then chosen from the plate to inoculate the overnight culture of the DH5α *E. coli* cells. The following day, a ZymoPURE Plasmid Miniprep Kit was used to extract the plasmid from the DH5α *E. coli* cells. A transformation was then performed the same way except with BL21 *E. coli* cells. Glycerol stocks of both BL21 and DH5α *E. coli* cells were made by mixing 1 mL of overnight growth with 1 mL of 60% glycerol in water.

***E. coli* cell culture and protein expression.** 3 mL overnight cultures were prepared by adding 3 mL of sterile LB media to culture tubes, and 3 µL of a 1000X KAN stock was added. A stab of the BL21 glycerol stock was added to the culture tubes and incubated at 37 °C overnight. The next morning, the cells were diluted: 3 mL LB media + 300 µL overnight culture + 3 µL KAN. After 2 hours, the OD<sub>600</sub> was between 0.6-0.8, and isopropyl β-d-1-thiogalactopyranoside (IPTG) was added in a final concentration of 1 mM to induce protein expression. Cells were then incubated for another 2 hours and then washed.

**SDS-PAGE.** Two overnight cultures were started and diluted the next morning as described above. When the diluted cells reached an OD<sub>600</sub> between 0.6-0.8, IPTG was added to one culture to induce protein expression. Both plus and minus IPTG cultures were then incubated at 37 °C for 26 hours. On the same day that these cells were induced, another two overnight cultures were grown. The next day, these cells were diluted, and IPTG was used to induce protein expression of one culture for two hours at 37 °C. 1 mL of media was collected from the plus and minus IPTG samples from both time points. These were centrifuged at 14000 rpm for 3 minutes. The supernatant was discarded, and the cells were resuspended in 400 µL PBS. 40 µL of the cell resuspension was mixed with 10 µL of a 5X SDS-PAGE sample loading buffer. This mixture was then boiled for 5 minutes to denature the proteins. To run the gel, 8 µL of Thermo Scientific™ PageRuler™ Plus Prestained Protein Ladder, 10 to 250 kDa, was added to the first well. The samples were loaded at 20 µL, and then gel was run at 240 V for 30 minutes.

**Luciferase permeability assay.** After the 2-hour IPTG incubation, washing was performed by first pelleting the cells in the centrifuge at 4000 rpm for 2-3 minutes. The supernatant was

discarded, and the cells were resuspended in 3 mL PBS. This was repeated 2 times. The cells were resuspended after the last wash in 3 mL PBS. In a 96-well black, flat-bottomed plate, the molecules of interest were added from their stocks for the final desired concentration in a total volume of 100  $\mu$ L. PBS was added to blank wells, negative control wells, and to any wells that were less than the maximum volume to ensure all wells would contain the same total volume and same number of cells (i.e., if the volume of the molecule in wells A was 10  $\mu$ L, but only 5  $\mu$ L was needed in wells B for the desired concentration, 5  $\mu$ L PBS would be added to B wells). CBT was added to the culture tube containing cells. Then, the same volume of cells was pipetted each well, mixed, and placed in the BioTek Synergy H1 Microplate Reader. The instrument was selected to run the endpoint/kinetic luminescence setting. Luminescence was set to read every 5 minutes for the duration of the run, usually between 30 minute-2 hours. Luminescence Fiber was the optics type. Gain was set to 240, and integration time was set to 0:01:00. Temperature was set to 37 °C.

**D-cystine-cipro-methyl-ester synthesis.** See Appendix A.4.

#### 4.6 References

1. CDC. "National Infection & Death Estimates for AR." Centers for Disease Control and Prevention. Available at: <https://www.cdc.gov/drugresistance/national-estimates.html>. Accessed March 18, 2023.
2. CDC. "COVID-19 & Antibiotic Resistance." Centers for Disease Control and Prevention. Available at: <https://www.cdc.gov/drugresistance/covid19.html>. Accessed March 18, 2023.
3. "A Metabolic-Tag-Based Method for Assessing the Permeation of Small Molecules Across the Mycomembrane in Live Mycobacteria - Liu - *Angewandte Chemie - Wiley Online Library*." Available at: <https://onlinelibrary.wiley.com/doi/abs/10.1002/ange.202217777>. Accessed March 4, 2023.
4. Jones, S. W., Christison, R., Bundell, K., et al. "Characterisation of cell-penetrating peptide-mediated peptide delivery: Cell-penetrating peptide-mediated peptide delivery," *British Journal of Pharmacology*, V. 145, No. 8, 2005, pp. 1093–102.
5. Fischer, R., Waizenegger, T., Köhler, K., et al. "A quantitative validation of fluorophore-labelled cell-permeable peptide conjugates: fluorophore and cargo dependence of import," *Biochimica et Biophysica Acta (BBA) - Biomembranes*, V. 1564, No. 2, 2002, pp. 365–74.
6. Illien, F., Rodriguez, N., Amoura, M., et al. "Quantitative fluorescence spectroscopy and flow cytometry analyses of cell-penetrating peptides internalization pathways: optimization, pitfalls, comparison with mass spectrometry quantification," *Scientific Reports*, V. 6, No. 1, 2016, p. 36938.
7. Ongwae, G. M., Lepori, I., Chordia, M. D., et al. "Measurement of Small Molecule Accumulation into Diderm Bacteria," *ACS Infectious Diseases*, V. 9, No. 1, 2023, pp. 97–110.
8. Roychaudhuri, R., Gadalla, M. M., West, T., et al. "A Novel Stereospecific Bioluminescent Assay for Detection of Endogenous D -Cysteine," *ACS Chemical Neuroscience*, V. 13, No. 23, 2022, pp. 3257–62.
9. Karatas, H., Maric, T., D'Alessandro, P. L., et al. "Real-Time Imaging and Quantification of Peptide Uptake *in Vitro* and *in Vivo*," *ACS Chemical Biology*, 2019, p. acschembio.9b00439.
10. Ammor, M. S. "Recent Advances in the Use of Intrinsic Fluorescence for Bacterial Identification and Characterization," *Journal of Fluorescence*, V. 17, No. 5, 2007, pp. 455–9.
11. Stewart, E. J. "Disulfide bond formation in the Escherichia coli cytoplasm: an invivo role reversal for the thioredoxins," *The EMBO Journal*, V. 17, No. 19, 1998, pp. 5543–50.

12. Korshunov, S., Imlay, K. R. C., and Imlay, J. A. "Cystine import is a valuable but risky process whose hazards *Escherichia coli* minimizes by inducing a cysteine exporter," *Molecular Microbiology*, V. 113, No. 1, 2020, pp. 22–39.
13. "Ciprofloxacin - StatPearls - NCBI Bookshelf." Available at: <https://www.ncbi.nlm.nih.gov/books/NBK535454/>. Accessed March 19, 2023.
14. Dalesandro, B. E., Kelly, J. J., Liu, Z., et al. "Measurement of Accumulation of Antibiotics to *Staphylococcus aureus* in Phagosomes," *Microbiology*, 2023.

## Summary and Future Outlooks

Bacteria are prevalent microorganisms that have the ability to cause diseases to the host that they infect. Three classes of bacteria exist (Gram-negative, Gram-positive, and mycobacteria), each differing in their cell envelope composition. The most common way to treat bacterial infections is with antibiotics. The Golden Age of Antibiotics was a period marked by a rapid increase in the discovery of antibiotics to treat bacterial infections. Unfortunately, these discoveries were followed by a significant increase in resistance to these antibiotics. Even today, antibiotic resistance is prevalent and is the cause of over a million deaths per year worldwide. In order to circumvent the resistance, new antibiotics must be developed. Not only must the drug have an important target, but it must reach its target to be effective, making permeability into the bacteria an important consideration. As such, the need to develop new drugs and monitor their permeability is vital to the fight against antibiotic resistance.

In this thesis, Chapter 3 describes modifications that eliminate a hydrogen-bond donor from molecules to make them more permeable into mycobacteria, which is the class of bacteria responsible for tuberculosis. By eliminating the hydrogen, the molecule forms fewer hydrogen bonds with the solvent, owing to a smaller desolvation penalty when the molecule enters the cell. The main modification studied here to eliminate the hydrogen bond was *N*-methylation. The nitrogen atoms in the backbone of peptides were systematically *N*-methylated and their permeability was tested using a click-chemistry based fluorescent assay. This study showed that increasing the methylation degree of a peptide increases the permeability across the mycomembrane to a certain extent. However, the addition of several methyl groups could potentially make the peptide too lipophilic, causing the peptide to interact too much with the mycomembrane and not permeate across. Another method studied here to eliminate hydrogen-bond donors was peptoid substitutions. Since peptoids are amino acid analogs with the side chain attached to the backbone nitrogen atom, the replacement of amino acids with their peptoid analogs allows for the elimination of a hydrogen-bond donor without the addition of any group to the peptide. Preliminary results with peptoid substitutions showed that this method also has the ability to modulate permeability of the molecules across the mycomembrane.

Moving forward in this project would involve investigating the cause of the highly methylated peptides not permeating across the mycomembrane. Additionally, several libraries of

differing amino acids could be synthesized and methylated and/or peptoid substituted. By doing so, the importance of the location of the methyl group or substitution could be addressed. In addition to changing the sequence of methylated and peptoid substituted peptides, another modification can be addressed. Some researchers have observed that an amide-to-ester bond substitution in the peptide backbone can also lead to increased permeability into mammalian cells. Thus, this modification can also be tested in mycobacteria.

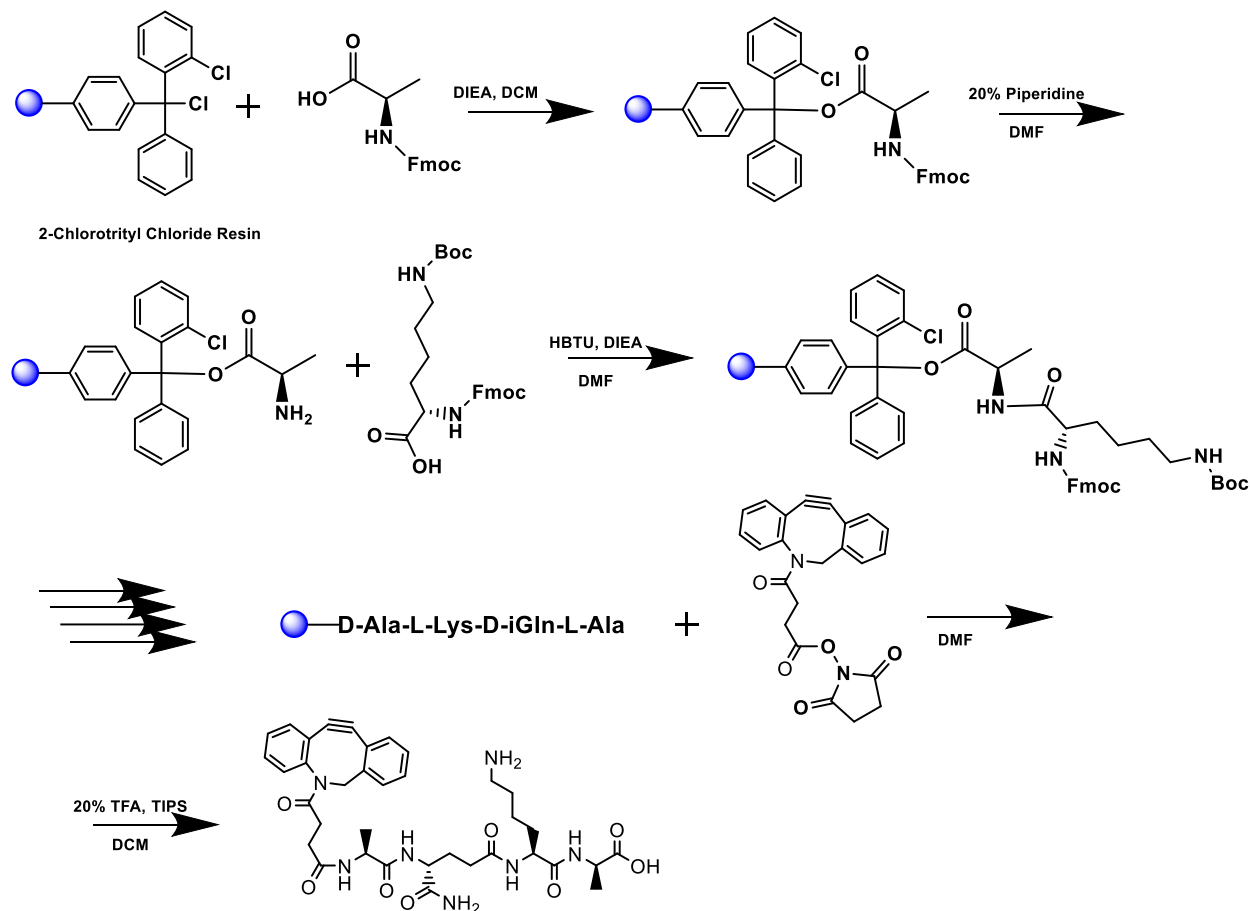
Testing permeability into *E. coli* is also an important step in drug development for treating antibiotic-resistant infections. Current methods for assessing permeability into *E. coli* cells are limited since they tend to have high background, large modifications, low signal, and/or several washing steps. Thus, Chapter 4 discusses a novel assay for monitoring molecule permeability into Gram-negative bacteria to address these limitations. This assay involves the expression of luciferase in *E. coli* cells followed by incubation with CBT and a D-cysteine-containing molecule. If the molecule permeates into the cell, the disulfide bond that held the D-cysteine to the molecule of interest will break, releasing free D-cysteine into solution. The free D-cysteine can then react with CBT to form D-luciferin, which is the substrate for luciferase. To develop this assay, we first monitored protein expression, followed by a CBT variant determination. We then tested the assay on D-cystine and D-cystine-cipro-methyl-ester. Assays with both compounds showed the ability of this assay to be used for monitoring permeability of molecules into the cytosol of *E. coli* in a quick method that does not involve washing.

While this assay produces a good signal-to-noise ratio, a limitation of this assay is that the molecule of interest must include an exposed sulfur atom for conjugation of a D-cysteine onto it. However, the addition of D-cysteine is a relatively small modification, especially for peptides. Nevertheless, this assay can be used as a method to monitor permeability of molecules into *E. coli*. For instance, this assay could be used to test the effects of *N*-methylation on peptide permeability into Gram-negative bacteria. Likewise, other modifications to peptides or small molecules could be evaluated using this assay in a high throughput manner.

## Appendix

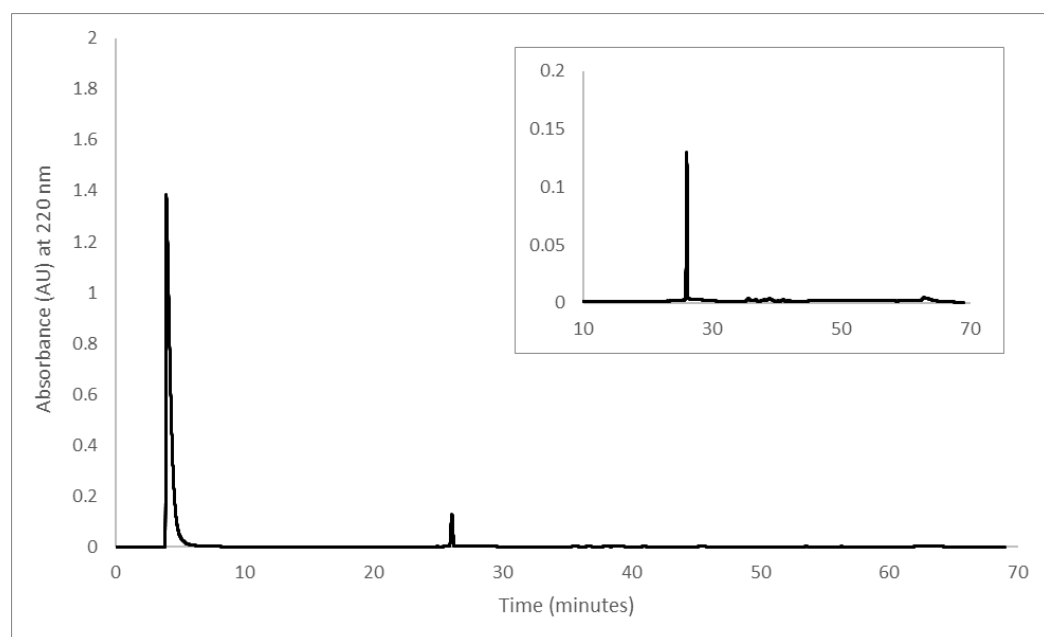
## A.3 Synthesis and Characterization of Compounds in Chapter 3

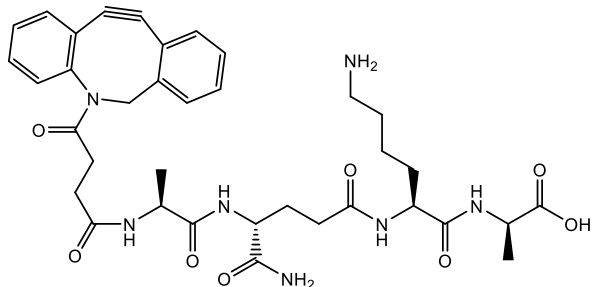
Scheme S1. Synthesis of tetraDBC0



A peptide vessel was placed in an 80 °C oven to dry for one hour. When cooled, 100 mg (0.107 mmol) of room temperature 2-chlorotrityl chloride resin was added to the vessel. 1.1 eq of Fmoc-D-Ala-OH was weighed out and dissolved in 5 mL dry DCM and 4.4 eq dry DIEA. This mixture was added to the resin and shook for one hour. The resin was then washed with alternating DCM and MeOH 2x and then washed twice more with DCM. Fmoc deprotection was performed by adding 20% piperidine in DMF to the resin and shaking for 30 minutes. The resin was then washed using the same washing procedure. Fmoc-L-Lys-OH was then coupled onto the peptide; 3 eq L-Lys, 3 eq HBTU, and 6 eq DIEA were dissolved in DMF and added to the resin to shake for 2 hours. The deprotection and coupling procedures were repeated for the coupling of Fmoc-D-

isoGln-OH and Fmoc-L-Ala-OH. The peptide was then deprotected after the addition of Fmoc-L-Ala-OH, and the resin was washed well and allowed to dry under vacuum. Then, 25 mg of DBCO-NHS was dissolved in DMF and added to the resin to shake overnight. The next morning, the resin was washed and transferred to a conical tube for cleaving. The cleaving was performed by adding 2 mL TFA, 8 mL DCM, and 100  $\mu$ L TIPS to the conical tube and rotating for 2 hours at room temperature. The resin was then filtered, and the resulting solution was concentrated. Cold diethyl ether was added to crash out the peptide, which was subsequently purified using RP-HPLC. The sample was analyzed for purity using a Shimadzu LC 2020 with a Phenomenex Luna 5 $\mu$  C18(2) 100 $\text{\AA}$  (30 x 2.00 mm) column; gradient elution with H<sub>2</sub>O/ACN. The large peak at the beginning of the spectra is from the DMSO that the peptide was dissolved in. An inset shows the rest of the spectra without the first peak. Molecular weight was confirmed using a Shimadzu MALDI-TOF Mass Spectrometer (MALDI-8020).

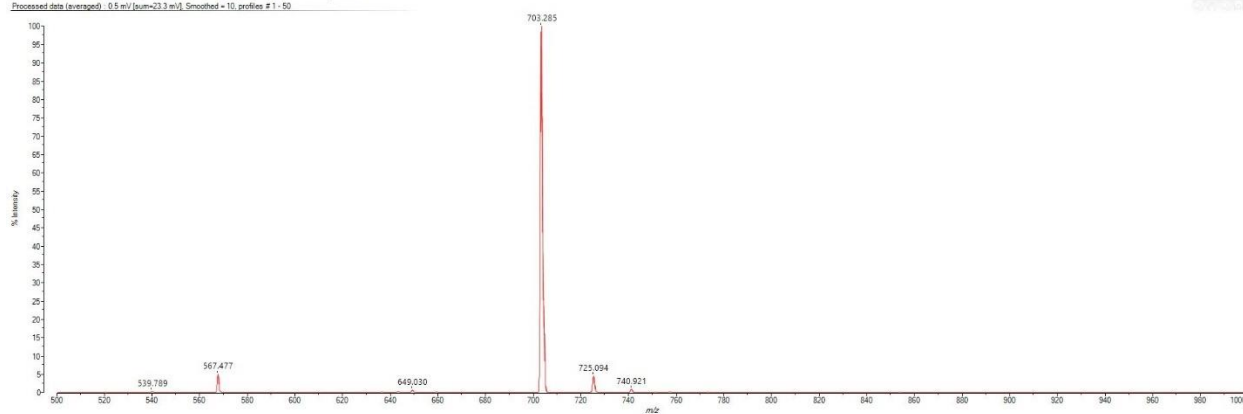


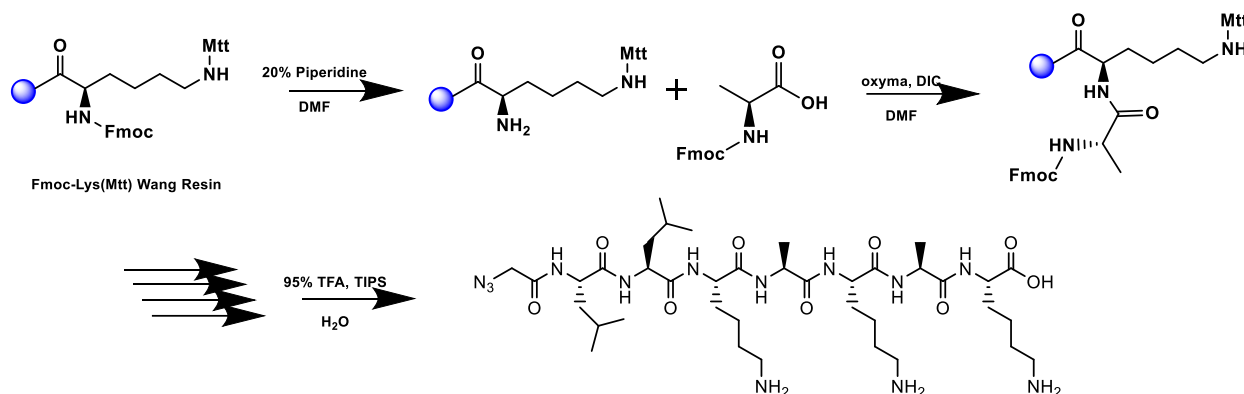


<b>tetraDBCO</b>	
Calculated m/z (M)	703.3330
M + H <sup>+</sup>	704.3408
M + Na <sup>+</sup>	726.3227
M + K <sup>+</sup>	742.2967
Masses found	703.285

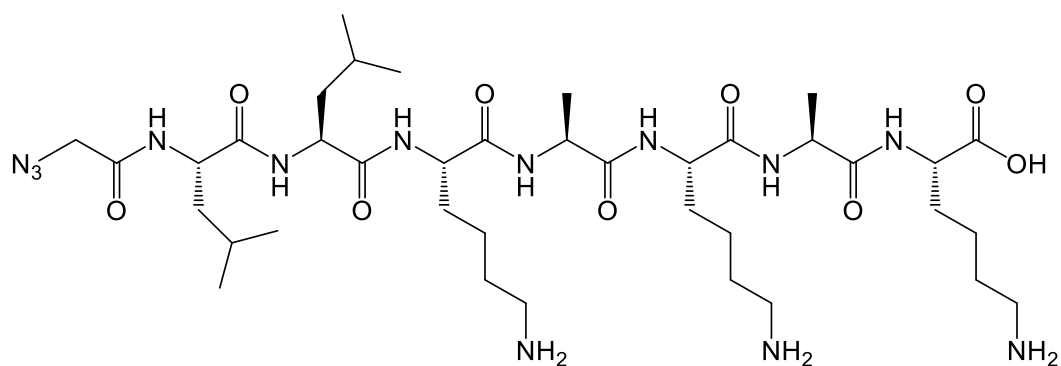
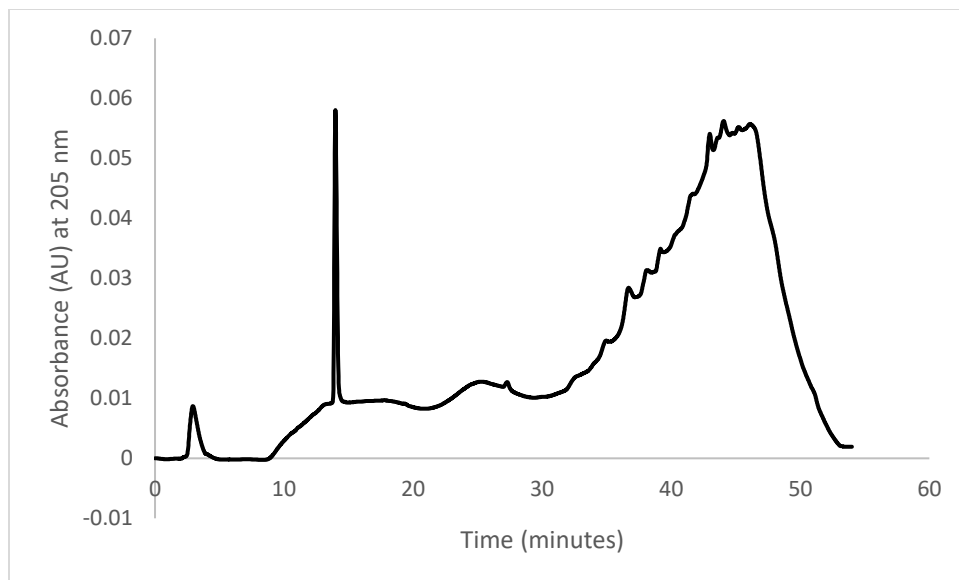
Created By: psy96k; Date: New Acquisition 3.83\_1 (Manual) July 25, 2022 6:30:07 PM Cal: Named Calibration "TOFMSX calibration better 7/1/2022" by klc2\rf on July 1, 2022 11:54:41 AM (Original)  
 Shimadzu MALDI-8020; Tuning: Linear; Power: 10; P. Ext at 556.00 (bin 57); Ion Gate Blanking: 500.00

Processed data (leveraged): 0.5 ml (sum=23.3 ml); Smoothed = 10; profiles # 1 - 50



**Scheme S2.** Synthesis of unmethylated AzLLKAKAK

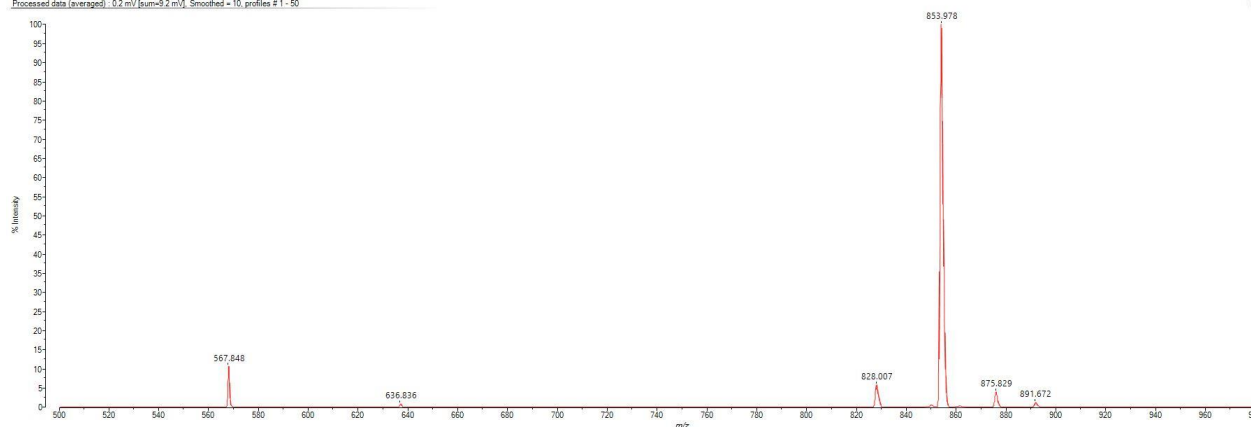
A 25 mL vessel of a CEM Discover Bio Manual Peptide Synthesizer was charged with 250 mg (0.12 mmol) of Fmoc-L-Lys(Mtt)-Wang resin. About 10 mL of 20% piperidine in DMF was added to the resin, and the Synergy software was used to run the deprotection protocol. The piperidine solution was drained and the resin was washed with DMF (4 x 10 mL). Fmoc-L-Ala-OH (5 eq), 1 M oxyma (5eq), and 1 M DIC (eq) in DMF (10 mL) were added to the reaction flask, and the coupling protocol was run. The amino acid solution was drained, and the resin was washed with DMF (2 x 10 mL). The Fmoc deprotection and the amino acid coupling was repeated for the following amino acids to make M0: Fmoc-L-Lys(Boc)-OH, Fmoc-L-Ala-OH, Fmoc-L-Lys(Boc)-OH. The resin was then transferred to a synthetic peptide vessel and the Fmoc was deprotected by shaking with resin with 20% piperidine in DMF for 30 minutes. The resin was washed with alternating DCM and MeOH 2x and then washed twice more with DCM. To couple on Fmoc-L-Leu-OH, the amino acid (3 eq), HBTU (3 eq), and DIEA (6 eq) were dissolved in DMF and added to the resin to shake for 2 hours. The resin was washed with DCM and MeOH as before. The process was performed again to couple another Fmoc-L-Leu-OH. After the addition of the last L-Leu, it was deprotected in the same way as before. To couple on the azide, 1 eq of azidoacetic acid-NHS ester and 6 eq DIEA were dissolved in DMF, and the mixture was added to the resin to shake overnight. The next morning, the resin was transferred to a conical tube for cleaving. The cleaving was performed by adding 95% TFA, 2.5% H<sub>2</sub>O, and 2.5% TIPS to the conical tube and rotating for 2 hours at room temperature. The resin was then filtered, and the resulting solution was concentrated. Cold diethyl ether was added to crash out the peptide, which was subsequently purified using RP-HPLC. The sample was analyzed for purity using a Shimadzu LC 2020 with a Phenomenex Luna 5 $\mu$  C18(2) 100Å (30 x 2.00 mm) column; gradient elution with H<sub>2</sub>O/MeOH. Molecular weight was confirmed using a Shimadzu MALDI-TOF Mass Spectrometer (MALDI-8020).

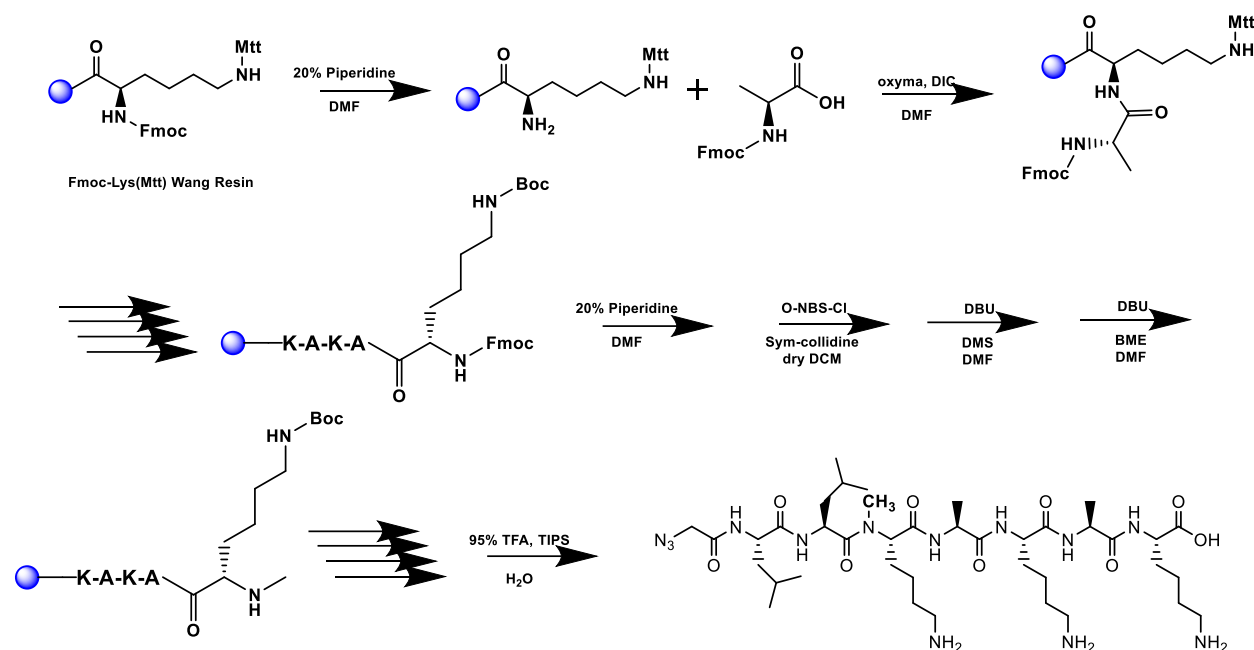


<b>Unmethylated AzLLKAKAK</b>	
Calculated m/z (M)	853.5498
M + H <sup>+</sup>	854.5576
M + Na <sup>+</sup>	876.5395
M + K <sup>+</sup>	892.5135
Masses found	853.978

Created By: psy9hk; Data: New Acquisition 17-11\_Manual; July 27, 2022 6:19:30 PM; Cal: Named Calibration "TOF MIX calibration better 7/1/2022" by klo2vrf on July 1, 2022 11:54:41 AM (Original)  
Shimadzu MALDI-8020; Tuning: Linear; Power: 10; P. Ext: at 558.00 (bin 57); Ion Gate Blanking: 500.00

Processed data (averaged): 0.2 mV [sum=9.2 mV], Smoothed = 10, profiles # 1 - 50



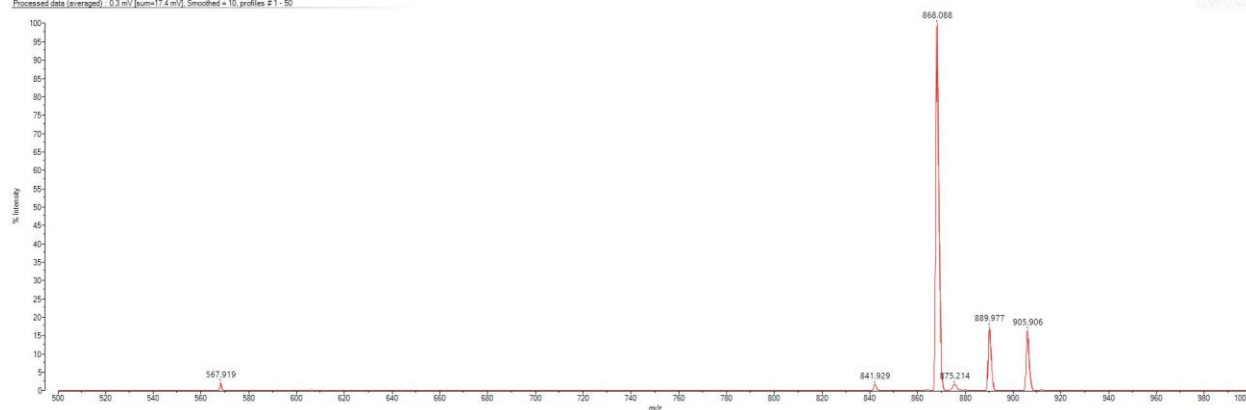
**Scheme S3.** Synthesis of methylated AzLLKAKAK


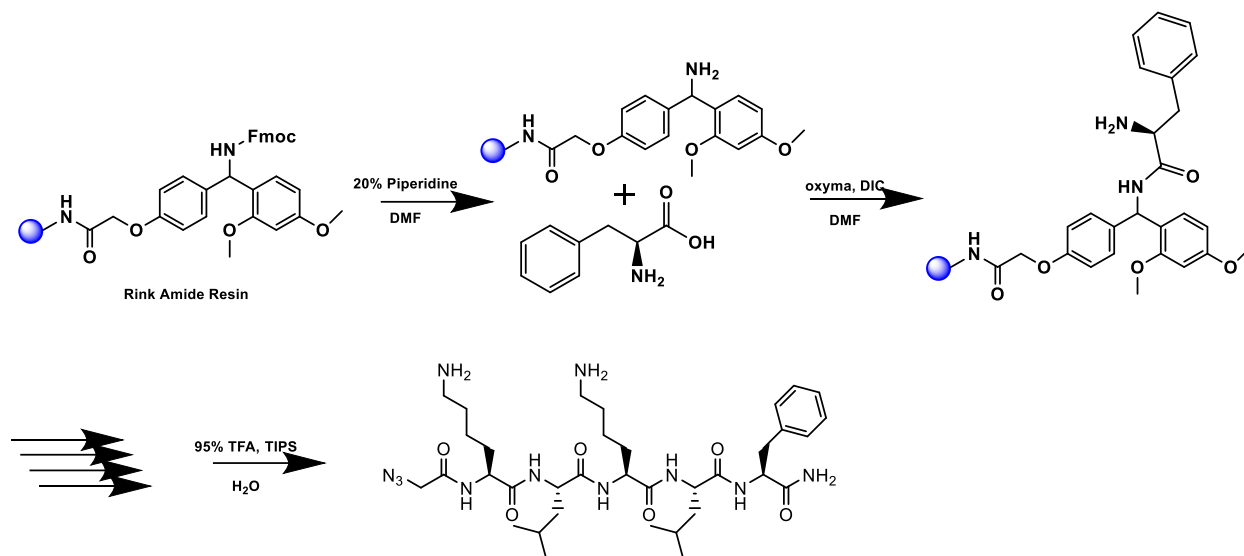
A 25 mL vessel of a CEM Discover Bio Manual Peptide Synthesizer was charged with 250 mg (0.12 mmol) of Fmoc-L-Lys(Mtt)-Wang resin. About 10 mL of 20% piperidine in DMF was added to the resin, and the Synergy software was used to run the deprotection protocol. The piperidine solution was drained and the resin was washed with DMF (4 x 10 mL). Fmoc-L-Ala-OH (5 eq), 1 M oxyma (5eq), and 1 M DIC (eq) in DMF (10 mL) were added to the reaction flask, and the coupling protocol was run. The amino acid solution was drained, and the resin was washed with DMF (2 x 10 mL). The Fmoc deprotection and the amino acid coupling was repeated for the following amino acids to make M0: Fmoc-L-Lys(Boc)-OH, Fmoc-L-Ala-OH, Fmoc-L-Lys(Boc)-OH. The resin was then transferred to a synthetic peptide vessel and the Fmoc was deprotected by shaking with resin with 20% piperidine in DMF for 30 minutes. Room temperature 2-Nitrobenzenesulfonyl chloride (o-NBS-Cl) (4 eq) and *sym*-collidine (10 eq) was dissolved in DMF and added to the resin to shake for 10 minutes. The resin was then washed 1x with DMF, and the procedure with o-NBS-Cl and *sym*-collidine was repeated with 10 min shaking. The resin was then washed 5x with DMF. to perform the methylation, 3 eq of DBU was dissolved in DMF and added to the resin. The resin shook vigorously for 3 min. 10 eq of DMS was then added to the resin (without draining DBU) and shook vigorously for 2 min. The resin was then washed 1x with DMF, and the protection procedure was repeated and washed with DMF 5x. To o-NBS deprotect, 10 eq of 2-mercaptoethanol (BME) and 5 eq of DBU were dissolved in DMF. This mixture was



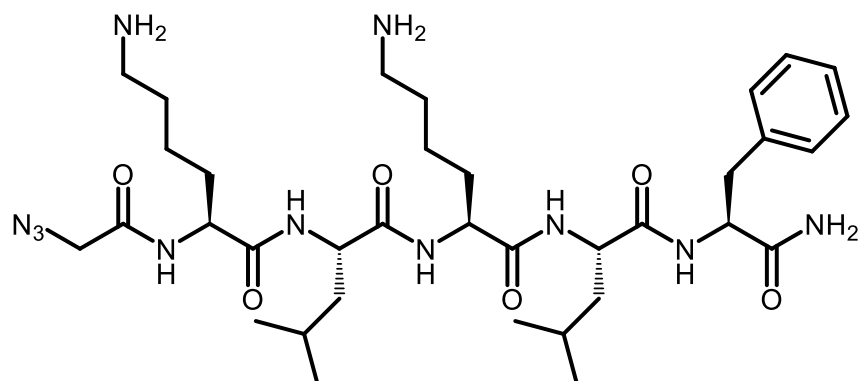
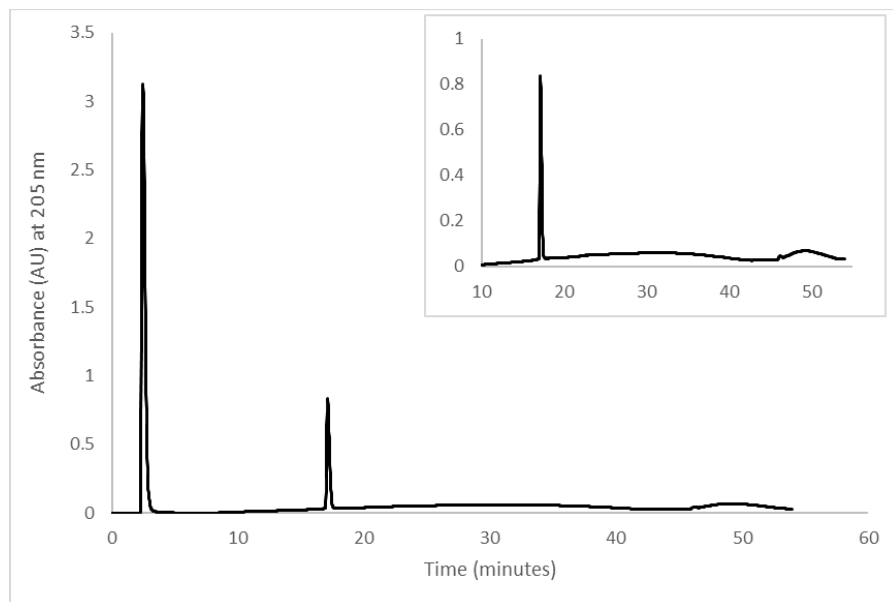
<b>Methylated AzLLKAKAK</b>	
Calculated m/z (M)	867.5654
M + H <sup>+</sup>	868.5732
M + Na <sup>+</sup>	890.5552
M + K <sup>+</sup>	906.5291
Masses found	868.088 889.977 905.906

Created By: psy98k, Data: New Acquisition 20.J1\_(Manual), July 28, 2022 4:54:32 PM Cal/Named Calibration "TOFMSX calibration better 7/1/2022" by kko2vt on July 1, 2022 11:54:41 AM (Original)  
Shimadzu MALDI-8020; Tuning: Linear; Power: 10; P.Ext at 556.00 (bin 57); Ion Gate Blanking: 500.00  
Processed data (averaged) - 0.3 ml<sup>2</sup> (sum=17.4 m<sup>2</sup>), Smoothed = 10, profile # 1 - 90



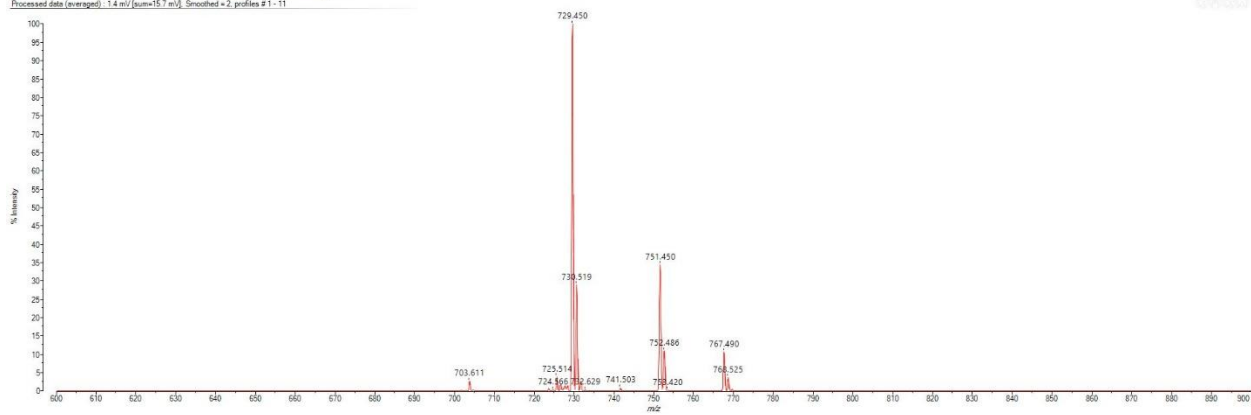
**Scheme S4.** Synthesis of AzKLKLF methylated library

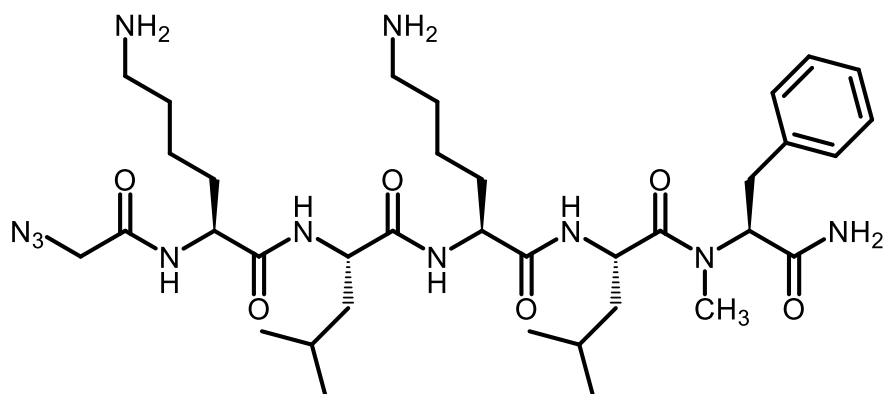
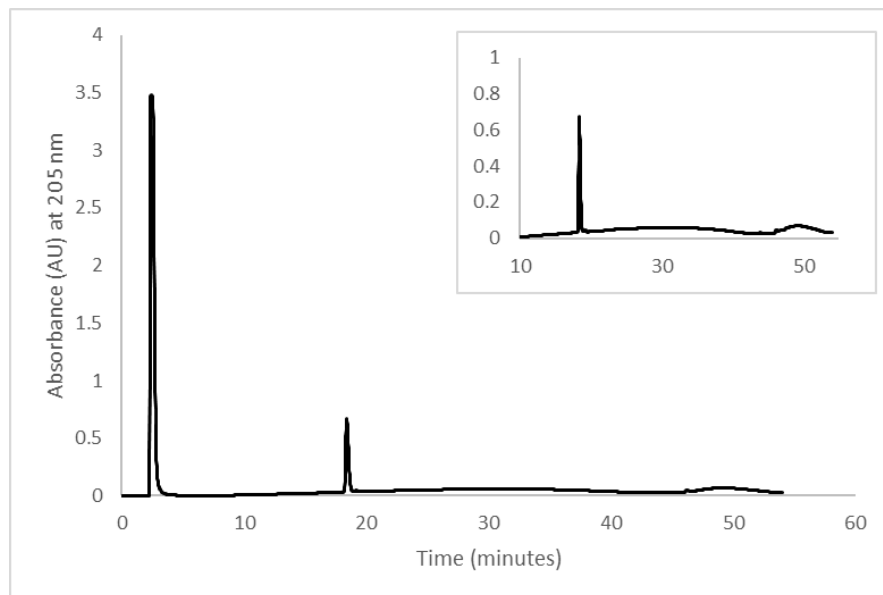
A 25 mL vessel of a CEM Discover Bio Manual Peptide Synthesizer was charged with 200 mg (0.096 mmol) of rink amide resin. About 10 mL of 20% piperidine in DMF was added to the resin, and the Synergy software was used to run the deprotection protocol. The piperidine solution was drained and the resin was washed with DMF (4 x 10 mL). Fmoc-L-Phe-OH (5 eq), 1 M oxyma (5eq), and 1 M DIC (eq) in DMF (10 mL) were added to the reaction flask, and the coupling protocol was run. The amino acid solution was drained, and the resin was washed with DMF (2 x 10 mL). The Fmoc deprotection and the amino acid coupling was repeated for the following amino acids to make M0: Fmoc-L-Leu-OH, Fmoc-L-Lys(Boc)-OH, Fmoc-L-Leu-OH, Fmoc-L-Lys(Boc)-OH, 2-azidoacetic acid. The same procedure was performed to make the M1-M4 peptides, but N-methylated amino acids were used for the respective methylated sites in the peptides. The resin was transferred to a conical tube for cleaving. The cleaving was performed by adding 95% TFA, 2.5% H<sub>2</sub>O, and 2.5% TIPS to the conical tube and rotating for 2 hours at room temperature. The resin was then filtered, and the resulting solution was concentrated. Cold diethyl ether was added to crash out the peptide, which was subsequently purified using RP-HPLC. The sample was analyzed for purity using a Shimadzu LC 2020 with a Phenomenex Luna 5 $\mu$  C18(2) 100Å (30 x 2.00 mm) column; gradient elution with H<sub>2</sub>O/ACN. The large peak at the beginning of the spectra is from the DMSO that the peptide was dissolved in. An inset shows the rest of the spectra without the first peak. Molecular weight was confirmed using a Shimadzu MALDI-TOF Mass Spectrometer (MALDI-8020).

**MO:**

<b>MO</b>	
Calculated m/z (M)	729.4650
M + H <sup>+</sup>	730.4728
M + Na <sup>+</sup>	752.4547
M + K <sup>+</sup>	768.4287
Masses found	729.450 751.450 767.490

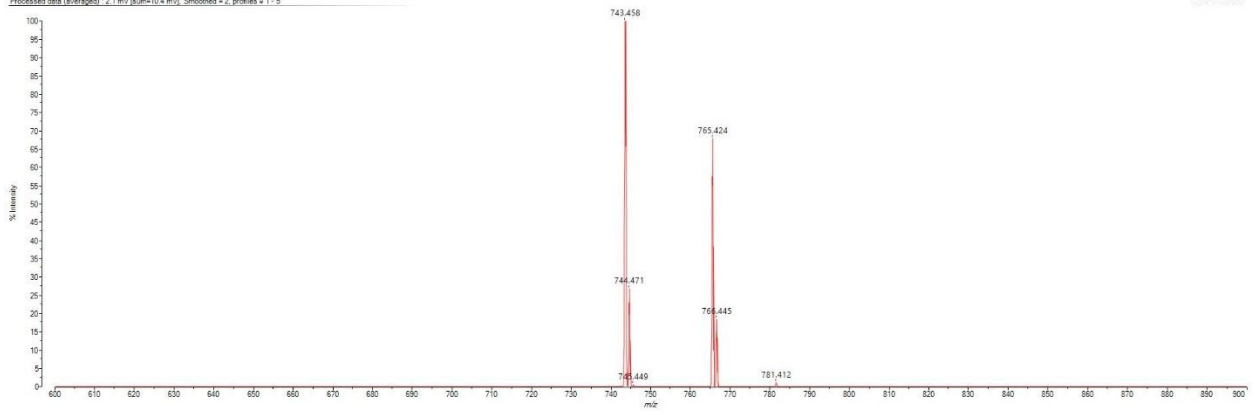
Created By psy9bk, Date: New Acquisition 17.01\_1 (Manual) February 6, 2023 2:36:20 PM Cal: Named Calibration "TOF mix 7.29.22" by bedffc on July 29, 2022 4:45:25 PM (Original)  
Shimadzu MALDI-TOF20: Tuning: Linear, Power: 5, P.E. at: 757.00 (Ion 97) Ion Gate: Blanking: 500.00  
Processed data (averaged): 1.4 ml (sum of 57 ml), Smoothed: x2, profiles # 1-11

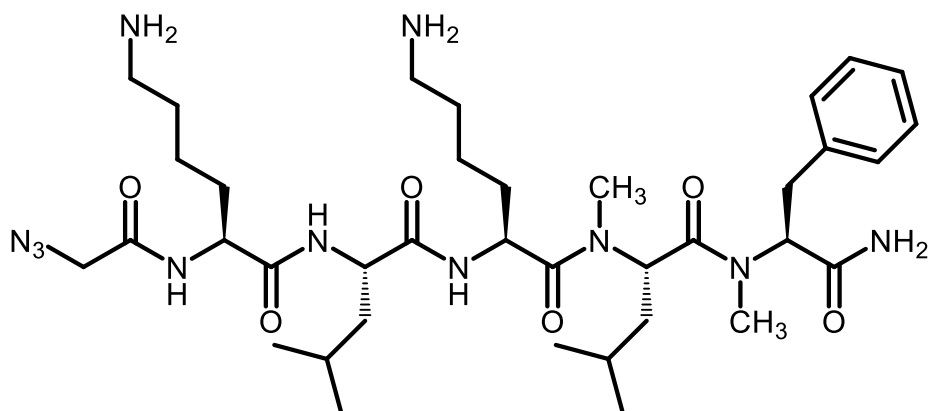
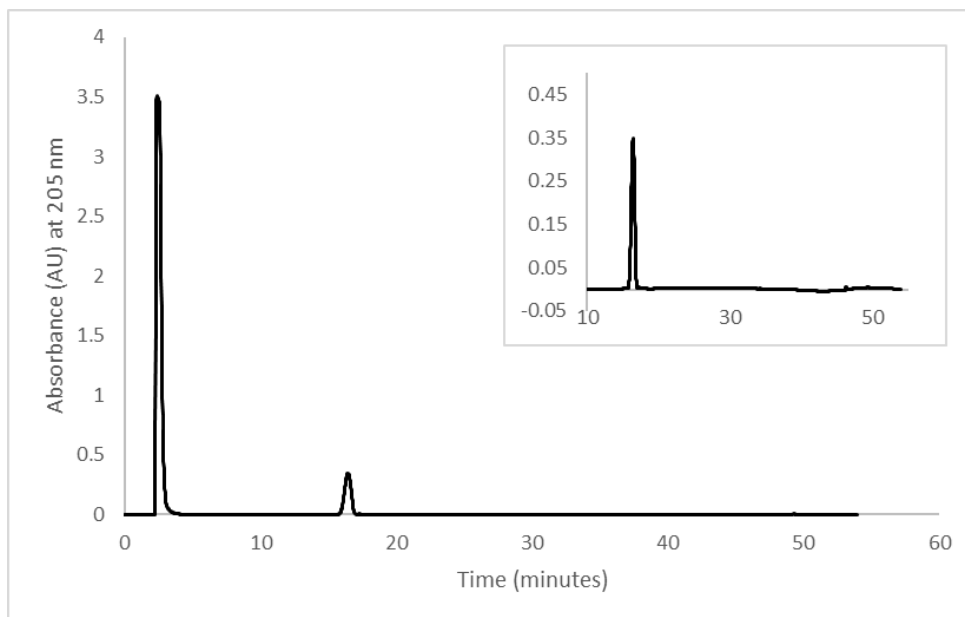


**M1:**

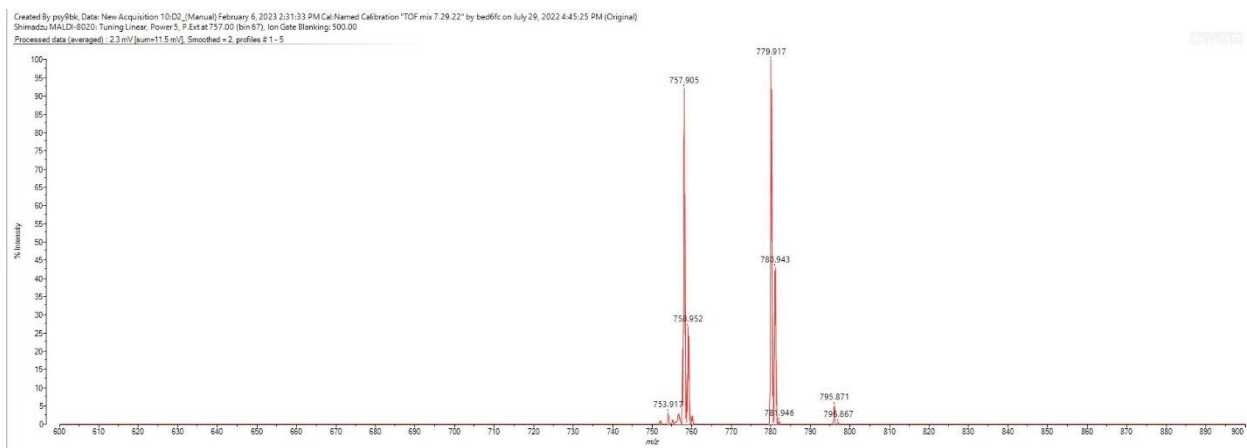
<b>M1</b>	
Calculated m/z (M)	743.4806
M + H <sup>+</sup>	744.4885
M + Na <sup>+</sup>	766.4704
M + K <sup>+</sup>	782.4443
Masses found	743.458
	765.424

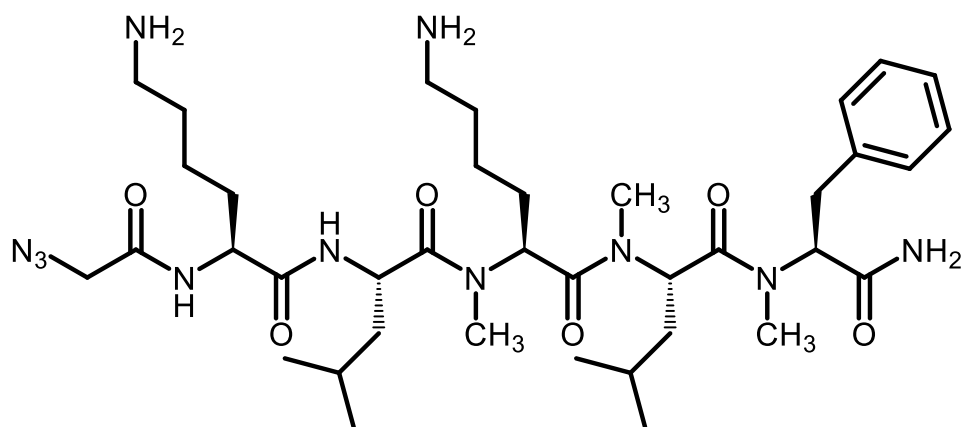
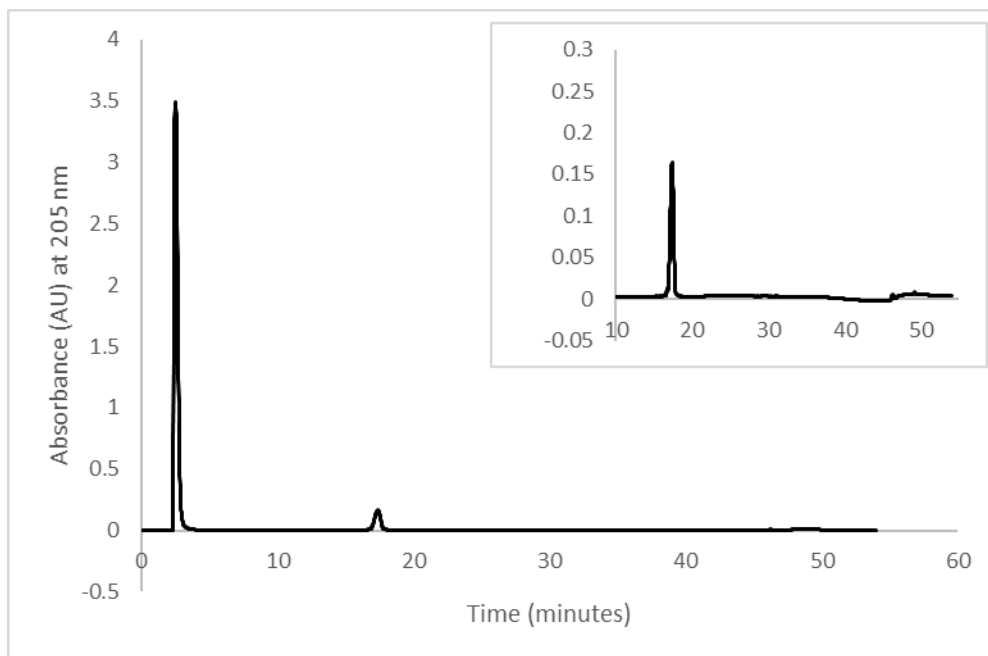
Created By: ppy/RLK, Date: New Acquisition 2.83\_1 (Manual) February 6, 2023 2:28:23 PM Cal: Named Calibration "TOF mix 7.29.22" by bedfrc on July 29, 2022 4:45:25 PM (Original)  
Shimadzu MALDI-8020: Tuning: Linear, Power: 5, P. Est: at 737.00 (Ion: 97), Ion Gate: Blanking: 500.00  
Processed data (averaged): 2.1 m/z (sum=114.4 m/z), Smoothed: +2, profiles # 1 - 5



**M2:**

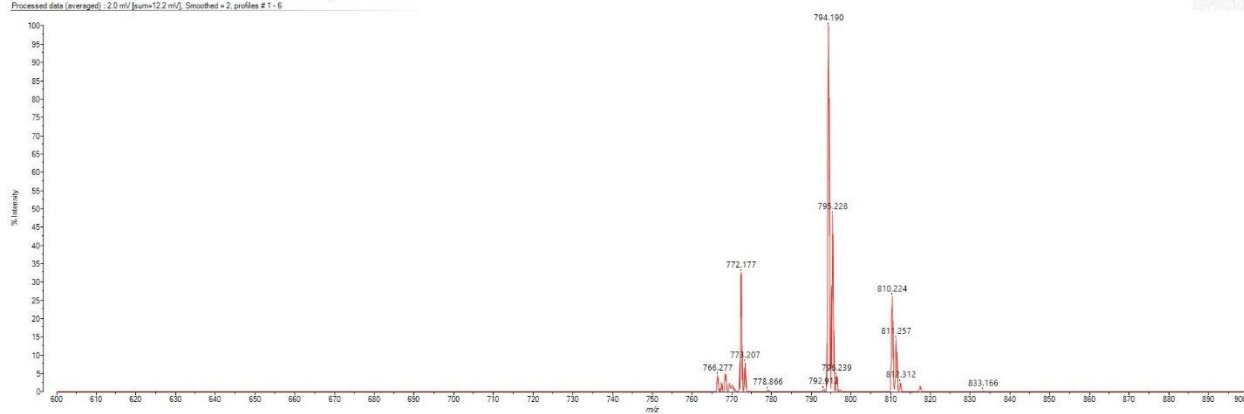
<b>M2</b>	
Calculated m/z (M)	757.4963
M + H <sup>+</sup>	758.5041
M + Na <sup>+</sup>	780.4860
M + K <sup>+</sup>	796.4600
Masses found	757.905
	779.917
	795.871

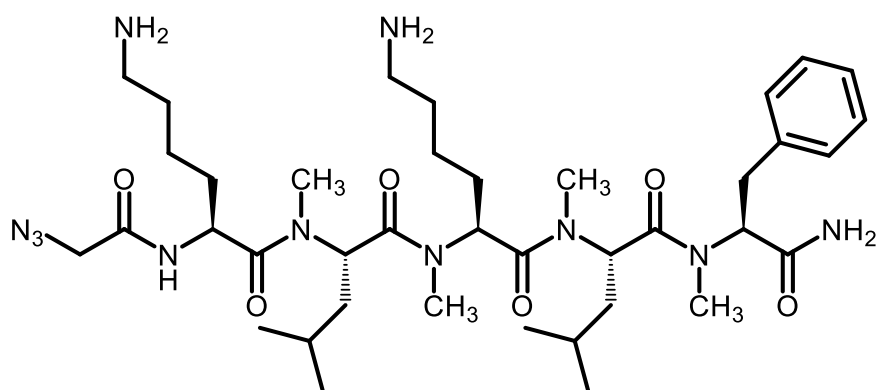
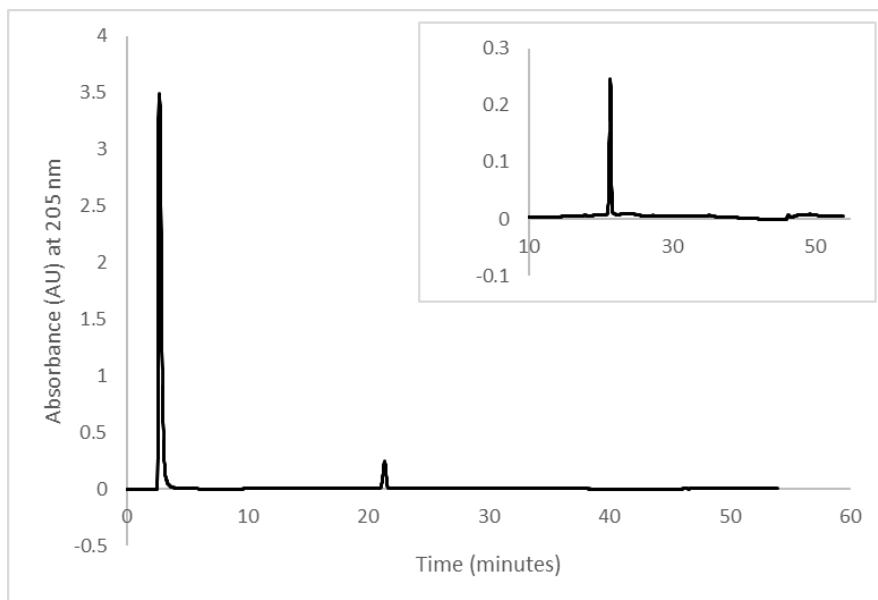


**M3:**

<b>M3</b>	
Calculated m/z (M)	771.5119
M + H <sup>+</sup>	772.5198
M + Na <sup>+</sup>	794.5017
M + K <sup>+</sup>	810.4756
Masses found	772.177
	794.190
	810.224

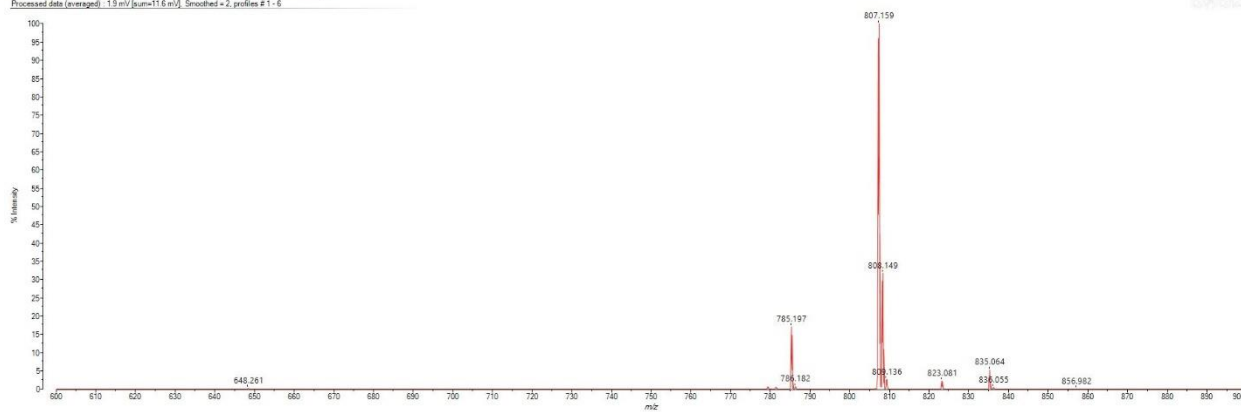
Created By pty9tk, Date: New Acquisition 6-14\_Manual February 16, 2023 11:33:39 AM Cal:Named Calibration "TOF mix 7.29.22" by bedffc on July 29, 2022 4:45:25 PM (Original)  
Shimadzu MALDI-8020: Tuning Linear, Power 10, P.Ext at 145.00 (bin 66), Ion Gate Blanking: 500.00  
Processed data (averaged): 2.0 ml (sum=12.2 ml), Scaled to 1, profiles # 1 - 6



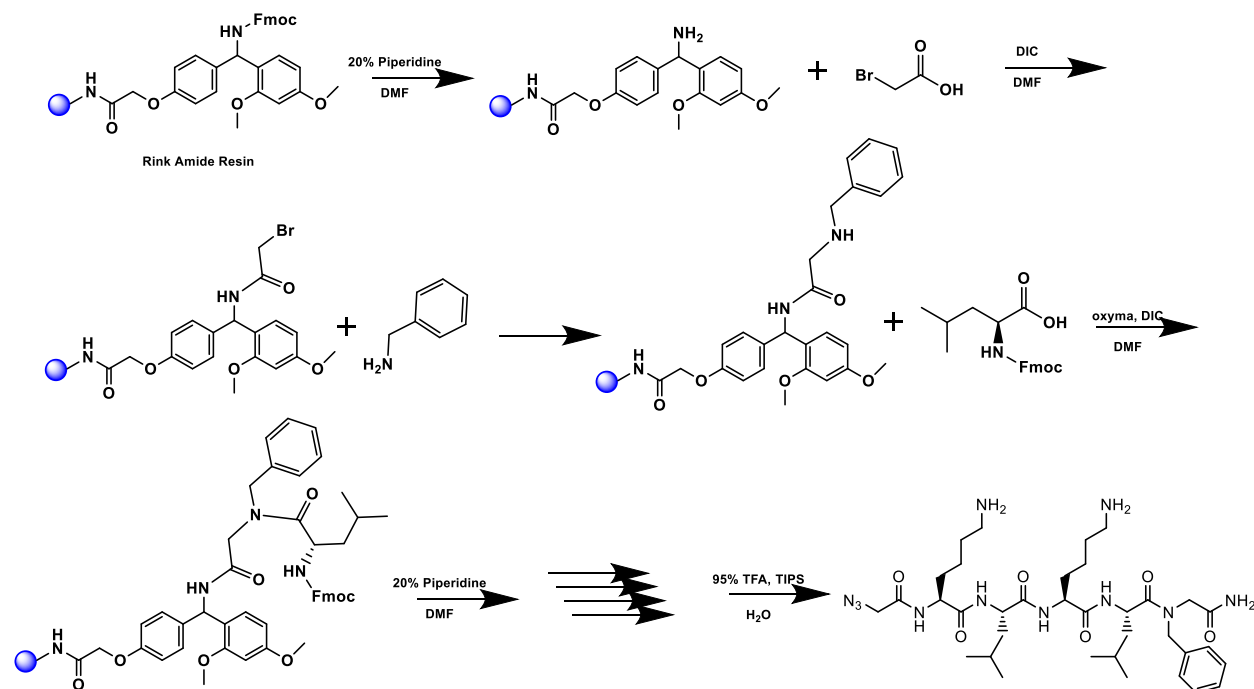
**M4:**

<b>M4</b>	
Calculated m/z (M)	785.5276
M + H <sup>+</sup>	786.5354
M + Na <sup>+</sup>	808.5173
M + K <sup>+</sup>	824.4913
Masses found	785.197
	807.159

Created By: psy9hk, Date: New Acquisition 4.A4\_1 (Manual) February 7, 2023 6:00:30 PM Cal: Named Calibration "TOF mix 7.29.22" by bedfic on July 29, 2022 4:45:25 PM (Original)  
Shimadzu MALDI-QTOF, Tuning: Linear, Power: 5, F: Ext at 785.00 (Ion 16), Ion Gate: Blanking: 500.00  
Processed data (averaged): 1.5 nV/beam(1.6 nV), Smoothed: 2, profiles: # 1 - 6

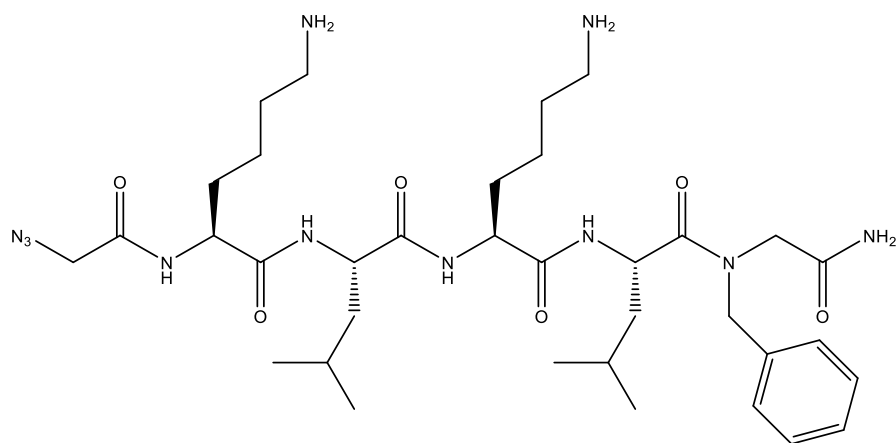
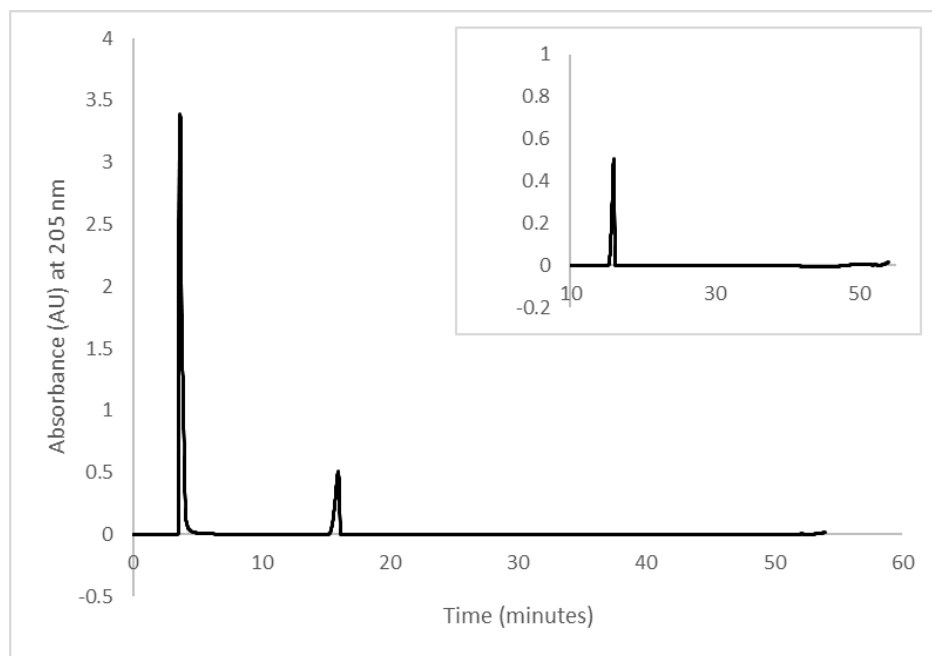


## Scheme S5. Synthesis of P1



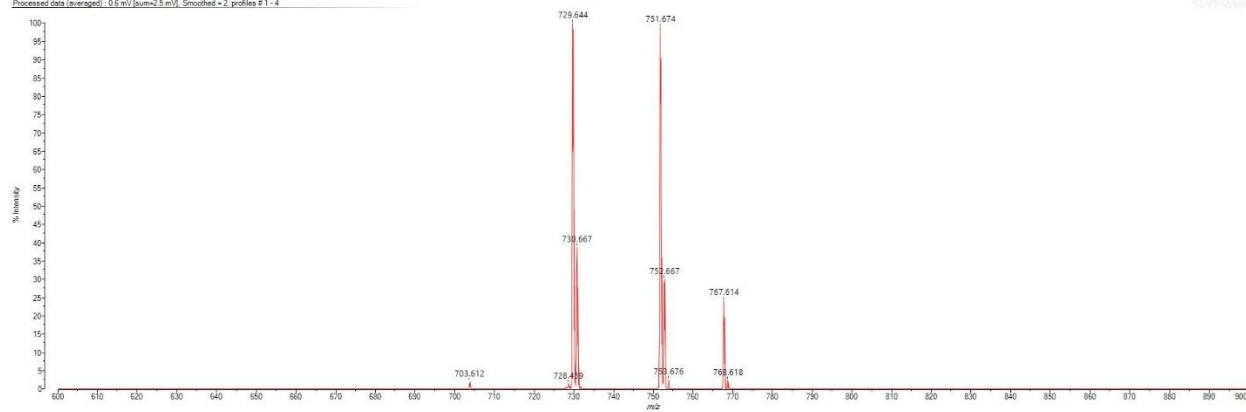
200 mg (0.096 mmol) of rink amide resin was added to a synthetic peptide vessel. The Fmoc group was deprotected by shaking with 20% piperidine in DMF for 30 minutes. The resin was then washed with alternating DCM and MeOH 2x and then washed twice more with DCM. A 0.6 M bromoacetic acid solution was made in DMF, and 1 mL of it was added to the resin. A 50% DIC in DMF solution was also made, and 200  $\mu$ L of this was also added to the resin. The vessel was set to shake for 20 minutes. The resin was then washed with DMF 3x. A 1.5 M solution of benzylamine in DMF was made, and 1 mL was added to the resin. After shaking for 1 hour, the resin was washed with DMF 3x. Fmoc-L-Leu-OH (5 eq), oxyma (5 eq), and DIC (5 eq) were dissolved in DMF and added to the resin. This mixture shook overnight. The resin was then washed with DCM and MeOH and the Fmoc deprotection were performed the same as before. Fmoc-L-Lys(Boc)-OH (5 eq), oxyma (5 eq), and DIC (5 eq) were dissolved in DMF and added to the resin to shake for two hours. The deprotection and coupling were repeated with the following amino acids: Fmoc-L-Leu-OH, Fmoc-L-Lys(Boc)-OH, 2-azidoacetic acid. The resin was transferred to a conical tube for cleaving. The cleaving was performed by adding 95% TFA, 2.5% H<sub>2</sub>O, and 2.5% TIPS to the conical tube and rotating for 2 hours at room temperature. The resin was then filtered, and the resulting solution was concentrated. Cold diethyl ether was added to

crash out the peptide, which was subsequently purified using RP-HPLC. The sample was analyzed for purity using a Shimadzu LC 2020 with a Phenomenex Luna 5 $\mu$  C18(2) 100 $\text{\AA}$  (30 x 2.00 mm) column; gradient elution with H<sub>2</sub>O/ACN. The large peak at the beginning of the spectra is from the DMSO that the peptide was dissolved in. An inset shows the rest of the spectra without the first peak. Molecular weight was confirmed using a Shimadzu MALDI-TOF Mass Spectrometer (MALDI-8020).

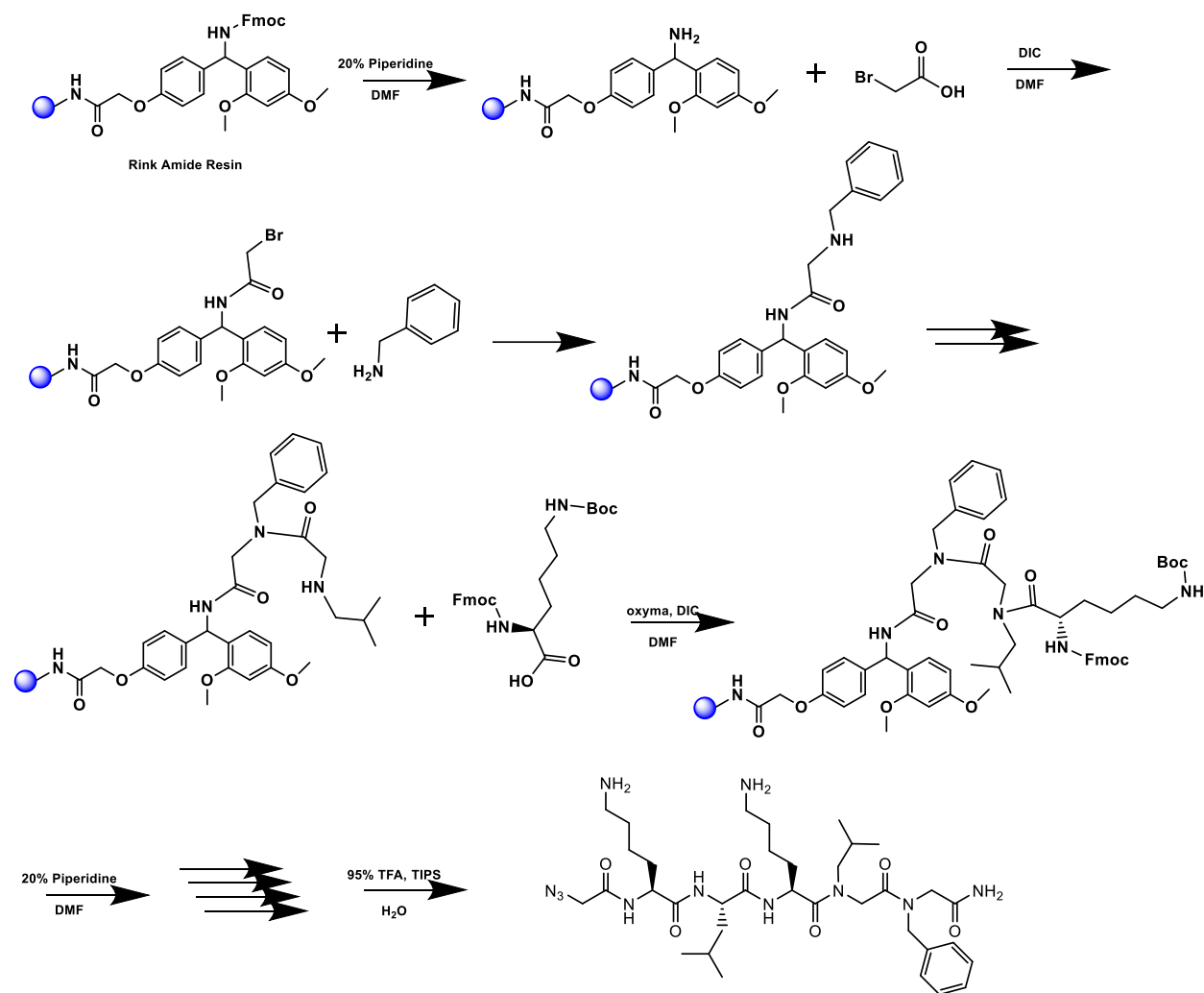


P1	
Calculated m/z (M)	729.4650
M + H <sup>+</sup>	730.4728
M + Na <sup>+</sup>	752.4547
M + K <sup>+</sup>	768.4287
Masses found	729.644 751.674 767.614

Created By: gpy9bk, Data: New Acquisition 3-82\_Manual, March 8, 2023 12:16:18 PM Cal: Named Calibration "TOF mix 7.29.22" by bde6fc on July 29, 2022 4:45:25 PM (Original)  
Shimadzu MALDI-S020; Tuning: Linear, Power: 7, P: Est: at 729.00 (in 66), Ion Gate: Blanking: 500.00  
Processed data (averaged): 0.6 mV (sum=2.5 mV), Smoothed = 2, profile # 1 - 4

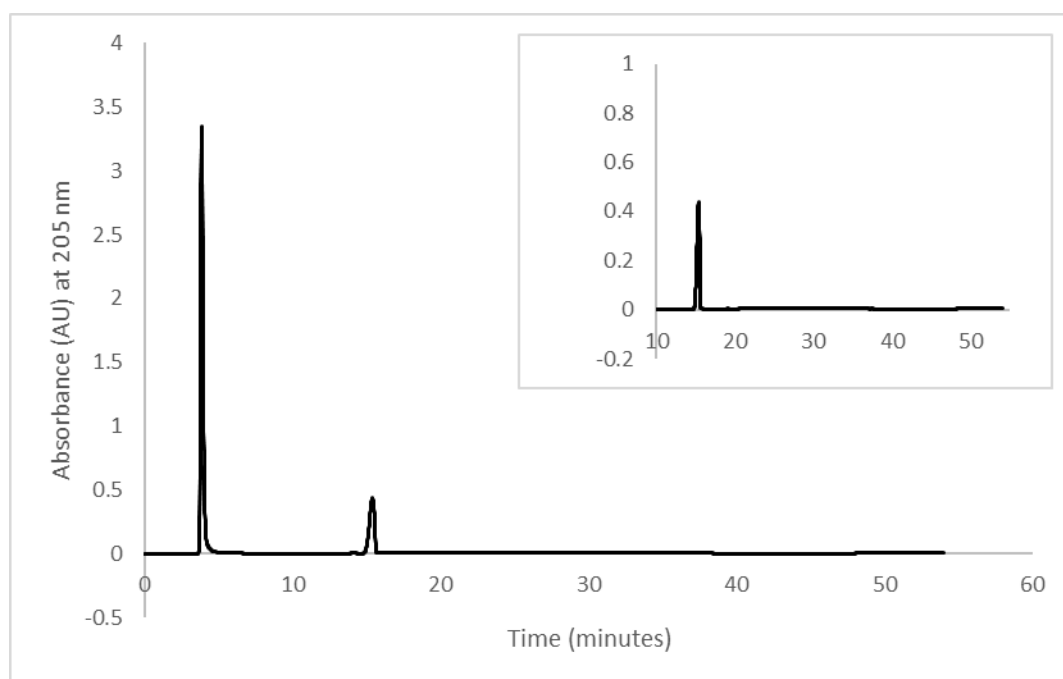


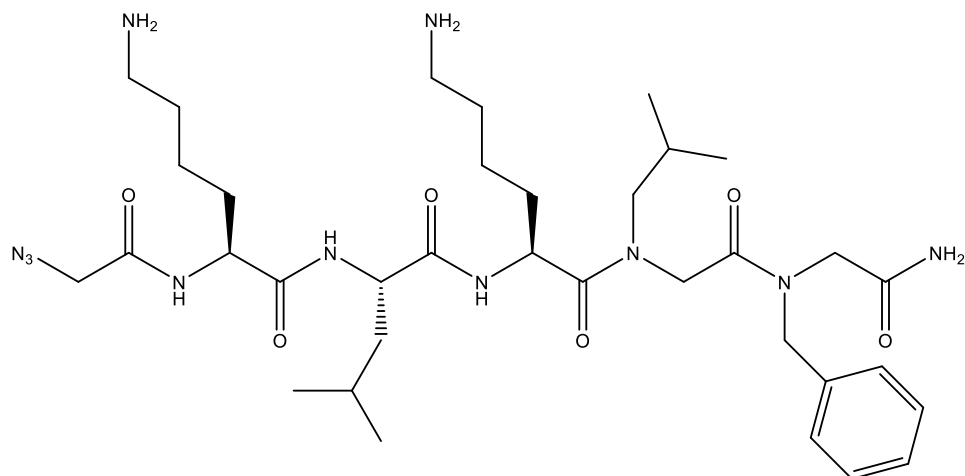
## Scheme S5. Synthesis of P2



200 mg (0.096 mmol) of rink amide resin was added to a synthetic peptide vessel. The Fmoc group was deprotected by shaking with 20% piperidine in DMF for 30 minutes. The resin was then washed with alternating DCM and MeOH 2x and then washed twice more with DCM. A 0.6 M bromoacetic acid solution was made in DMF, and 1 mL of it was added to the resin. A 50% DIC in DMF solution was also made, and 200  $\mu$ L of this was also added to the resin. The vessel was set to shake for 20 minutes. The resin was then washed with DMF 3x. A 1.5 M solution of benzylamine in DMF was made, and 1 mL was added to the resin. After shaking for 1 hour, the resin was washed with DMF 3x. The 0.6 M bromoacetic acid solution (1 mL) and the 50% DIC in DMF (200  $\mu$ L) were added to the resin again and was shook for 20 minutes. The resin was washed with DMF 3x. A 1.5 M solution of isobutylamine in DMF was made, and 1 mL of it was added to the resin to shake for 1 hour. The resin was washed with DMF again. Fmoc-L-Lys-OH (5 eq), oxyma (5 eq), and DIC (5 eq) were dissolved in DMF and added to the resin. This mixture shook

overnight. The resin was then washed with DCM and MeOH and the Fmoc deprotection were performed the same as before. Fmoc-L-Leu-OH (5 eq), oxyma (5 eq), and DIC (5 eq) were dissolved in DMF and added to the resin to shake for two hours. The deprotection and coupling were repeated with the following amino acids: Fmoc-L-Lys(Boc)-OH, 2-azidoacetic acid. The resin was transferred to a conical tube for cleaving. The cleaving was performed by adding 95% TFA, 2.5% H<sub>2</sub>O, and 2.5% TIPS to the conical tube and rotating for 2 hours at room temperature. The resin was then filtered, and the resulting solution was concentrated. Cold diethyl ether was added to crash out the peptide, which was subsequently purified using RP-HPLC. The sample was analyzed for purity using a Shimadzu LC 2020 with a Phenomenex Luna 5 $\mu$  C18(2) 100Å (30 x 2.00 mm) column; gradient elution with H<sub>2</sub>O/ACN. The large peak at the beginning of the spectra is from the DMSO that the peptide was dissolved in. An inset shows the rest of the spectra without the first peak. Molecular weight was confirmed using a Shimadzu MALDI-TOF Mass Spectrometer (MALDI-8020).

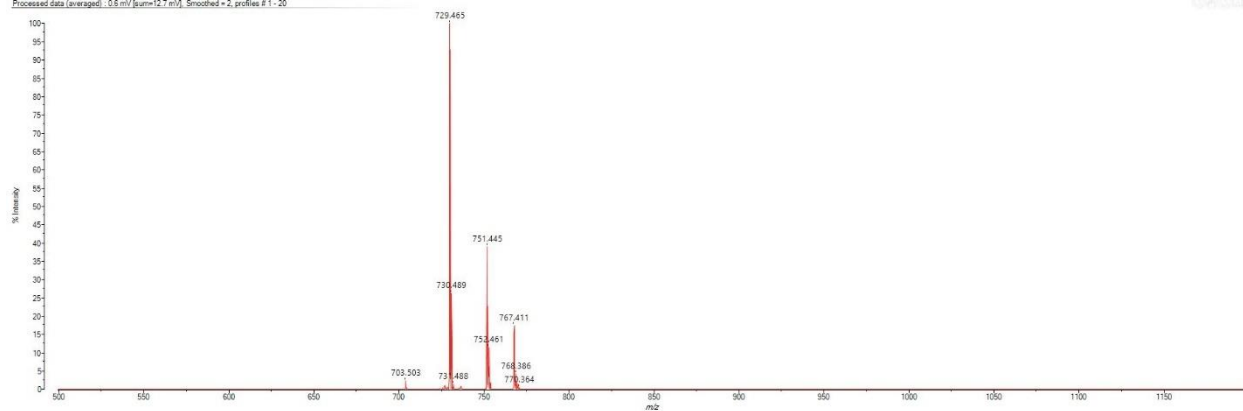




P1	
Calculated m/z (M)	729.4650
M + H <sup>+</sup>	730.4728
M + Na <sup>+</sup>	752.4547
M + K <sup>+</sup>	768.4287
Masses found	729.465 751.445 767.411

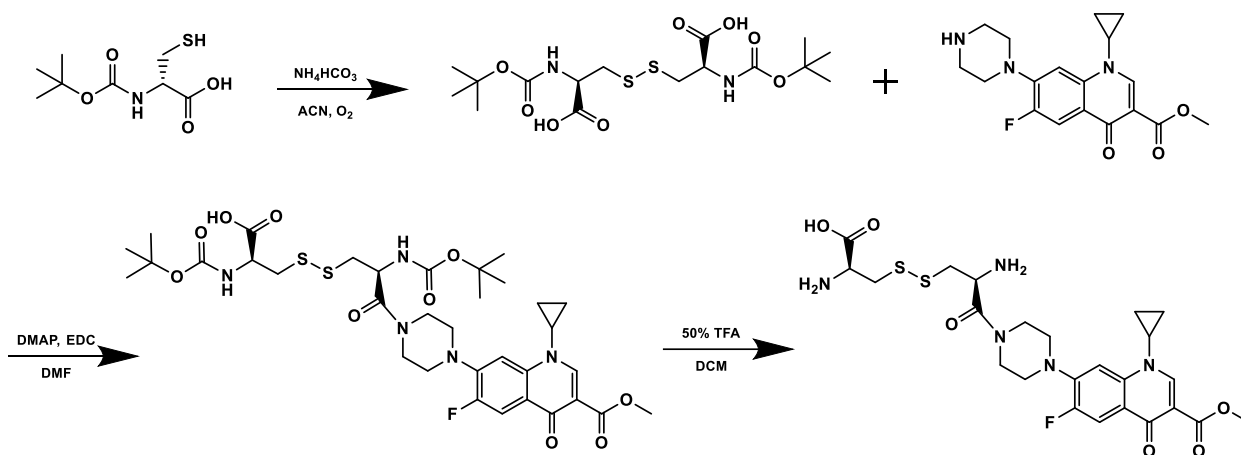
Created By: pro9k; Date: New Acquisition 1651; (Manual) March 13, 2023 10:08:30 AM Cal: Named Calibration "TOF mix 7.29.22" by bed6fc on July 29, 2022 4:45:25 PM (Original)  
Shimadzu MALDI-8020; Tuning: Linear; Power: 7; P.Ext: et 729.00 (ion 66); Ion Gate: Blanking: 500.00

Processed data (averaged): 0.6 nL (sum=12.7 nL); Smoothed = 2; profiles # 1 - 20

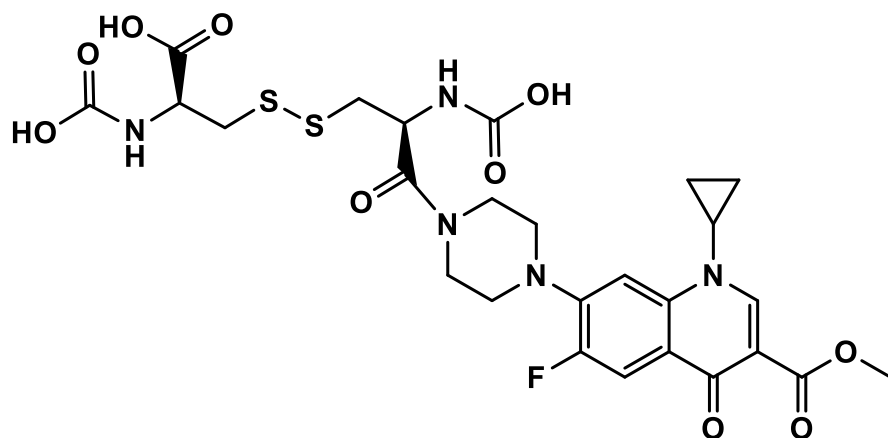
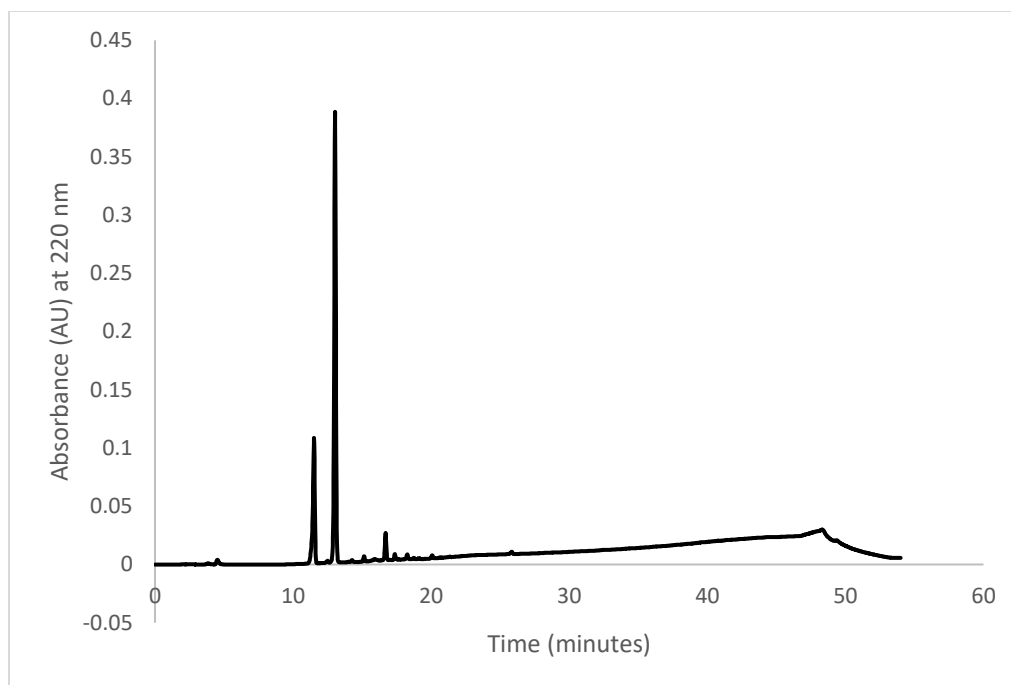


#### A.4 Synthesis and Characterization of Compounds in Chapter 4

**Scheme S1.** Synthesis of D-cystine-cipro-methyl-ester



First, N-Boc-D-cysteine was oxidized to N-diBoc-D-cystine by dissolving 200 mg of N-Boc-D-cysteine in a solution containing 22.5 mL acetonitrile and 7.5 mL 0.5 M ammonium bicarbonate. The solution was bubbled with air overnight. An Ellman's test was performed to test for free thiols. After passing the Ellman's test, the solution was rotovapped and lyophilized, yielding 185 mg. To conjugate N-Boc-D-cysteine to cipro-methyl-ester, the following was dissolved in 10-15 mL dimethylformamide (DMF): 50 mg cipro-methyl-ester, 135 mg N-Boc-D-cystine, 4 mg DMAP, and 25 mg EDC. This reaction stirred overnight. Thin layer chromatography (TLC) and electrospray ionization (ESI) was used to monitor the reaction progress. The compound was extracted from the DMF using liquid-liquid phase extraction with DCM and 0.1 M HCl. A silica column was used to purify the D-cystine-cipro-methyl-ester (DCCME). Chloroform with increasing concentration of methanol was used to elute the compound from the column. TLC was used to confirm the collection of the compound. The fractions were rotovapped, and 0.5 mL TFA + 0.5 mL DCM were added to Boc-deprotect the compound for 2 hours. The solution was rotovapped again, and ether was added to crash out the compound. DCCME was then purified *via* preparatory high performance liquid chromatography (HPLC) on a C8 column with H<sub>2</sub>O + 0.1% TFA and acetonitrile + 0.1% TFA. Collected fractions were rotovapped and lyophilized. The remaining compound was dissolved in water to make a stock. The sample was analyzed for purity using a Shimadzu LC 2020 with a Phenomenex Luna 5 $\mu$  C18(2) 100 $\text{\AA}$  (30 x 2.00 mm) column; gradient elution with H<sub>2</sub>O/ACN. Molecular weight was confirmed using a Shimadzu MALDI-TOF Mass Spectrometer (MALDI-8020).



<b>D-cystine-cipro-methyl-ester</b>	
Calculated m/z (M)	567.1622
M + H <sup>+</sup>	568.1700
M + Na <sup>+</sup>	590.1519
M + K <sup>+</sup>	606.1259
Masses found	567.612 589.453

Created By psj96k, Data: New Acquisition 2A1\_1 (Manual) February 23, 2023 1:26:48 PM Cal: Named Calibration "TOF mix 7.29.21" by beddfc on July 29, 2022 4:45:25 PM (Original)  
Shimadzu MALDI-8020; Tuning: Linear; Power: 5, P: Ext: at 560.00 (0th 50); Ion Gate: Blanking: 500.00  
Processed data (averaged): 8.8 mV (sum=52.3 mV), Smoothed = 2, profiles # 1 - 6

